From the Institute for Cardiogenetics
at the University of Lübeck
Acting Director: Prof. Dr. med. Malte Spielmann

The Impact of the Pro-Atherogenic *MRAS* gene in Smooth Muscle Cells

Dissertation

for Fulfilment of the Requirements
for the Doctoral Degree
at the University of Lübeck

from the Department of Natural Sciences

Submitted by

Pashmina Wiqar Shah

From Islamabad (Pakistan)

Lübeck, 2024

First referee: Prof. Dr. Malte Spielmann

Second referee: Prof. Dr. Tanja Zeller

Date of oral examination: February/26/2025

Approved for printing, Lübeck, March/07/2025

List of Contents

List of Figures

List of Tables

1. Abstract

Cardiovascular disease (CVDs) including coronary artery disease (CAD), cardiomyopathy, myocardial infarction and stroke, are the leading cause of death globally. The preeminent cause of CVDs is atherosclerosis, an inflammatory thickening of the vessel wall. Numerous risk factors including smoking, alcohol consumption, obesity, hypertension, stress, age, gender and genetic predisposition, contribute to its development. Genome wide association studies (GWAS) have pinpointed more than 393 loci marked by single nucleotide variants significantly associated with CAD. However, the causal mechanisms behind these associations remain unclear for which functional follow-up studies are very essential to identify the causal genetic variation or gene, to better understand the link between these loci and the disease.

A study by Erdmann *et al.* in 2009, revealed a region on 3q22.3, which encompasses the *MRAS* gene as a risk factor for CAD. In this doctoral dissertation, the CAD-risk gene *MRAS* was investigated. *MRAS* encodes muscle Ras, a small GTPase that acts as a signal transducer in tumour necrosis factor (TNF) signalling and other related acute phase response signalling pathways. According to eQTL data, *MRAS* risk variants for CAD increase *MRAS* mRNA levels primarily in the arterial tissue. Recently, it has been indicated that functional *MRAS* variants are specific to vascular smooth muscle cells (SMCs). The exact role of *MRAS* in atherogenesis, the underlying mechanism of CAD, and the therapeutic potential of targeting *MRAS* is still elusive. Therefore, we investigated the function of *MRAS* in vascular SMCs, one of the key cell types in the etiology of atherosclerosis and plaque stabilization. Human primary aortic SMCs transfected with *MRAS*-specific siRNA and murine aortic SMCs derived from our *Mras*$^{-/-}$*ApoE*$^{-/-}$ double knockout (dKO) mouse model was subjected to functional assays including proliferation, migration and apoptosis. The siRNA mediated knockdown of *MRAS* in human SMCs increased migration and proliferation with and without stimulation of TNF, IL-6 and IL-1ß. In line with that, the absence of *Mras* in murine SMCs led to significant increase in proliferation, enhanced migration and reduced apoptotic activity compared to control *B6.ApoE*$^{-/-}$ SMCs. Stimulation with TNF, IL-6 and IL-1ß enhanced the proliferative effect of *Mras* deficiency, indicating an interplay of these cytokines and MRAS pathways. Moreover, bulk RNA sequencing revealed that *Mras* knockout in murine SMCs led to differential gene expression of numerous genes involved in cGMP and cAMP signalling, suggesting that SMCs upregulate cGMP/cAMP signalling to compensate for the loss of *Mras*. The *in vivo* atherosclerosis study on plaque characteristic revealed that the impact of *Mras* deficiency was sex-specific as significant differences in plaque size, collagen content and macrophage staining were only observed in male mice. Male *Mras*$^{-/-}$*ApoE*$^{-/-}$ dKO mice showed significantly higher levels of collagen content, MoMa content and SMC content as compared to *B6.ApoE*$^{-/-}$ male mice. In conclusion, our data indicates that lower MRAS levels in the vessel wall, particularly in SMCs, provides protection against CAD by stabilizing atherosclerotic plaques, and thereby decreasing the risk of plaque rupture and subsequent hospitalization.

2. Zusammenfassung

Erkrankungen des Herz-Kreislaufsystems, einschließlich Koronarer Herzkrankheit (KHK), Kardiomyopathie, Herzinfarkt (HI) und Schlaganfall, sind weltweit die Haupttodesursache. Die Ursache für KHK ist Atherosklerose, eine entzündliche Verdickung der Gefäßwände. Zahlreiche Risikofaktoren wie Rauchen, Alkoholkonsum, Fettleibigkeit, Bluthochdruck, Stress, Alter, Geschlecht und genetische Veranlagung tragen zu ihrer Entstehung bei. Genomweite Assoziationsstudien (GWAS) haben mehr als 393 Genorte identifiziert, die durch Einzelnukleotid-Polymorphismen gekennzeichnet sind, die signifikant mit KHK assoziiert sind. Die kausalen Mechanismen hinter diesen Assoziationen sind jedoch nach wie vor unklar, weshalb funktionelle Folgestudien sehr wichtig sind, um die kausalen genetischen Variationen oder kausale Gene zu identifizieren, und damit den Zusammenhang zwischen diesen Genorten und der Krankheit besser zu verstehen.

In einer Studie von Erdmann et al. aus dem Jahr 2009 wurde die Genregion auf 3q22.3, als Risikofaktor für KHK entdeckt, die das *MRAS*-Gen beinhaltet. In dieser Dissertation wurde das CAD-Risikogen *MRAS* untersucht. *MRAS* kodiert für das muskulären Ras, eine kleine GTPase, die als Signalüberträger in der Tumornekrosefaktor (TNF)-Signalgebung und anderen Akutephase-Signalwegen fungiert. Den eQTL-Daten zufolge erhöhen *MRAS*-Risikovarianten für KHK die MRAS-mRNA-Spiegel hauptsächlich im arteriellen Gewebe. Kürzlich wurde festgestellt, dass funktionelle *MRAS*-Varianten spezifisch für vaskuläre glatte Muskelzellen (*engl.* Smooth Muscle Cells, SMCs) sind. Die genaue Rolle von MRAS bei der Atherogenese, der zugrundeliegende Mechanismus der KHK und das therapeutische Potenzial einer gezielten Beeinflussung von MRAS sind noch nicht geklärt. Daher untersuchten wir die Funktion von *MRAS* in vaskulären SMCs, einem der wichtigsten Zelltypen bei der Ätiologie der Atherosklerose und der Plaquestabilisierung. Humane primäre Aorten-SMCs, die mit *MRAS*-spezifischer siRNA transfiziert wurden, und murine Aorten-SMCs, die aus einem *Mras*$^{-/-}$*ApoE*$^{-/-}$-Doppelknockout-Mausmodell stammen, wurden funktionellen Tests unterzogen, darunter Proliferation, Migration und Apoptose. Die siRNA-vermittelte Ausschaltung von *MRAS* in menschlichen SMCs erhöhte die Migration und Proliferation mit und ohne Stimulation durch TNF, IL-6 oder IL-1ß. In Übereinstimmung damit führte das Fehlen von *Mras* in murinen SMCs zu einem signifikanten Anstieg der Proliferation, verstärkter Migration und verringerter apoptotischer Aktivität im Vergleich zu *B6.ApoE*$^{-/-}$ SMCs. Die Stimulation mit TNF, IL-6 und IL-1ß verstärkte die proliferative Wirkung des *Mras*-Mangels, was auf ein Zusammenspiel dieser Zytokine und MRAS-Signalwege hinweist. Darüber hinaus ergab die RNA-Sequenzierung, dass der Verlust von Mras in murinen SMCs zu einer veränderten Genexpression zahlreicher Gene führte, die an der cGMP- und cAMP-Signalübertragung beteiligt sind. Deutet darauf hin, dass SMCs die cGMP/cAMP-Signalübertragung aktivieren, um den Verlust von *Mras* zu kompensieren. Die *In vivo*-Atherosklerose-Studie zeigte, dass der *Mras*-Mangel geschlechtsspezifische Auswirkungen auf die Plaque-Eigenschaften hat, da nur bei männlichen Mäusen signifikante Unterschiede in der Plaque-Charakteristik zeigten. Männliche *Mras*$^{-/-}$*ApoE*$^{-/-}$ dKO-Mäuse wiesen im Vergleich zu männlichen *B6.ApoE*$^{-/-}$-Mäusen

signifikant höhere Werte des Kollagen-, Monocyten und Magrophagen und SMC-Gehalts auf. Zusammenfassend deuten unsere Daten darauf hin, dass niedrigere MRAS-Spiegel in der Gefäßwand, insbesondere in SMCs, vor KHK schützen, indem sie atherosklerotische Plaques stabilisieren und dadurch das Risiko einer Plaqueruptur und damit eines anschließenden Krankenhausaufenthalts verringern.

3. Introduction

3.1 Cardiovascular Disease

Cardiovascular disease (CVD) is the leading cause of death globally according to the (1). CVDs comprise of stroke, cardiomyopathy, coronary artery disease (CAD) and myocardial infarction (MI). The foremost cause of CVDs is atherosclerosis, an inflammatory process characterized by deposition of lipids in the endothelial layer of walls in the blood vessel. These lipid deposits called plaques or atherosclerotic lesions, narrow the blood vessels causing disrupted or reduced blood flow. Plaque's rupture and can induce thrombus formation, and ultimately cause complete vessel occlusion initiating interruption in the blood flow and cutting off the oxygen supply to downstream tissues. Severe tissue death is a consequence of all these processes, that is in the form of stroke in the brain and MI in the heart (2).

3.1.1 Atherosclerosis

Atherosclerosis is a chronic condition characterized by the deposition of lipids in the intima, the inner vessel wall of arteries (3). There are numerous stages in the development of atherosclerosis (4). Monocytes are recruited to the early lipid depositions in the intima, where they differentiate into macrophages and clear up the lipid deposits by phagocytosis (5). Accumulation of lipid-laden macrophages, or foam cells, is the first stage which can occur in an early stage in life (6, 7). The second stage is the formation of "fatty streaks" which are the precursor of advanced lesions (8). Advanced lesions develop in life later, as an inflammatory response (9) mediating vascular remodelling (10, 11). If lipids accumulate in higher amounts, the macrophages become overstressed and rupture (12), thereby releasing cellular content that fuels the lipid-rich, necrotic core (13). The necrotic core is often covered by a layer of collagen and smooth muscle cells (SMCs). SMCs are recruited from the media, *e.g.,* by signals released from macrophages (14). The SMCs change phenotypically from the contractile to the synthetic form (15–17) and start migrating towards the intima. The SMCs start proliferating and synthesizing collagen (18, 19) to form the fibrous cap (20) which stabilizes the plaque and preserves residual functionality of the vessel (21).

Stenosis may be caused by advanced lesions growing larger towards the lumen of the vessel (4). The plaques can grow by two processes i.e., continued lipid deposition (slow growth) (22), and rupture and healing of vulnerable plaques (rapid growth) (23, 24). Plaques with thin fibrous caps are defined as vulnerable plaques (25, 26). An injury to the fibrous cap by mechanical stress (27) can lead to the release of thrombotic material into the blood stream (24). SMC growth and collagen secretion contribute to the subsequent healing (28) of the plaque surface (29, 30).

Atherosclerotic plaques are formed by various cells originating from the vessel wall, which has three layers anatomically: the tunica intima (inner layer consisting of a monolayer of endothelial cells), the tunica media (middle layer consisting of multiple layers of vascular smooth muscle cells (VSMCs), and the tunica extrema (the outer layer composed of fibroblasts, perivascular cells, collagen and nerve endings) (31).

3.1.2 Genome-wide Association Studies for Coronary Artery Disease

Genetics contribute highly to the risk of coronary artery disease (32). Family burden serves as an indicator of the hereditary risk associated with atherosclerosis (33). Family members with higher occurrence of MI are at a higher risk for atherosclerosis (33–35). Identical twins showed increased risk for MI (36). Moreover, the identified variants are often rare, exhibit strong effect sizes, and are specific to certain families, which limits their ability to fully explain the global incidence of atherosclerosis and myocardial infarction (MI) in the general population. Atherosclerosis is a complex disease with rare, familial (or mendelian) variants driven by a mixture of many genetic factors (3, 37). To solve the problem of the lack of explainable genetic heritability in the general population, genome-wide association studies (GWAS) were conducted that focus on common single nucleotide variants with an allele frequency of more than 5 percent. However, common genetic variants do not cause MI themselves. They modify the susceptibility of the individual to conditions that favour the onset of the disease (38–40).

Common variants have a lower effect than rare variants (41, 42) but are widely distributed among the population and account for a late onset-disease pattern (43). Whereas rare (or familial) variants mostly lead to a disease phenotype emerging in an early stage of life (35).

GWAS is a method to study the genetics of complex diseases like coronary artery disease and atherosclerosis (44, 45). The association of variations in the human genome to the disease is analysed through GWAS. Identification of large number of single nucleotide variants (SNVs) within cohorts of populations (43, 46–48), selection of tag SNVs based on their haplotypes (49, 50), and rapid SNV genotyping using DNA microarray chips (51–53) were the approaches used through GWAS.

A GWAS's requisite is large groups of cases and controls i.e., people with or without a disease within populations (54). DNA samples were collected from each individual that was part of a GWA study and the DNA was genotyped for the SNVs of interest, and the SNV frequencies were calculated. Multiple testing for the statistical significance level of the large number of SNVs was carried out leading to a significance threshold of $p < 5 \times 10^{8}$, famously known as the Bonferroni correction (55, 56). When the GWAS was conducted, a risk gene was assigned for each locus that was in close proximity to the significant SNV (57).

The first GWAS for CAD identified a risk locus on chromosome 9 and was published in 2007 (44, 45, 58, 59). Many more risk loci of CAD were identified in the following years (60–67). Unexpectedly, most of the mapped genes were either of unknown function or involved in pathways not readily contributing to CAD/MI. After decades, recent findings from three large CAD consortia have identified 393 loci that are significantly associated with CAD (68–72), one of which is the 3q22.3 risk locus that comprise the candidate causal gene *MRAS* (62).

Other approaches in combination with GWAS are also used to diagnose more CAD risk genes, including expression quantitative trait locus (eQTL)-data approach (57, 73) and approach to find out how gene-gene or gene-environment interactions modulated the effects of risk genes (74).

GWAS in combination with eQTL data, *in vitro* studies using atherosclerosis-relevant cell types such as SMCs or endothelial cells (75), and *in vivo* studies using mouse models to capture complex traits of the disease, is the most efficient and crucial step in understanding and interpreting the association of an SNV with the disease phenotype and moving towards translational approaches (76–79).

3.2 The Candidate CAD Risk Gene, *MRAS*

Muscle RAS (*MRAS*) is a putative oncogene located in a CAD susceptibility locus that was first identified by Erdmann *et al.* in a GWA study in 2009 (62). The 3q22.3 risk locus (Table 1) was identified by analysis of three genome-wide CAD datasets from 1,222 German individuals with MI and 1,298 healthy controls (n = 1,298) in a study that identified four SNVs (rs1199338, rs2347252, rs3732837, and rs9818870) associated with CAD (62). Furthermore, another study was conducted in populations of European ancestry involving meta-analysis of 14 CAD GWAS, comprising of 22,233 cases and 64,762 controls, followed by analysis of 60,738 additional individuals, confirming the *MRAS* CAD risk locus (67).

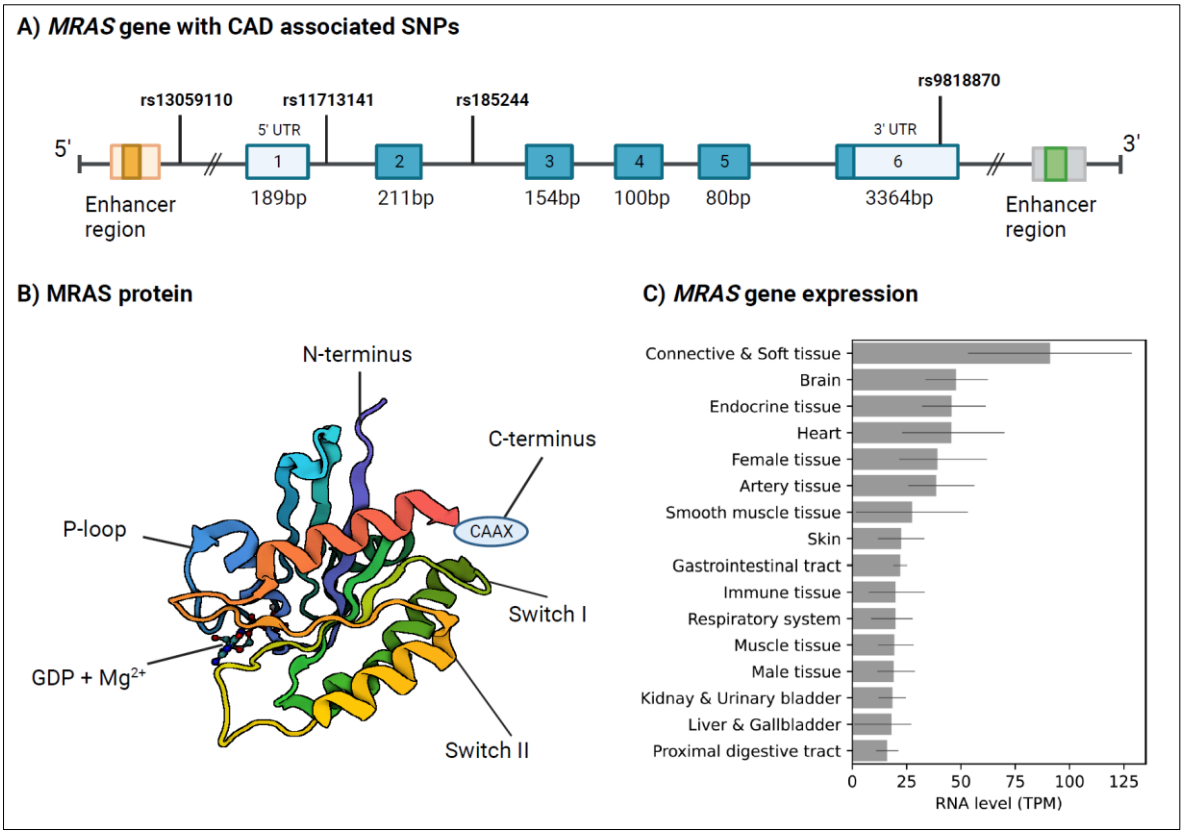

Figure 1 – Schematic representation of the MRAS gene (A), protein structure (B) and gene expression (C)

A: (Canonical transcript ENST00000423968.7; coding regions are depicted blue) with its genetic variants associated with CAD sequentially arranged according to their chromosomal position. **B:** Model of the MRAS protein (PDB: 1X1R) depicting the N-termini (purple) with its phosphate-binding loop (P-loop) and the two switch regions i.e. Switch I (green), Switch II (yellow), carboxy terminus with its CAAX motif (red), and GDP and Mg2+ (blue sticks and red sphere). **C:** Gene expression of *MRAS* as transcripts per million (TPM) in different tissues from the Expression Atlas (**https://www.ebi.ac.uk/gxa/home**). The Figure is taken from (80).

MRAS (Ensembl ID ENSG00000158186) is located on human chromosome 3q22.3 and mouse chromosome 9. The human canonical *MRAS* gene consists of six exons, five of which are coding (Figure 1)**.** The first exon, 189 bp in length, resides in the 5'-untranslated region (UTR), while the second to fifth coding exons are 211, 154, 100, and 80 bp, respectively. The sixth exon is the largest at 3364 bp, including the 3'-UTR, which plays a regulatory role by binding microRNAs (miRNAs) (81).

The gene structure of *MRAS* (Figure 1) is highly conserved among all vertebrates, with identical splice site junctions and conserved sequences in its five exons in human, zebrafish, mouse, and Xenopus. The human *MRAS* genes shares 99.5% similarity with its chimpanzee orthologue, and 97.0%, 89.4% and 60.6% with lizard, mouse and nematode orthologues, respectively (https://www.genecards.org/).

The human *MRAS* gene encodes a 208-amino-acid membrane-bound small GTPase protein (82) with an 10-amino acid N-terminal extension, a 117-amino acid catalytic domain, and a C-terminal membrane localization domain (82) (Figure 1). The N-termini of RAS family members, including

RRAS, KRAS, HRAS, NRAS, and MRAS, share significant primary sequence homology, particularly in the phosphate-binding loop (P-loop) and the two switch regions (switch I and II) within the G-domain crucial for nucleotide binding and hydrolysis (83). MRAS is anchored to the plasma membrane (84, 85) via a RAS GTPase-specific CAAX motif in its C-terminal region, which serves as a lipophilic anchor following post-translational modifications like isoprenylation (86).

The MRAS protein was first identified in mice and rats through the screening of skeletal myocyte and brain cDNA libraries respectively (86), while the human *MRAS* cDNA was cloned from an embryonic lung fibroblast cDNA library (87). The amino acid sequence predicted from the murine C2 cell *MRAS* cDNA contains an open reading frame that encodes a 208-amino acid protein (82) with a molecular mass of 23,901 Da, which is identical to its counterpart identified in rat brain. Cloning and overexpression of *MRAS* resulted in the formation of micro-spikes in cultured cells; therefore, the protein was named MRAS, where 'M' indicates 'muscle' or 'micro-spikes' (60).

The highest levels of *MRAS* transcripts are found in the connective/soft tissue, brain, endocrine tissue, and muscle tissues (heart, skeletal and smooth muscle) (Figure 1)**.** *MRAS* expression is cell type enriched in adipocytes and eccrine sweat gland cells (skin) (refer to Human Protein Atlas). However, the MRAS protein is present in nearly all tissue types at moderate to high levels. *MRAS* expression is regulated by the Krüppel-like factor 5 (KLF5) transcription factor (88), which stimulates its transcription in certain regions of the brain, heart, and developing bones in mice (86, 89). According to GeneCards/GeneHancer (90), the high-scored enhancer (GeneHancer ID: GH03J138347) contains 69 transcription factor binding sites, indicating a much more complex gene regulation. Moreover, in humans, eight protein-coding transcripts are reported for *MRAS* (Ensembl ID: ENST00000423968.7).

3.2.1 *MRAS* and Coronary Artery Disease

Several non-coding single nucleotide variants (SNVs) located within the *MRAS* locus are reported to be associated with CAD and CAD causing traits like dyslipidaemia and hypertension (Figure 1 and Table 1)**.**

In the Han Chinese population, 3q22.3 was also detected as a novel CAD-associated locus and the association was significant in females (91). Furthermore, the rs6782181 and rs9818870 *MRAS* SNVs were highly associated to CAD in the Saudi Arabian population. *MRAS* has been identified as a causal risk gene for CAD in certain ethnic groups (92).

However, the precise molecular mechanisms by which *MRAS* variants influence the development of atherosclerosis remain unclear. An explanation is SNVs rs9818870 and rs40593 acting as predictors of cardiovascular disease risk in CAD-free individuals (93) and cerebral infarction (94), respectively. Both SNVs are located in the 3’ UTR of *MRAS*, adjacent to a cluster of miRNA binding sites. These

sites are increasingly recognized for their role in regulating *MRAS* gene expression, translation, and protein levels (94) by altering the mRNA structure (81). Moreover, the majority of SNVs associated with CAD are in the non-coding regions, suggesting regulatory function (95).

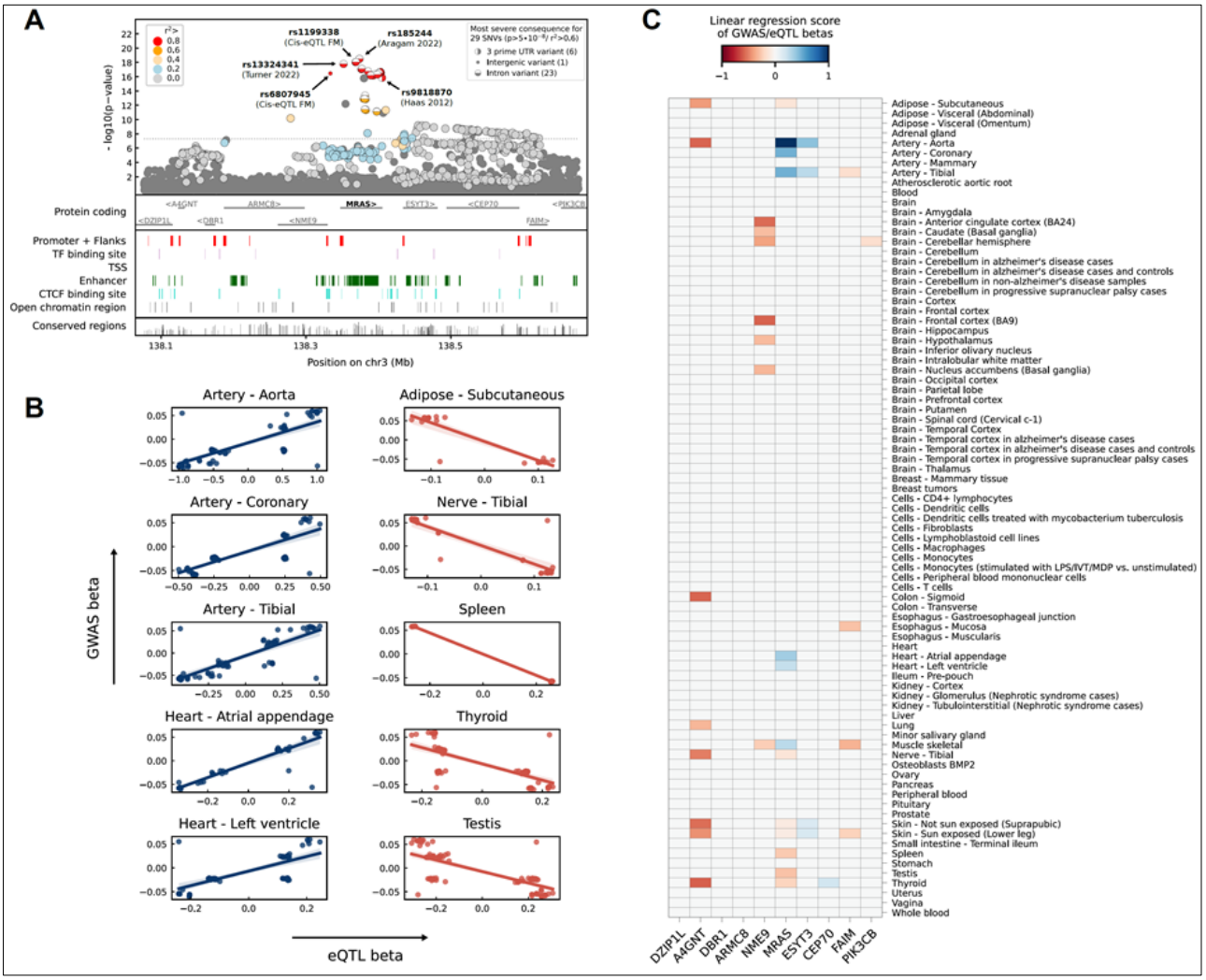

Figure 2 – *MRAS* genetic variants associated with CAD

A) Regional association plot showing the genome-wide significant *MRAS* locus. Genetic features and linkage disequilibrium (LD) values (r2) were obtained from Ensembl (release 110). The intronic index variant, rs185244 (68), overlaps with a broad enhancer region (green) and is considered one of the causal variants. Besides rs185244, other variants in high LD also show high evidence of causality based on eQTL fine mapping (FM), which are rs1199338 from DAP-G (96) and rs6807945 from CAVIARBF (97) with a Bayesian posterior probability >0.99 in artery and heart tissue. In addition, rs9818870 is another putative causal variant as it alters the local mRNA structure in the 3'-untranslated region of *MRAS* transcripts and thus their interaction with microRNAs, resulting in differential gene expression (81). **B) Exemplary regression plots of GWAS beta effects and eQTL beta effects for *MRAS* variants in moderate LD (r2>0.2).** Artery and heart tissue show a significant positive correlation between *MRAS* expression and CAD risk (all p<10-11). In contrast, variants that result in higher *MRAS* levels in nerve, spleen, testis, or thyroid appear to reduce CAD risk (and vice versa). **C) Heatmap** of relative regression scores from regression analysis for all proximal genes in the *MRAS* locus (±0.5 Mb window) and all tissues listed in the QTLizer database (98) . Relative linear regression scores (-1 to 1) are derived from the absolute maxima of eQTL beta values multiplied by the sign of the slope of linear regression obtained from the *Python* function *stats.linregress* as implemented in SciPy. Only scores from regression analysis with $p < 10^{-6}$ are shown for simplification. This figure was taken from (80).

3.2.2 Risk Factors contributing to Atherosclerosis

Divergent factors are known to promote atherosclerosis, and can be divided into two categories i.e., clinical and molecular risk factors (99). Family history of heart disease, gender, age, smoking, diabetes, obesity, unhealthy diet, lack of physical activity, hypertension, high blood cholesterol, and oxidized low-density lipid cholesterol are all clinical risk factors of coronary artery disease (3, 100). Molecular risk factors consist of Apolipoprotein B/A-I levels, number of triglycerides in the blood, LDL-C, and C-reactive protein levels (101). Furthermore, risk factors can also be divided into controllable and non-controllable categories (102). Controllable risk factors, often referred to be as behavioural or life style factors, are factors that can be changed meaning adopting healthy habits i.e., healthy diets, no alcohol consumption, engagement in regular physical activity, quitting smoking, and managing diseases like hypertension, and diabetes. Medication to lower cholesterol and blood pressure may even be taken to prevent and reduce the risk of atherosclerosis. In contrast, factors that cannot be controlled are age, gender, and genetic predisposition (101, 102).

3.2.3 *MRAS* is associated with Obesity, Dyslipidaemia, and Hypertension

Numerous non-coding SNVs in the *MRAS* locus were identified to be significantly associated with obesity-related traits, like BMI, body fat percentage, or waist-to-hip ratio **(Table 1).** Notably, rs6782181, initially linked to CAD, was also associated with hypercholesterolemia, hypertriglyceridemia, low HDL and obesity (92). This variant was associated to dyslipidaemia in Chinese Han and Mulao populations (94, 103, 104). Another SNV, rs253662 was associated to reduced HDL levels (94). Moreover, three SNVs – rs751357, rs6782181, and rs40593, were positively associated with high serum total cholesterol levels, thereby increasing the risk of cardiovascular disease (94). It was speculated that the interaction between *MRAS* and obesity may be the primary factor driving its impact on dyslipidaemia-related events. Additionally, *MRAS* expression is enriched in adipocytes (refer to Human Protein Atlas). Hypertension-related SNVs (rs4678408, rs6807945, rs6766859) (105, 106) were linked to systolic blood pressure and the use of agents acting on renin-angiotensin-aldosterone system respectively (Table 1).

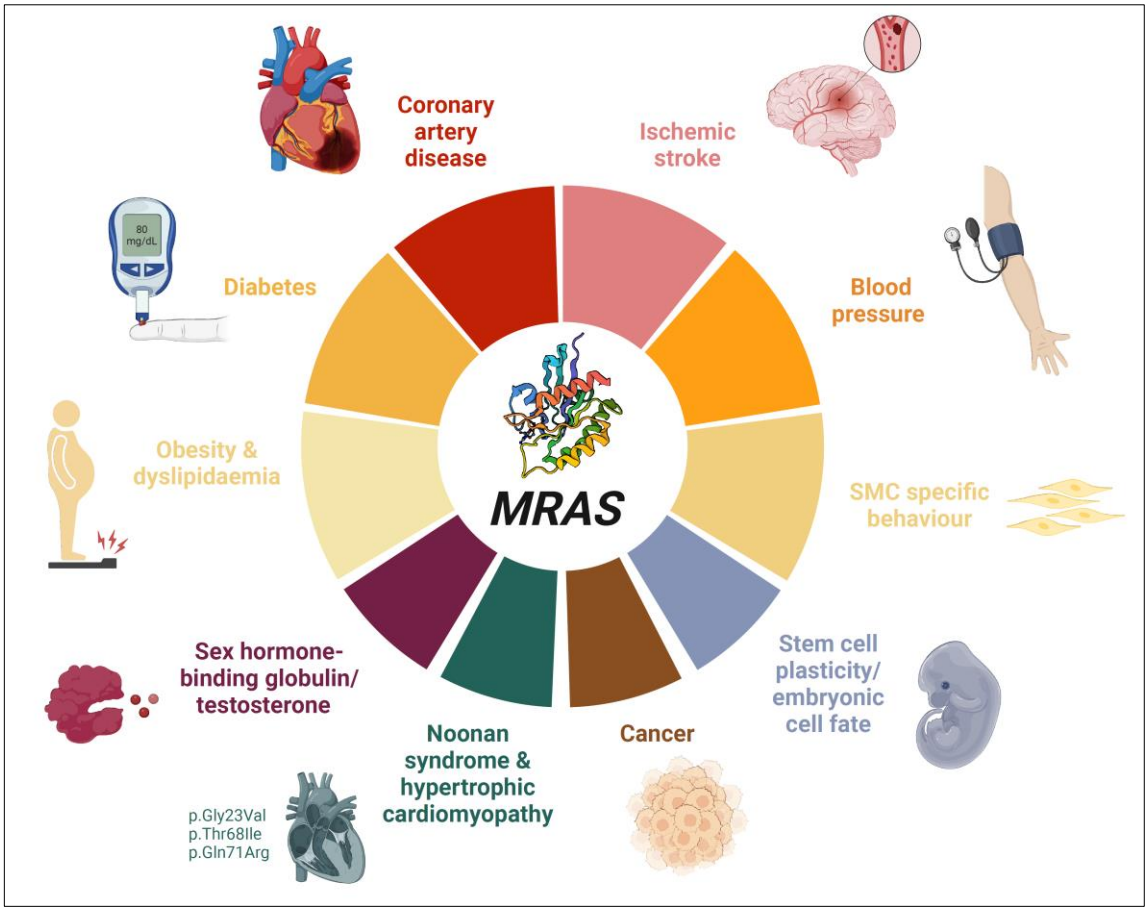

Figure 3 – *MRAS* and associated traits

MRAS variants are associated with a variety of common genetic conditions, including coronary artery disease, Noonan syndrome, or cardiac hypertrophy. It is also involved in metabolic disorders like diabetes, obesity, and dyslipidaemia. Apart of its active role in diseases, *MRAS* is also a novel stemness marker impacting mouse embryonic stem cell plasticity and Xenopus embryonic cell fate. Recently, it was demonstrated that *MRAS* risk variants are specific to smooth muscle cell (SMC) behaviour (106). This figure was created with BioRender and taken from (80).

Table 1 – *MRAS* index variants associated with coronary artery disease (CAD) and related traits

Trait	rsIDs	Variant ID	P	Beta	Location	Regulome score	*MRAS* eQTLs	Study ID
Coronary artery disease	rs13059110	3_138278900_G_T	1.0E-09	0.080	Intergenic	0.51	0.66	FINNGEN_R6
	rs11713141	3_138348784_C_T	1.0E-09	-0.020	Intron	0.55	-0.13	GCST010479
	rs185244	3_138374047_C_T	3.2E-19	0.030	Intron	0.99	0.50	GCST90132314
	rs9818870	3_138403280_C_T	2.6E-17	0.030	3' UTR	0.22	0.22	GCST000338
Body mass index (BMI)	rs1308362	3_138385085_A_T	6.0E-09	0.030	Intron	1.00	0.16	GCST004557
	rs9818870	3_138403280_C_T	4.0E-10	0.014	3' UTR	0.22	0.34	GCST90179150
Body fat percentage	rs9851766	3_138402667_A_G	1.0E-11	0.014	3' UTR	0.22	0.24	GCST90020232
Waist-to-hip ratio	rs9872754	3_138399143_C_T	8.0E-16	0.031	Intron	0.9	0.24	GCST90020025
Triglyceride	rs2306374	3_138401110_T_C	1.0E-10	0.017	Intron	0.67	0.24	GCST90025957
HDL cholesterol levels	rs2306374	3_138401110_T_C	1.0E-11	-0.017	Intron	0.67	0.24	GCST90025956
Body height	rs140371629	3_138348474_G_C	4.0E-09	n.d.	Intron	0.55	-0.20	GCST007841
Essential hypertension	rs4678408	3_138348474_G_C	9.0E-09	n.d.	Intergenic	0.51	-0.15	GCST010774
Systolic blood pressure	rs6807945	3_138333912_C_T	3.0E-11	n.d.	Intergenic	0.55	-0.27	GCST007087
Diastolic blood pressure	rs185244	3_138374047_C_T	4.0E-13	0.203	Intron	0.99	0.50	GCST90132904
Use of agents acting on renin–angiotensin system	rs6766859	3_138336294_C_T	1.0E-10	-0.033	Intergenic	0.55	-0.16	GCST007930
Type 2 diabetes mellitus	rs6766859	3_138336294_C_T	1.0E-12	-0.033	Intergenic	0.55	-0.16	GCST010555
Hemoglobin A1c	rs9818870	3_138403280_C_T	1.0E-28	0.029	3'UTR	0.22	0.34	GCST90025974
Lung function	rs730158	3_138359356_T_C	1.0E-09	n.d.	Intron	0.55	-0.13	GCST007081
Sex hormone-binding globulin	rs9872754	3_138399143_C_T	5.0E-08	-0.035	Intron	0.90	0.24	GCST90104277
Testosterone	rs6766859	3_138336294_C_T	1.0E-21	0.035	Intergenic	0.55	-0.03	GCST90012113
Noonan syndrome	rs1576359216	3_138372951_G_T	n.d.	n.d.	Missense	n.d.	n.d.	RCV000787303
	rs1576387876	3_138397333_C_T	n.d.	n.d.	Missense	n.d.	n.d.	RCV000787304
	rs1576387885	3_138397342_A_G	n.d.	n.d.	Missense	n.d.	n.d.	RCV000787305

Data is from GWAS Catalog or Open Targets Platform. Variants with high linkage disequilibrium (r2>0.4) associated with the same trait are not shown; except for rs9818870, as it was the first reported *MRAS* risk variant for CAD by (62) and co-workers in 2009. Variant locations/ consequences are from Ensembl (release 110). The RegulomeDB probability score ranges from 0 to 1, with 1 being most likely to be a regulatory variant. *MRAS* eQTL values are from the GTEx Portal and represent the median of normalized effect sizes with $p<10^{-6}$ including several tissues. This table is taken from a review article published by (80).

3.2.4 *MRAS* Pathways

The RAS superfamily, named after the Rat sarcoma virus, includes guanosine triphosphate binding proteins encoded by the prototypic RAS oncogenes – *NRAS*, *KRAS*, and *HRAS* – as well as *MRAS* (107). While *MRAS* shares functional similarities with the classical RAS family members, it also has unique roles, e.g., by acting through specific effectors that dephosphorylate Raf and activate the extracellular signal-regulated kinase (ERK) pathway (Figure 4).

As *MRAS* is present in a variety of cell types and functions as a signal transducer for growth factors (such as nerve growth factors in dendrite development (108) or bone morphogenetic protein-2 (85) and cytokines IL-6 (60) or TNF (109), its signalling is part of several biological processes such as cell differentiation, proliferation, migration, apoptosis and adhesion (Figure 4).

MRAS plays a critical role in RAS/MAPK pathway by forming a ternary network with the leucine rich repeat-containing scaffold protein (SHOC2), and protein phosphatase 1 (PP1). The SHOC2-PP1 complex acts as an effector of *MRAS*. When active *MRAS* binds to the SHOC2-PP1 complex, it stimulates PP1 activity, which further activates RAF proteins by dephosphorylating a conserved inhibitory site. This process ultimately leads to the activation of the ERK pathway (110–112). The significance of the MAPK/ERK pathways in *MRAS* signalling is highlighted by the identification of three missense mutations in *MRAS* (p.Gly23Val, p.Thr68Ile, and p.Gln71Arg) in patients with Noonan syndrome. Noonan syndrome is a developmental disorder within the RASopathies group. This syndrome is characterized by features such as cardiac hypertrophy, which is likely involving effects on SHOC2/PP1 complex activity in RAS/MAPK/ERK pathway activation (113, 114).

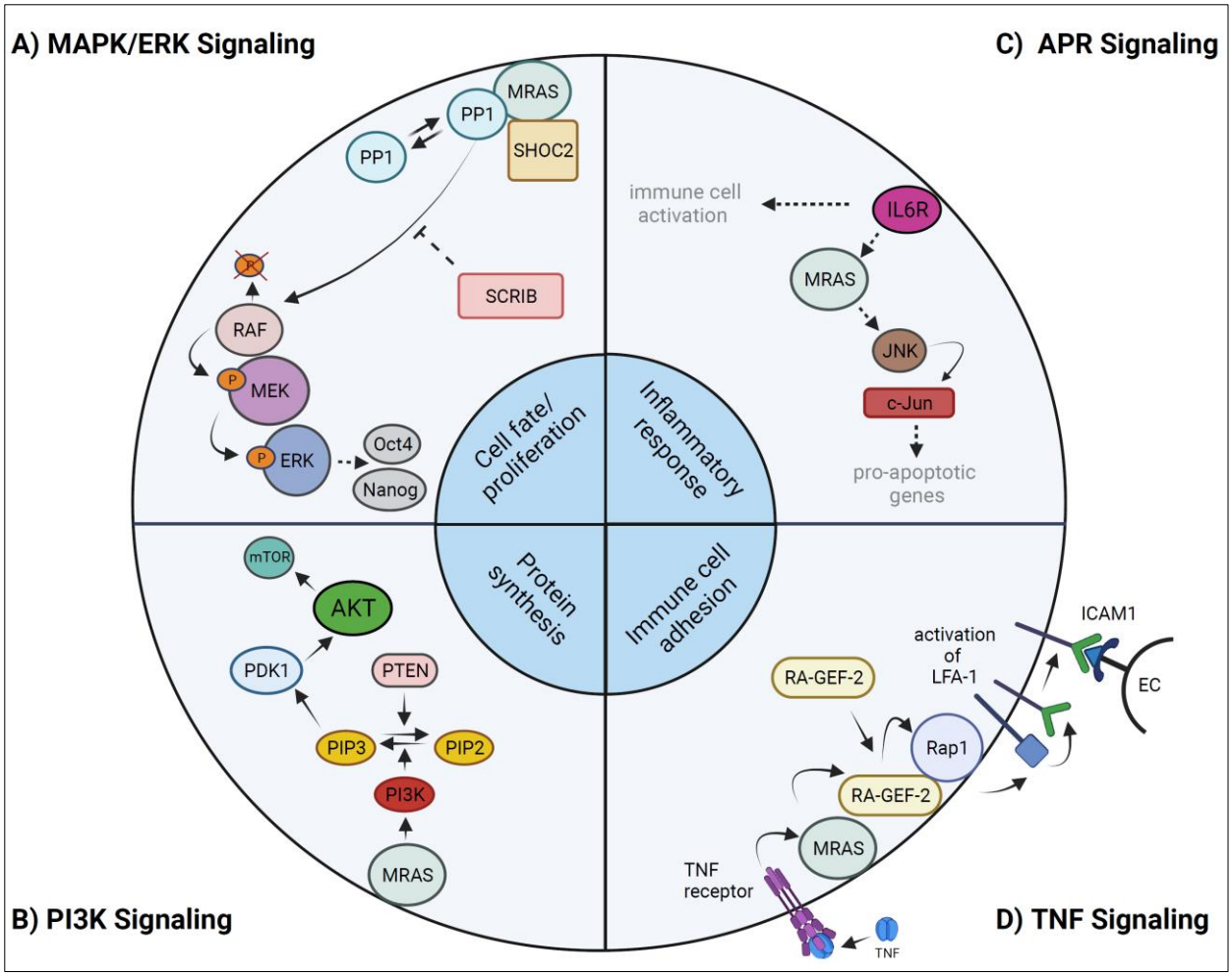

Figure 4 – MRAS signalling pathways

A) MAPK/ERK Signalling: *MRAS* forms the ternary complex with the leucine rich repeat-containing scaffold protein (SHOC2) and protein phosphatase 1 (PP1) that stimulates PP1 activity. The Rat sarcoma virus (RAS) recruits the Rapidly accelerated fibrosarcoma (RAF) to the plasma membrane causing phosphorylation of RAF which further activates the mitogen-activated ERK kinase (MEK) and then the extracellular signal-regulated kinase (ERK) cascade (110–112). **B) PI3K/AKT/mTOR Signalling:** *MRAS* activates the Serine/Threonine Protein Kinase AKT by interacting directly with the phosphatidylinositol-kinase (PI3K) which converts phosphatidylinositol 4,5-bisphosphate (PIP_2) to phosphatidylinositol (3,4,5)-trisphosphate (PIP_3) further stimulating Pyruvate Dehydrogenase Kinase 1 (PDK1) activity (115, 116). This cascade is inhibited by Protein Tyrosine Phosphatase (PTEN). **C) APR Signalling:** Interleukin 6 (IL-6) and tumour necrosis factor (TNF) are inflammatory cytokines involved in the acute phase response signalling pathway and both activate *MRAS* as a signal transducer (60, 109). *MRAS* activates the c-Jun amino terminal kinase (JNK) signalling cascade propagating apoptosis and cell survival (85). **D) TNF Signalling:** *MRAS* is an active player in the TNF adhesion signalling cascade. TNF triggers *MRAS* activation recruiting Rap Guanine Nucleotide Exchange Factor 2 (RA-GEF2) to the plasma membrane and thus activating Ras-related protein 1 (RAP1). The RA-GEF2-actiavted RAP1 causes the activation of lymphocyte function-associated antigen 1 (LFA-1) and enables inflammatory cells to bind to intercellular adhesion molecule-1 (ICAM-1) expressed by endothelial cells (EC) (109). This figure was created with BioRender.com and is taken from (80).

MRAS also directly interacts and activates PI3K, which in turn activates the serine/threonine kinase AKT (Figure 4). Furthermore, AKT activates various proteins, including mTOR. PI3K signalling is crucial for promoting cell survival and inhibiting apoptosis (115–117). *MRAS* increases AKT activity by 5-10-fold in neuronal-like PC12 cells (115). A promising approach for treating atherosclerosis is by targeting the PI3K/AKT/mTOR pathway with rapamycin or rapalogs (e.g. wortmannin or LY294002) (118).

Additionally, *MRAS* also play's a crucial role in the TNF-stimulated adhesion signalling cascade in splenocytes including lymphocytes, dendritic cells, and macrophages (109). *MRAS* mediates the activation of integrin proteins, particularly lymphocyte function-associated antigen 1 (LFA-1). TNF activates *MRAS*, which then recruits Rap guanine nucleotide exchange factor 6 (RapGEF6) to the plasma membrane (Figure 4) and activates Ras-related protein 1 (RAP1). This further leads to the activation of LFA-1. The activated LFA-1 allows inflammatory cells to bind to intracellular adhesion molecule- 1 (ICAM-1) on endothelial cells (109), playing a key role in atherosclerosis progression (119).

MRAS has also been reported to moderately activate the c-Jun amino terminal kinase (JNK) cascade (also known as MAP kinase 8 cascade) (Figure 4) (85), which functions downstream of the IL-6 receptor and facilitates stress-induced cellular responses including apoptosis (115).

It has been identified that *MRAS* can induce epithelial-to-mesenchymal transition (EMT) through the PI3K and ERK pathways (120), highlighting its complex roles in both physiological and pathological conditions.

3.3 Cytokines and their Role in Atherosclerosis

Pro-inflammatory cytokines accelerate atherosclerosis progression and strongly impact the disease development (121). Divergent immune cells are present in the arterial wall and their number elevates with atherosclerosis progression. Immune cells normally migrate into the aortic wall and return to the blood circulation. Cytokines promote the influx and activation of inflammatory cells like macrophages, T-helper, T and B lymphocytes facilitating their retention within the plaque. This leads to the accumulation of these cells in the plaque and the surrounding adventitia (121).

Cytokines consist of more than 100 secreted factors divided into divergent classes: interleukins (ILs), tumor necrosis factors (TNFs), interferons (IFNs), transforming growth factors (TGFs), colony-stimulating factors (CSFs), and different chemokines (122). T-cells, SMCs, monocytes, macrophages, endothelial cells, platelets, and adipocytes produce cytokines in response to inflammation. Cytokine-induced activation of endothelial cells lead to the expression of adhesion molecules and chemokines, which facilitates the migration of immune cells (lymphocytes, monocytes and neutrophils) to the site of atherosclerosis (123). Cytokines also influence SMC behaviour by promoting their proliferation, and migration (124). In the later stages of atherosclerosis, pro-inflammatory cytokines can also contribute to the destabilization of atherosclerotic plaques, thereby accelerating plaque rupture and thrombus formation (Figure 5) (124, 125).

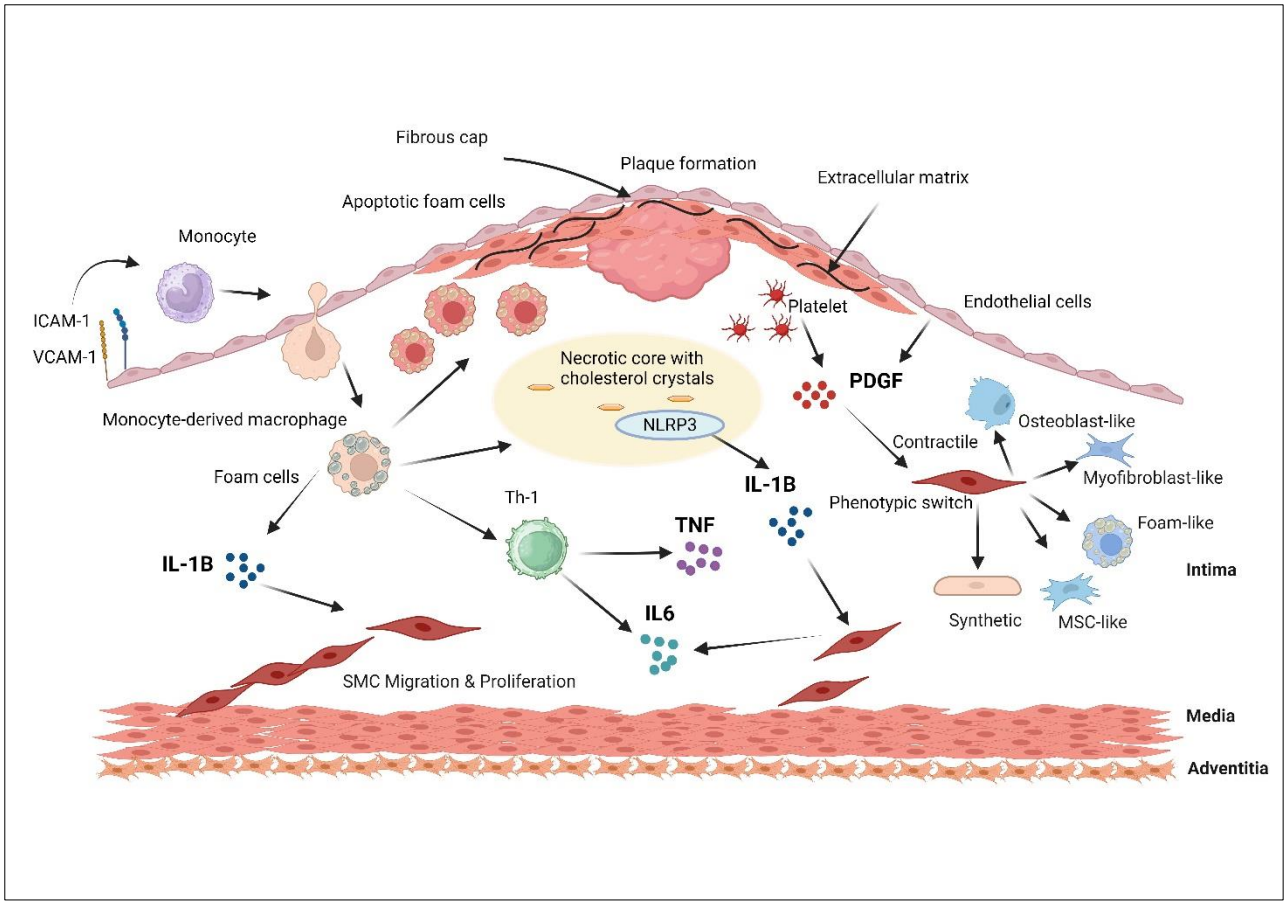

Figure 5 – The role of cytokines during the development of atherosclerosis

Immune cell accumulation increases at the site of plaque formation. Monocytes are recruited from the bloodstream after adhesion molecules (VCAM-1 & ICAM-1) are expressed on the surface of activated endothelial cells (126). The monocytes diffuse into the arterial wall and differentiate into monocyte-derived macrophages. Furthermore, these macrophages uptake lipoproteins through scavenger receptors (127) and form the foam cells that then undergo apoptosis or necrosis contributing to the formation of a lipid-rich necrotic core. Cholesterol crystals form within the foam cells that activate the NLRP3 inflammasome leading to release of IL-1ß. This in turn, stimulates SMCs to produce IL-6, which has an proinflammatory effect (127). Divergent proinflammatory cytokines influence the different stages of plaque development. Activated macrophages separately secrete various cytokines like TNF, IL-1, IL-6. These cytokines promote the recruitment and activation of additional inflammatory cells, leading to their retention in the plaque and further accumulation of immune cells in both the plaque and the surrounding adventitia (128). These cytokines activate Th1 cells, that produce TNF and IL-6, which can also be secreted by natural killer cells. Apart of PDGF being produced by endothelial cells, it is produced and stored in the platelets and when released, it stimulates VSMCs migration and phenotypic transformation from the contractile phenotype to the synthetic one (129). VSMCs proliferate, migrate, and undergo phenotypic transformation from the media to the intima and transdifferentiate into mesenchymal cell like (MSC-like), foam-like, myofibroblast-like, osteoblast-like cells. Over time, a fibrous cap forms over this core due to the migration of the SMCs from the media into the intima and the secretion of extracellular matrix. Continuous foam cell formation and inflammation leads to the growth of the atherosclerotic plaque which may become unstable and thus rupture (126). This figure was created by biorender.com.

3.3.1 TNF

Tumour necrosis factor (TNF) is a type I cytokine predominantly produced by activated macrophages, T-cells and natural killer cells (130). TNF, being a pro-inflammatory cytokine, plays a vital role in the development of atherosclerosis and is involved in cell homeostasis and immune response regulation (131). As the TNF levels increase in the atherosclerotic plaque and the blood, the progression of atherosclerosis elevates (132). Experiments with double knockout of TNF and *ApoE* in mice showed a significant reduction in the plaque size in the aortic sinus of $TNF^{-/-}ApoE^{-/-}$

mice compared to the wild type control *ApoE*$^{-/-}$ group (133). This reduction was attributed to decreased expression of ICAM-1 and VCAM-1 adhesion molecules, as well as monocyte chemotactic protein-1 (MCP-1) (133). Anti TNF therapy decreased the occurrence of CVD events in rheumatoid arthritis patients prone to CVD (134).

3.3.2 IL-6

IL-6 belongs to the superfamily of cytokines that are dimeric molecules signalling dimeric receptor complexes (135). The gp130 receptor chain is involved in the formation of certain receptor complexes within this cytokine superfamily. IL-6, a heterodimer, consists of IL-6R and gp130 (135).

IL-6 is secreted from T and B lymphocytes, macrophages, fibroblasts, and SMCs and its concentrations get higher in stress, infection, trauma and aging (136). Increased levels of IL-6 can be related to a higher risk of heart failure, therefore, IL-6 can be utilized as a biomarker for therapeutically targeting and preventing heart failure with preserved ejection fraction (HFpEF) (137, 138).

The role of IL-6 in atherosclerosis can be either pathogenic or protective depending on the stage of the disease (139). IL-6 can stimulate the expression of IL-1 receptor (IL-1RA) antagonist and release of soluble TNF receptor, both of which significantly reduce IL-1 and TNF activity, respectively (140).

Research studies have demonstrated the pro-inflammatory role of IL-6 in atherosclerosis by incorporating recombinant IL-6 in *ApoE*$^{-/-}$ mice that resulted in a two-fold increase in the area of atherosclerotic lesions (141). Similarly, accelerated plaque formation with decreased collagen content, reduced accumulation of inflammatory cells within the lesions and reduced IL-10 production was associated with *ApoE*$^{-/-}$ *IL-6*$^{-/-}$ double knock down mice (142). Another research study depicted that IL-6 signals through its soluble form (sIL-6R) beside its classical cell surface IL-6 receptor. The IL-6/sIL-6R complex binds directly to the gp130, which is present on nearly all cells in the body, and thus activates a pro-inflammatory response called trans-signalling (143). Conversely, the tissue regeneration and anti-inflammatory effects of IL-6 are regulated by the classical IL-6R signalling pathway. In another research study, it was shown that soluble gp130 (sgp130) inhibited the IL-6/sIL-6R complex but did not affect the classical IL-6R-dependent signalling pathway (144).

3.3.3 IL-1ß

Interleukin 1 (IL-1) family includes IL-1α and IL-1ß pro-inflammatory cytokines that are produced by myeloid cells (145). Atherosclerotic aortas consist of elevated levels of secretion and expression of IL-1 family cytokines and their receptors respectively (146). IL-1ß plays a crucial role in Th17

cell differentiation that can intensify inflammation in the vascular wall (147). Proatherogenic properties of both IL-1α and IL-1ß, contributing to the upregulation of adhesion molecules expression in endothelial cells and activation of macrophages was validated in mouse model experiments (146, 148). IL-1ß is highly secreted by activated macrophages that have a destructive effect on myocardial remodelling (149). High serum levels of IL-1ß are linked to increased risk of mortality and recurrent major adverse cardiovascular events in acute heart failure and myocardial infarction patients (150). Inhibiting IL-1ß by Canakinumab can reduce the risk of recurrent cardiovascular events by inducing an anti-inflammatory effect (151). Treatment with recombinant IL-1RA (or Anakinra), a scavenger receptor of IL-1ß, also reduces inflammation in atherosclerosis (152), while deficiency of IL-1RA intensifies the disease.

The IL-1 receptor possesses endogenous anti-inflammatory effects as it inhibits IL-1 signalling. In atherosclerosis, IL-1ß production is driven by NLRP3 inflammasome activation, triggered by cholesterol crystal accumulation in macrophages, which destroys lysosomes (153). The CD36/ TLR-6/ TLR-4 receptor complex is essential for binding modified lipoproteins, activating NLRP3, and producing IL-1ß. Knockout of any component in this complex reduces IL-1ß production and atherosclerotic plaque (146, 154, 155). Fatty acids also stimulate IL-1α production through an NLRP3- independent pathway (154).

Administering recombinant IL-1RA or overexpressing it in *ApoE*$^{-/-}$ mice significantly reduced plaque build-up (156). Contrastingly, *IL-1-RA knockout C57BL/6J* mice on a high-fat diet showed increased foam cell accumulation in the aortic wall, accelerating disease progression (156, 157).

3.3.4 PDGF-BB

The platelet-derived growth factor (PDGF) family consists of 5 members including PDGF-AA, PDGF-BB, PDGFAB, PDGF-CC and PDGF-DD (158). Amongst all of them, PDGF-BB is found to be a potential stimulant of switching phenotypical SMCs from a contractile to a synthetic one (159, 160). PDGF is produced in smooth muscle cells and endothelium and is stored in higher concentrations in the platelets (158, 159).

PDGF plays a crucial role in morphogenesis, tumorigenesis and development of CVD (159). In VSMCs, PDGF-BB was reported to enhance cell migration in a dose-dependent manner by regulating epithelial-mesenchymal transition (161). PDGF is also involved in regulating blood vessel formation/ stability by influencing VSMC proliferation and migration (161) as well as facilitating pericyte vessel coverage (162).

3.4 Vascular Smooth Muscle Cells – as Cell Model for Atherosclerosis

Vascular Smooth muscle cells, one of the key cell types in the etiology of atherosclerosis and plaque stabilization were the prime focus of this study as according to the GTEx, several *MRAS* risk variants for CAD increase *MRAS* mRNA levels primarily in the arterial and cardiac tissue, showing the strongest effect in the aorta (106) (Figure 2). Moreover, an intronic CAD susceptibility locus, in *MRAS*, rs13324341, resulted in alteration of a myocyte enhancer factor 2 (MEF2) binding site specifically in SMCs (106). An altered MEF2 binding site is linked to SMC growth responses during atherosclerosis (106).

Generally, the VSMCs provide structural support to vascular blood vessels and enable contraction, blood pressure regulation, and control of vessel diameter and blood flow (163–167). VSMCs and pericytes excrete extra-cellular matrix like collagen and elastin (166), which influence the mechanical properties of mature vessels. Primary VSMCs display divergent phenotypes and have the ability to switch between phenotypes but do not differentiate conclusively. Many research studies admit the fact that the phenotypic plasticity of VSMCs may contribute to the development of vascular disorders (165, 166, 168).

VSMCs in the tunica media have a contractile phenotype essential for regulating vascular tone (168). These cells possess a fully functional contractile apparatus and respond to small molecules like acetylcholine and norepinephrine (167). This contractile phenotype is characterized by tightly bundled myofilaments, minimal rough endoplasmic reticulum (ER), a reduced golgi apparatus, fewer free ribosomes, and reduced connective tissue (165, 167). Contractile VSMCs proliferate slowly and express distinct contractile proteins, ion channels, and signalling molecules (166). Contractile VSMCs exhibit a spindle-shaped morphology and express typical contractile marker proteins such as SMαA, smooth muscle myosin heavy chains (MYH11) SM-1 and SM-2, SMC lineage-restricted protein 22-kDa (SM22α/tagln), ACTA2 and smoothelin (SMTN) in the normal arterial media (17, 165, 167).

In inflammatory milieus, VSMCs partly lose the contractile capacity, increasing their ability to proliferate, migrate and secrete ECM protein and cytokines (169). Synthetic VSMCs exhibit a fibroblast-like shape, express fewer contractile proteins and secrete large amounts of extra-cellular matrix. They feature an extensive rough ER, a well-defined Golgi apparatus and numerous free ribosomes. Their broad morphology causes overlapping, creating a "hill and valley" pattern and promoting higher proliferation rates (17, 165, 167). Caldesmon 1 (CALD1), tropomyosin 4 (TPM4), myosin heavy chain 10 (MYH10), retinol binding protein 1 (RBP1) and vimentin (VIM) are proteins specifically expressed by synthetic VSMCs (167).

VSMCs can switch between contractile and synthetic phenotypes, often adopting a hybrid state with traits of both. The synthetic phenotype is mediated by factors like platelet derived growth factor (PDGF), basic fibroblast growth factors (bFGF), insulin-like growth factors (IGFs), epidermal growth factor (EGF), α-thrombin, factor Xa, angotensin-II (ANG-II), enothelin-1, and unsaturated lysophosphatidic acid (167), while the contractile phenotype is promoted by heparin, TGFß, ANG-II and IGF1 as well (167, 170). This phenotypic switch involves reduced expression of VSMC-selective differentiation markers, increased migration and proliferation and ECM synthesis for vascular repair (166).

We hypothesize that *MRAS* is an important regulatory element of SMC phenotype switching. Therefore, we investigate the influence of *MRAS* on SMC behaviour such as migration, proliferation, and apoptosis in human and murine SMCs (Figure 6).

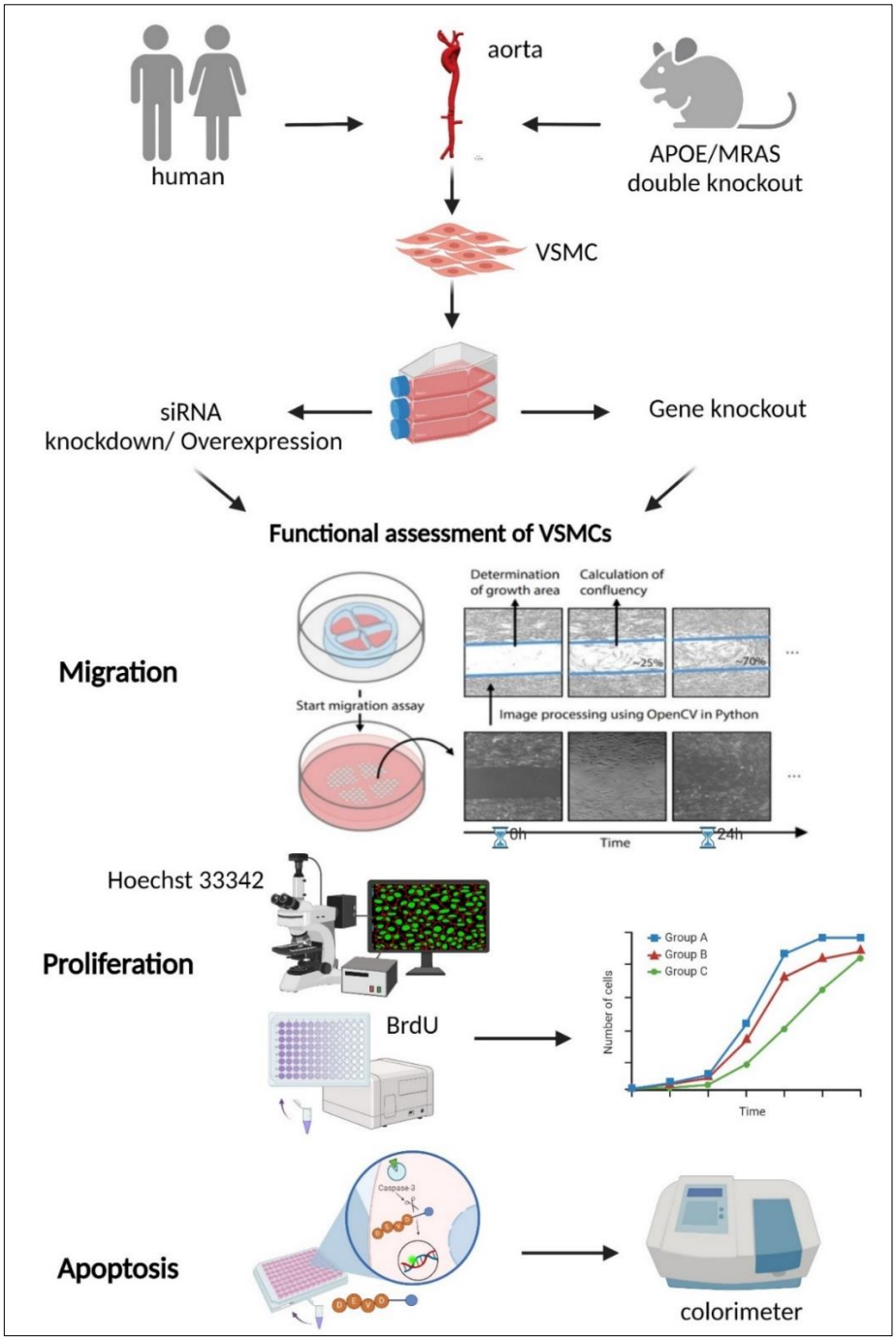

Figure 6 – Functional assessment of VSMCs

A graphical representation of all the experiments conducted in this research is depicted. The figure was made by biorender.com.

3.5 Aims of this Thesis

Several GWASs have linked genomic regions of *MRAS* to CAD/MI, but still the exact underlying patho-mechanism and functional link to CAD is still unclear. This doctoral thesis addressed the role of *MRAS* in atherosclerosis and relevant risk factors. The impact of *MRAS* on atherosclerosis-relevant

phenotypes specifically in SMCs was the main study of this research. The following aims were defined to the present thesis:

1. To investigate the role of the *MRAS* gene in atherosclerosis using human aortic SMCs through RNA interference.
2. To validate the findings of *MRAS* siRNA knockdown experiments in overexpression experiments of the *MRAS* gene in human aortic SMCs.
3. To confirm these findings in mouse aortic SMCs isolated from a double knockout *Mras*$^{-/-}$ *ApoE*$^{-/-}$ mouse model.
4. To perform transcriptomic analysis of murine *Mras*$^{-/-}$*ApoE*$^{-/-}$ SMCs using RNA sequencing.
5. To determine the plaque characteristics in the double knockout *Mras*$^{-/-}$*ApoE*$^{-/-}$ mouse model.

4. Material and Methods

4.1 Vascular Aortic Smooth Muscle Cells

4.1.1 Isolation of Human SMCs (HSMCs)

Human aortic smooth muscle cells (HSMCs), isolated from three donors, were purchased from three different companies (Table 2).

Table 2 – HSMC donor information

Cell line Type	Name	Donor	Age (years)	Gender	Order No.
Human Aortic Smooth Muscle Cells (HSMCs)	HSMC IV	Thermo Fisher Scientific	27	m	#C-007-5C
	HSMC VI	Cell Applications	26	m	#354-05a
	HSMC VIII	Promocell	38	f	#C-12533

4.1.2 Isolation of Murine Smooth Muscle Cells

Material

Table 3 – Material, buffers, and devices for isolation of murine SMCs (MSMCs)

Category	Name	Manufacturer/Composition
Material	Reaction tubes (1.5, 15 and 50 ml)	Sarstedt
	Biosphere Filter Tips (10, 100 and 1000 µl)	Sarstedt
	Serological Pipettes (2, 5, 10 and 25 ml)	Sarstedt
	Cell culture dish (60 mm)	Grenier Bio-one (#628160)
	6- well plate (Nunclon™ Delta Surface Multidish)	Thermo Scientific (#140675)
	Culture flask 25 cm^2 – TC Flask T75	Sarstedt (#83.3911.002)
	Culture flask 75 cm^2 – TC Flask T175	Sarstedt (#83.3912.302)
	Cell strainer 40 µm Nylon	BD Falcon (#352340)
	Cell scraper 25 cm	Sarstedt (#83.1830)
	Vial-Cassette™	Chemometec (#941-0012)
Buffers	Cell culture medium (for murine cells)- Dulbecco's modified eagle medium	DMEM 1x+GlutaMax™-I Gibco (#31966-021), supplemented with 10% FBS and 1% P/S

	FBS	Superiorstabil® Bio&Sell (#FBS.S 0615)
	P/S 10,000 U/ml	Penicillin/Streptomycin Biochrome (#A2213)
	Collagenase Type II (10 mg/ml)	Cell systems (#LS004176), in culture medium, sterile filtered
	PBS	Capricorn Scientific Dulbeco's PBS w/o Ca & Mg, w/o Phenol Red (#PBS1A9)
	Trypsin- EDTA	Capricorn Scientific (#TRY-1B10); for trypsinization → dilute 1:10 in PBS
	Trypsin neutralizer solution 1x	Cascade Biologics™ Gibco (#R-002-100)
	StemPro™ Accutase™ Cell Dissociation Reagent	Accutase/Biotase Bio and Sell (#BS.L 2193) with 0.5mM EDTA; sterile filtered
	Gelatine (0.1%)	Pork skin (#G1890, Sigma) in PBS, sterile autoclaved
Devices	Centrifuge 5702R	Eppendorf
	Thermomixer 5436	Eppendorf
	CO_2-Incubator Hera cell	Heraeus
	Laminar Flow Clean Bench	CleanAir
	NucleoCounter® System NC-200™	Chemometec

Method – Protocol

All animal experiments were performed in accordance with the German animal studies committee of Schleswig- Holstein. Murine aortic smooth muscle cells (MSMCs) were isolated from the thoracic aortas of WT (*B6.ApoE*$^{-/-}$) and dKO (*Mras*$^{-/-}$*ApoE*$^{-/-}$) in both genders (male and females). The aorta was cut off the diaphragm and washed in PBS, and put into a cell culture dish with culture Medium. The adventitia was removed and the aorta was pre-digested with collagenase II at 37°C for 6h in a thermo-shaker. After the complete tissue dissociation and digestion, the tubes were centrifuged for 10 min at 10000 rpm and the supernatant discarded. The pellet (isolated cells) was resuspended in gelatine-coated 6-well plates in a culture medium (DMEM supplemented with 10% Fetal Bovine Serum (FBS) and 1% PenStrep (penicillin/streptomycin)) and kept in the incubator for 3 to 5 days until the first medium change. Primary aortic SMCs were first passaged when the cells in the 6-well plate were 100% confluent. Medium was removed and cells were washed with PBS. After removing

PBS, 0.5 ml of Trypsin-EDTA or StemPro™ Accutase™ Cell Dissociation Reagent were added per well in the 6-well plate and left for incubation for 20 to 30s until the cells have detached. Cell scraper was used when the cells were very dense and would not detach easily. After neutralization with Trypsin neutralizer, a centrifugation step is performed for 10 min at 3000 rpm and the supernatant was discarded and cells from the pellet were resuspended in a fresh gelatine coated culture flask (25 cm^2/ 75 cm^2) with the culture medium.

The experiments of all murine SMCs were performed with cultures between passages P4 and P14. To ensure that only single cells were used for the experiments, the cell solution after trypsinization and centrifugation was filtered through a 40 µm pore size cell filter to remove big chunks of cells.

4.2. Cell Culture Experiments

4.2.1 siRNA Knockdown – RNA Interference (RNAi)

Material

Table 4 – Material, buffers, and devices for siRNA knockdown in SMCs

Category	Name	Manufacturer/Composition
Material	Reaction tubes (0.5, 1.5, and 2.0 ml)	Sarstedt
	Biosphere Filter Tips (10, 100 and 1000 µl)	Sarstedt
	Serological Pipettes (2, 5, 10 and 25 ml)	Sarstedt
	6- well plate (Nunclon™ Delta Surface Multidish)	Thermo Scientific (#140675)
	Vial-Cassette™	Chemometec (#941-0012)
	GenMute™ Transfection Kit	SignaGen® Labs (#SL100568-SMC)
Buffers	Cell culture medium (for human cells)- Human vascular SMC basal medium	M231 Gibco (#M-231-500), supplemented with SMGS (Smooth Muscle Growth Supplement) Cascade Biologics™ Gibco 20x (#S-007-25)
	DNase/RNase free water	Invitrogen UltraPure™ Life Technologies Limited, Distilled water DNase/RNase free (#10977-035)
	siRNA hs.Ri.MRAS.13.1, 13.2, 13.3	IDT (#234428468, #236042620, #235059915), 10 nM lyophilized and dissolved in 1 ml DNase/RNase free water
Devices	CO_2-Incubator Hera cell	Heraeus

	Laminar Flow Clean Bench	CleanAir
	NucleoCounter® System NC-200™	Chemometec

Method – Protocol

Human aortic SMCs were seeded in cell culture plates (6-well plates) in culture medium (M231 supplemented with SMGS) and let grown for 24h prior to transfection for the cell density to reach an optimal confluency of 70% or more at the time of transfection. Optimization of transfection with siRNA was needed with different concentrations of siRNA (10 nM-40 nM). The GenMute™ siRNA Transfection Kit for primary human SMCs was used for siRNA knockdown in HSMCs. Three different siRNA for *MRAS* silencing were used for these experiments **(Table 5).**

Table 5 – Detailed information about different siRNA used for knockdown

Name	Duplex Sequences	Manufacturer
hs.Ri.MRAS.13.1	5‘-CGGGUUUACUUGGAAUGAAAGAUAC-3‘ 3’-CAGCCCAAAUGAACCUUACUUUCUAUG-5‘	IDT (#234428468)
hs.Ri.MRAS.13.2	5’-CAAUAUUCCGUACAUAGAAACCAGU-3‘ 3‘-GUGUUAUAAGGCAUGUAUCUUUGGUCA-5‘	IDT (#236042620)
hs.Ri.MRAS.13.3	5’-AGGUCGAUUUGAUGCACUUGAGGAA-3’ 3’-GUUCCAGCUAAACUACGUGAACUCCUU-5’	IDT (#235059915)

Evenly distributed and healthy cells were transfected with siRNA by preparation of the transfection mix (Table 6). The transfer buffer needed for transfection has to be diluted 1:5 from the stock solution with RNase-free water before adding to the mix i.e., (1 ml Transfer buffer 1x = 200 µl 5x Transfer buffer + 800 µl RNase-free water).

Table 6 – Transfection mix for 6-well plate

Reagents (Mix) for 6-well plate (9.6cm^2/well)	
Number of cells	3x10^5 cells
Transfer buffer 1x	231.56 µl
GenMute™ SMC	5.44 µl
siRNA (20nM)	3 µl
Medium Volume	1260 µl
Master mix volume per well	1500 µl

The mix was incubated at room temperature for 20 min for the complex to build. The transfection mix was added to each well in the 6-well plate and the plate was shaken with circular movements to ensure even distribution of the mix over the cells. The cells were left for incubation at 37°C for 24-72 hours (varying for each siRNA). siRNA knockdown was the most efficient with hs.Ri. MRAS.13.2 being 80%.

4.2.2 Overexpression - Plasmid

Material

Table 7 – Material, buffers, and devices for isolation of plasmid

Category	Name	Manufacturer/Composition
Material	Reaction tubes (0.2, 0.5, 1.5, 2.0, 15 and 50 ml)	Sarstedt
	Biosphere Filter Tips (10, 100 and 1000 µl)	Sarstedt
	Serological Pipettes (2, 5, 10 and 25 ml)	Sarstedt
	Inoculation loop (1 µl)	Sarstedt (#86.1567.010)
	Inoculation spreader	Sarstedt (#86.1569.001)
	Chemically competent E. coli DH5α™	NEB (#C29871)
	High Efficiency Transformation Kit	New England Biolabs (NEB) (#C29871)
	QIAfilter Plasmid Maxi Kit	EndoFree® Plasmid Maxi Kit - Qiagen (#12362)
Buffers	LB broth powder (Lennox)	Sigma (#L3022-250G)
	LB Agar (Lennox) MRAS Human Tagged ORF Clone Plasmid	Sigma (#L2897-250G) Origene (#RC212259)
	Antibiotics	Kanamycin 100 mg/ml
	SOC outgrowth medium	Thermo Fischer (#15544034)
Devices	Thermomixer 5436	Eppendorf
	Compact shaker KS 15 control	Edmund Bühler GmbH
	Centrifuge Rotanta 460R	Hettich
	Nanophotometer N60 Touch	Implen GmbH (#T62326)

Method – Protocol

LB-broth liquid media was prepared in a Corning® Erlenmeyer baffled cell culture flask by mixing 3 g LB broth powder (L3022-250G) in 150 ml of distilled water. LB broth with agar (Lennox) was also prepared by dissolving 3.5 g agar in 100 ml of distilled water. 25 µg/ ml Kanamycin was added to the LB-broth and agar broth.

MRAS Human Tagged ORF Clone Plasmid (pellet form) pCMV6-Entry was dissolved in 100 µl making it 100 ng/µl. A further dilution of 1:500 was made from the stock plasmid solution and 5 µl of diluted plasmid was added to 100 µl of bacterial cells. Bacterial cells used were NEB 5-alpha Competent E. coli (high-efficiency). The transformation of cells was done according to the High Efficiency Transformation Protocol. 100 µl of the bacterial mix was spread onto an LB-agar plate containing Kanamycin 25 µg/ml and incubated overnight at 37°C.

After overnight incubation, two individual clones of bacteria were picked up using a small pipette tip and gently moved to Eppendorf tubes with SOC outgrowth medium. Both the tubes were left on a shaker for 1h for formation of more colonies in the tubes. The content from the tubes was transferred into 5 ml liquid LB-medium containing 25 µg/ml Kanamycin and incubated overnight in a shaking incubator at 37°C and 220 rpm. On the next day, tubes were centrifuged for 10 min at 4500 rpm to pellet the bacteria. The supernatant was discarded and the pellets were kept.

The plasmids were isolated using the QIAfilter Plasmid Maxi Kit according to the manufacturer's instructions and eluted in 150 µl of elution buffer. Concentrations of both the clones from the plasmid were measured using the Nanodrop Quantification machine and the plasmids were stored at -20°C.

Sequencing was performed to ensure the clones containing the correct inserts. Samples were prepared and sent to Seqlab- Sequence Laboratories Göttingen (GmbH), Göttingen, Germany. Two primers were used i.e., XL39 and VP1.5. Both the clones were sent with both the primers. 700 to 1000 ng of purified plasmid DNA were filled up to 12 µl of distilled water, 3 µl of 10 µM primer solution were added, reaching a final volume of 15 µl, and four samples were thus sent for sequencing.

4.2.3 Amaxa Nucleofection – Electroporation

Material

Table 8 – Material, buffers, and devices for overexpression in SMCs

Category	Name	Manufacturer/Composition
Material	Reaction tubes (0.2, 0.5, 1.5, 2.0 and 50 ml)	Sarstedt
	Biosphere Filter Tips (10, 100 and 1000 µl)	Sarstedt
	Serological Pipettes (2, 5, 10 and 25 ml)	Sarstedt

	Culture flask 25 cm^2 – TC Flask T75	Sarstedt (#83.3911.002)
	Culture flask 75 cm^2 – TC Flask T175	Sarstedt (#83.3912.302)
	Amaxa™ Nucleofector™ Kit	Lonza (#VPI-1004)
Buffers	Cell culture medium (for human cells)- Human vascular smooth muscle cell basal medium	M231 Gibco (#M-231-500), supplemented with SMGS (Smooth Muscle Growth Supplement) Cascade Biologics™ Gibco 20x (#S-007-25)
	F-12 Ham DMEM culture medium DMEM/ F12 (1:1) 1x	Dulbecco's modified eagle medium nutrient mixture; DMEM/F-12 Ham (+ L-Glutamine & 15 mM Hepes) Gibco (#11330-032)
	Geneticin® G418 (50 mg/ml)	Active Geneticin® Gibco (#10131-035)
Devices	CO_2-Incubator Hera cell	Heraeus
	Laminar Flow Clean Bench	CleanAir
	NucleoCounter® System NC-200™	Chemometec
	Centrifuge 5702R	Eppendorf
	Centrifuge 5415R	Eppendorf
	Amaxa Nucleofector® device	Amaxa Biosystems
	Keyence Microscope BZ-X 810	Life Sciences

Method – Protocol

Human aortic SMCs (Passage 4) were seeded in a 75 cm^2 flask and incubated in a CO_2-incubator at 37°C for 48 h. Prior to the nucleofection, the medium was changed. Each nucleofection reaction was performed in duplicates. When the cell concentration and confluency reached $1x10^6$ cells and 90% respectively, the cells were detached from the flask with Trypsin-EDTA and counted. Then, $2x10^6$ cells/ml were put in 2 ml reaction tubes. The tubes were centrifuged at 4000 rpm for 12 min at room temperature and the supernatant discarded. The pellet was dissolved in 100 µl of Nucleofector™ Solution and 1-5 µg of each plasmid (pCMV6-GFP, pCMV6-empty, pCMV6-MRAS (clone 1 or 2)) respectively. The supplement for the Nucleofector™ solution was added before using the kit in 4.5:1 ratio. The cell suspension was transferred into a certified cuvette (inclusive of the Nucleofector kit) and the cap on the cuvette closed. The A-033 and U-025 programs in the Nucleofector™ Programs were the most efficient of all. The A-033 was selected and the cuvette with the cell suspension was inserted in the Nucleofector™ Cuvette Holder within the nucleofection machine. Once the program was finished, the electroporated cell suspension was transferred with a sterile plastic pipette (also

supplied in the kit) into 50 ml falcon tubes containing pre-warmed F-12 Ham DMEM culture media (500 µl). After 15 min of incubation of the falcon tube in the water bath, the contents of the tube were transferred to a 25 cm^2 culture flask with pre-warmed culture media. The flask was gently rocked to allow even distribution, and the cells were incubated for 3-4 days for complete transfer of the plasmids into the cells. The medium was changed 6h post nucleofection. pCMV6-GFP was used as a control for detection of transfected plasmid with the Keyence microscope throughout the days. When the nucleofection was not efficient at times, a selection marker (Geneticin G418 in 0.2-0.8 mg/ml) was added for the survival of only those cells that contained the plasmid. Transfection of the plasmid was higher with the addition of geneticin to the culture media. The nucleofection was stable for 7-10 days only.

All the functional assays (proliferation, migration and apoptosis) were performed with the overexpressed cells to compare the siRNA knockdown of *MRAS* to the overexpression of *MRAS*.

4.2.4 Stimuli – PDGF-BB, TNF, IL-6 & IL-1ß

For all the experiments (human and murine SMCs), different stimuli were used in different concentrations. The following (Table 9) depicts the variable conditions for each stimulus.

Table 9 – Detailed information about different stimuli used

Reagent	Species	Stock conc.	Volume	Working conc.	Manufacturer
PDGF	Recombinant PDGF	100 µg/ml	1 ml PBS+0.1% BSA	10 ng/ml 30 ng/ml	Peprotech (#100-14B)
TNF	Recombinant Human TNF-α	50 µg/ml	1 ml PBS+0.1% BSA	10 ng/ml	Peprotech (#300-01A)
	Recombinant Murine TNF-α	20 µg/ml	1 ml PBS+0.1% BSA	10 ng/ml	Peprotech (#315-01A)
IL-6	Recombinant Human IL-6	5 µg/ml	1 ml PBS+0.1% BSA	5 ng/ml 10 ng/ml	Peprotech (#200-06)
	Recombinant Murine IL-6	2 µg/ml	1 ml PBS+0.1% BSA	5 ng/ml 10 ng/ml	Peprotech (#216-16)
IL-1ß	Recombinant Human IL-1ß	2 µg/ml	1 ml PBS+0.1% BSA	5 ng/ml 10 ng/ml	Peprotech (#200-01B)
	Recombinant Murine IL-1ß	2 µg/ml	1 ml PBS+0.1% BSA	5 ng/ml 10 ng/ml	Peprotech (#211-11B)

4.3 Gene/ Protein expression Analysis

4.3.1 RNA Isolation

Material

Table 10 – Material, buffers, and devices for RNA isolation

Category	Name	Manufacturer/Composition
Material	Reaction tubes (0.2, 0.5, 1.5, 2.0 and 50 ml)	Sarstedt
	Biosphere Filter Tips (10, 100 and 1000 µl)	Sarstedt
	innuPREP RNA Mini Kit 2.0	Innuscreen GmbH (#845-KS-2040250)
Buffers	DNase/RNase free water	Invitrogen UltraPure™ Life Technologies Limited, Distilled water DNase/RNase free (#10977-035)
	Lysis buffer (Guandinium Thiocyanate)	Innuscreen GmbH (#31-00536)
	Ethanol abs.	J.T. Baker (64-17-5)
Devices	Centrifuge 5415R	Eppendorf
	Nanophotometer N60 Touch	Implen GmbH (#T62326)

Method – Protocol

RNA isolation was performed with the innuPREP RNA Mini Kit 2.0 Standard protocol for eukaryotic cells. Two washing solutions from the kit needed preparatory steps: 70 ml ethanol was added to HS washing solution and 160 ml ethanol was added to the LS washing solution. All steps were performed at room temperature.

1.5 ml reaction tubes with transfected cells suspended in the lysis buffer (400 µl) were incubated at room temperature for 3 min. The contents of the tubes were transferred to a column (Filter D) that selectively eliminates genomic DNA. The Filter D was placed in a collector tube and the tube was centrifuged at 11,000 rpm for 2 min. The column was discarded and 70% ethanol (equal volume as the lysis buffer i.e., 400 µl) was added to the filtrate/flow-through. The filtrate was transferred to another column (Filter R) which is responsible for the selective binding of RNA. The Filter R with a collector tube was processed to centrifugation for 2 min at 11,000 rpm again. The flow-through was discarded and bound RNA was washed with two washing steps i.e., 500 µl of Washing Solution HS, followed by centrifugation for 1 min/11,000 rpm and 700 µl Washing Solution LS, followed by centrifugation for 1 min/11,000 rpm. Flow-through was discarded and excessive ethanol was dried by performing an empty spin for 3 min at 11,000 rpm. Finally, the filter R was then placed on new

collector tubes where RNA was eluted with 30 µl RNase-free water by spinning for 1 min at 13,000 rpm. Eluted RNA was transferred into smaller tubes (0.2 ml) for storage, aliquots were taken for measuring the concentration, and samples were immediately frozen at -80°C.

Concentration and purity of RNA- samples were determined using the Nanodrop photometer. 2 µl of samples were measured at wavelength of 260 nm. Furthermore, samples were measured at 280 nm (absorbance of protein), and the purity of the RNA samples was assessed by the ration of $Absorbance_{260}/Absorbance_{280}$ (2.0 for pure RNA).

4.3.2 cDNA Synthesis

Material

Table 11 – Material, buffers, and devices for cDNA synthesis

Category	Name	Manufacturer/Composition
Material	Reaction tubes (0.2, 0.5, 1.5, 2.0 and 50 ml)	Sarstedt
	Biosphere Filter Tips (10, 100 and 1000 µl)	Sarstedt
	M-MLV Reverse Transcriptase Kit	Thermo Fisher (#28025021)
Buffers	DNase/RNase free water	Invitrogen UltraPure™ Life Technologies Limited, Distilled water DNase/RNase free (#10977-035)
	5X First Strand Buffer	Invitrogen (#28025021)
	Dithiothreitol (DTT) 100 mM	Invitrogen (#28025021)
	2'-deoxyribonucleoside-5'-triphosphates (dNTPs) 4 mM	Promega (#U1330)
	Hexanucleotide Random- Primer Mix	Carl Roth (#HP28.1)
	RiboLock RNase Inhibitor 40 U/µl	Thermo Scientific (#EO0381)
	M-MLV RT 200 U/µl	Invitrogen (#28025021)
Devices	PCR cycler	SensoQuest Labcycler

Method – Protocol

RNA was reverse transcribed into cDNA with the M-MLV Reverse Transcriptase Kit for eukaryotic cells. 1-5 µg of total RNA per sample, filled up to a volume of 10 µl with DNase/RNase-free water were used. RNA samples were denatured at 68°C for 5 min in the PCR- cycler, then put on ice. A master mix reaction (

Table ***12*)** was prepared on ice with pipetting of the enzymes, M-MLV-RT and Ribolock to the RNA samples at the end, making the total reaction volume to 20 µl. The samples were proceeded further for PCR in the PCR-cycler for 60 min at 37°C, followed by an inactivation step for the enzymes for 5 min at 95°C. The cDNA was stored at -20°C until further use.

Table 12 – Reaction mix for one reaction cDNA synthesis

Reagents (Mix)	**1x**
5x Strand buffer	4 µl
DTT (100mM)	2 µl
dNTPs (4mM)	1 µl
Ribolock (40u/µl)	1 µl
M-MLV RT (200U/µl)	1 µl
Master mix volume per sample	10 µl

4.3.3 Quantitative Polymerase Chain Reaction (qPCR)

Material

Table 13 – Material, buffers, and devices for qPCR

Category	**Name**	**Manufacturer/Composition**
Material	Reaction tubes (0.2, 0.5, 1.5, 2.0 and 50 ml)	Sarstedt
	Biosphere Filter Tips (10, 100 and 1000 µl)	Sarstedt
	384-well PCR plates	Applied Biosystems (#4309849)
Buffers	DNase/RNase free water	Invitrogen UltraPure™ Life Technologies Limited, Distilled water DNase/RNase free (#10977-035)
	PowerUp™ SYBR® Green Master mix	LifeTechnologies (#A25777)
	Primer mix 5 pmol/µl	Eurofins Genomics
Devices	7900HT Fast Real-Time PCR System	Applied Biosystems (#4329001)

Method – Protocol

To examine/measure the expression of *MRAS* on transcript level, cDNA, reverse transcribed from RNA was used. Sample reactions were pipetted in 0.2 ml tubes respectively and placed in the thermocycler 7900HT Fast Real-Time PCR System to carry out the PCR. A master mix with the

following composition as show in (Table 14) was processed and added to a 384-well plate in triplicates.

Table 14 – Reaction mix for one reaction in a qPCR plate

Reagents (Mix)	**1x**
PowerUp™ SYBR® Green Master Mix	3.75 µl
Primer mix (5pmol/µl)	1.125 µl
DNase/RNase-free water	1.125 µl
Master mix volume per sample	6 µl

DNase/RNase-free water was used as a negative control and the housekeeping gene (*GAPDH*) as an internal standard (reference gene). The PCR conditions were as shown in (Table 15).

Table 15 – PCR program conditions

Purpose	**°C**	**(min)**	**Cycles**
Initial denaturation	95	5:00	1x
Denaturation	95	0:15	40x
Annealing and Elongation	60	1:00	1x
Final dissociation	95	10:00	1x
Cooling	4	∞	1x

4.3.3.1 $2^{-\Delta\Delta CT}$ method for Calculation of Relative Gene Expression

Relative gene expression levels were calculated using the $2^{-\Delta\Delta CT}$ method (171). The threshold cycles (Cts) are used to coordinate to the number of cycles required for the fluorescent signal to reach the threshold. Ct values were generated for each sample by the SDS 2.2.2 software and evaluated with the $2^{-\Delta\Delta CT}$ method.

The difference in threshold cycle between the target gene and the internal standard (GAPDH) was calculated, leading to the ΔCt value.

ΔCt = Ct (target gene) – Ct (reference gene)

Then, the difference between the target and reference sample, the ΔΔCT value was calculated:

ΔΔCt = ΔCt (target sample) – ΔCt (reference sample)

The fold change due to the reference or the relative gene expression level is further obtained.

Relative gene expression level = $2^{\wedge-\Delta\Delta Ct}$

Three replicates per plate were taken into consideration and the median/mean of their expression levels was calculated. Three technical replicates were compared and plotted through GraphPad vs. 9.5.1.

4.3.4 Primer Design

Primers for target genes were designed using the open-source tool Primer3Plus and the NCBI database. Primers were designed in such a way that they spanned through the exon-exon junction to lessen the possibility of genomic DNA amplification in qPCR. The primer pairs were checked for sequence specificity in the human reference genome using the Primer BLAST took from NCBI. Primer specificity was also validated through a test qPCR, including the monitoring of the standard and dissociation curve. Primers used, are shown in (Table 16).

Table 16 – Primers for qPCR

Gene	Forward primer	Reverse primer	Product Size (in bp)
h*MRAS*-rt1	GTCACTGACAAGGCCAGCTT	TCCTCAAGTGCATCAAATCG	124
h*MRAS*- rt2	GAAGATCACCAGGGAGCAAG	GAGGTCATGGAAGGCTTTGT	112
m*Mras*-rt1	TGTCTACTCCGTCACCGACA	TGCATCAGATCCACCTTGTT	126
m*Mras*-rt2	TCATTCCCAATGATCCTCGT	GGTCCTTGGCACTGGTCTCT	127
h*GAPDH*	GGATTTGGTCGTATTGGG	GGAAGATGGTGATGGGATT	205
m*Gapdh*	GACCACAGTCCATGCCATCAC	CCGTTCAGCTCTGGGATGAC	169

4.3.5 Protein Isolation and Western Blotting

Material

Table 17 – Material, buffers, and devices for Western Blotting

Category	Name	Manufacturer/Composition
Material	Reaction tubes (0.2, 0.5, 1.5, 2.0 and 50 ml)	Sarstedt
	Biosphere Filter Tips (10, 100 and 1000 µl)	Sarstedt
	Nitrocellulose Protran®Amersham™ Filter paper (0.2 µm)	Carl Roth (#10600001)
Buffers	StemPro™ Accutase™ Cell Dissociation Reagent	Accutase/Biotase Bio and Sell (#BS. L 2193) with 0.5 mM EDTA; sterile filtered

	Lysis buffer (Guandinium Thiocyanate)	Innuscreen GmbH (#31-00536)
	Trypsin- EDTA	Capricorn Scientific (#TRY-1B10); for trypsinization → dilute 1:10 in PBS
	Nonidet P40	USB (#19628)
	cOmplete™ Mini Protease Inhibitor	Sigma Aldrich (#11836153001)
	RIPA buffer	150mM NaCl, 1% Nonidet P40, 1% DOC, 0.1% SDS, 25mM Tris-HCL pH 7.6, 1 tablet cOmplete™ Mini Protease Inhibitor Cocktail per 10ml, 1 tablet PhosSTOP™ per 10ml
	DC Protein Assay	BioRad Labs (#5000112)
	Self-made protein standards	1% stock BSA per 1 ml of RIPA lysis buffer
	DL- Dithiothreitol (DTT)	Sigma Aldrich (#D0632); 500 mM DTT dissolved in water
	TBS	5 ml 10X TBS, 45ml distilled water
	10X Tris-buffered saline (TBS)	24,2 g TRIS, 90 g NaCl, 16 ml HCL 32% pH 7.5
	Tween 20	BioRad Labs (#1706531)
	TBS with Tween 20 (TBS-T)	1x TBS, 0.1 (v/v) Tween-20
	NuPAGE™ 4-12% Bis-Tris Protein Gel (10 well)	Thermo Fisher (#NP0321BOX)
	NuPAGE™ LDS Sample Buffer	Thermo Fisher (#NP0007)
	NuPAGE™ SDS Running Buffer	Thermo Fisher (#NP0002)
	Precision Plus Protein™ Standards All Blue	BioRad Labs (#161-0373)
	NuPAGE™ Transfer Buffer	ThermoFisher (#NP0006-1)
	Western Blotting Kit V RD	Li-cor Biosciences (#926-35010)
	Powdered milk	Carl Roth (#T145.2); 1% (w/v) powder milk dissolved in TBS-T
Devices	XCell SureLock™ Blot Module	Invitrogen (#E19051)
	Tube Rotator	VWR International

	Super Signal West Pico PLUS Chemiluminescent Doc MP Imaging System	BioRad Labs
	Shaker Vibrax-VXR	IKA
	Duomax 1030 Shaker	Heidolph
	Synergy HT Microplate Plate Reader	Biotek

Method – Protocol

Cells were detached from the culture flasks (75 cm^2) by incubation with StemPro™ Accutase™ Cell Dissociation Reagent or 0.05% Trypsin-EDTA in PBS depending on the cell species i.e., mouse cells through accutase and human cells through trypsin. Then the cell suspension was resuspended in 100-500 µl of lysis buffer depending on the number of cells harvested. After addition of cell lysis buffer, the suspension was incubated for 60 min at 4°C on a shaker. The cell lysate was then proceeded to centrifugation at 10,000 rpm for 15 min at 4°C. The supernatant was discarded and the pellet was stored at -80°C for further use. All subsequent procedures were conducted at room temperature.

50/100 µl of RIPA buffer was added to the protein pellets depending on the number of cells in the pellet meaning the bigger the pellet, the more RIPA. 40x strong resuspensions of the pellet in RIPA were carried out and the samples were then stored on ice for a time interval of 25 min. Resuspensions were carried out every 10 min on ice. The samples were then transferred to new tubes.

Protein determination was carried out by measuring the total protein concentration in the samples via a colorimetric protein assay. Eight protein standard series with defined protein concentrations ranging from 0.25 to 8 mg/ml, working Reagent A, Reagent B and Reagent S were prepared. A master mix with Reagent S and A at a ratio of 1:50 was prepared. 3 µl of the respective standards or the protein samples were added to a 96-well plate as duplicates. RIPA buffer served as a negative control. 25 µl of Reagent A was added to each well followed by addition of 200 µl Reagent B. The plate was stored for 20 min at room temperature but in the dark. Protein concentration was measured using the Plate Reader with a concentration ranging between 1 and 2 mg/ml.

Samples with a maximum of 10 µg protein in RIPA+DTT+ Loading Dye (NuPAGE™ LDS Sample Buffer) were prepared with a maximum volume of 10 µl per sample to be loaded onto the gel. The samples were denatured at 95°C for 4 min in the thermocycler and stored at -20°C for the gel electrophoresis experiment on the next day.

Western Blotting was employed to visualize specific proteins within a biological sample, with separation based on molecular weight. The samples were loaded onto a NuPAGE 4-12% Bis-Tris-polyacrylamide gel. A molecular weight standard, Precision Plus Protein, was also applied to the sample gel. Protein separation was conducted at 100 V for 10 min followed by 130V for 70-80 min.

The proteins were subsequently transferred to a 0.2 µm nitrocellulose or PVDF membrane using 32 V for 70 min within an XCell SureLock Blot Module. The membrane was blocked with 4 ml of 1% (w/v) milk-TBS-T (0.5 g milk powder and 50 ml TBS) for 1 h while gently agitating on a rotator. The membrane was subjected to overnight incubation at 4°C with the primary antibody, which was diluted (1:1000 of antibody in 4 ml of milk = 4 µl) in 1% (w/v) milk-TBS-T while gently rotating. The next day, the membrane was washed 3 times with 1x TBS-T for 5 min each. Subsequently, a horseradish peroxidase-conjugated secondary antibody in 1% (w/v) milk-TBS-T was applied to the membrane. This was followed by a 60 min incubation while rotating, and three subsequent washing steps with TBS-T. Protein visualization was achieved using the Super Signal West Pico PLUS Chemiluminescent Doc MP Imaging System. Detected protein bands were quantified using the Image Lab Software (BioRad). ß- Actin and GAPDH served as internal standards for target protein quantification.

Table 18 – List of antibodies and their description

Antibody	Host species	Clonality	Protein Size	Dilution	Manufacturer
MRAS	rabbit	monoclonal	24 kDa	1:1000	ab176570, abcam
hGAPDH	rabbit	polyclonal	37 kDa	1:1000	ab9458, abcam
ß-Actin	mouse	monoclonal	43 kDa	1:1000	sc- 47778, Santa Cruz

4.4 RNA Sequencing

Material

Table 19 – Material, buffers, and devices for RNA sequencing

Category	Name	Manufacturer/Composition
Material	Reaction tubes (1.5, 2.0 and 50 ml)	Sarstedt
	Biosphere Filter Tips (10, 100 and 1000 µl)	Sarstedt
	Culture flask 75 cm^2 – TC Flask T175	Sarstedt (#83.3912.302)
	RNeasy® Mini Kit	Qiagen (#74136)
	Agilent RNA 6000 Pico Kit	Agilent Technologies (#5067-1513 #Q32856)
	Illumina stranded mRNA Prep Kit	Illumina®
	Agilent DNA 1000 Kit	Agilent Technologies (#5067-1504)

Buffers	DNase/RNase free water	Invitrogen UltraPure™ Life Technologies Limited, Distilled water DNase/RNase free (#10977-035)
	Chloroform	Sigma (#C2432-500)
	Trizol® Reagent	Ambion by Life Technologies™ (#15596018)
	Ethanol	Sigma (#E7023)
Devices	Centrifuge 5415R	Eppendorf
	Agilent 2100 Bioanalyzer	Agilent Technologies
	Vortex mixer	IKA-Model MS3

Method – Protocol

Murine vascular aortic SMCs ($2x10^6$ cells) were seeded in 75 cm^2 flasks for 24h and kept in the incubator and left to be grown in the flasks for 48h and then trypsinized followed by yielding a pellet of cells. The cell pellet was frozen in 1 ml Trizol and kept at -80°C for further use.

Table 20 – Samples and their concentrations used for RNA sequencing

Cell line Type	**Gender**	**#**	**WT= *B6.ApoE*$^{-/-}$ wild-type** ***Mras* KO= *Mras*$^{-/-}$*ApoE*$^{-/-}$ double knockout**	**Concentration (ng/ml)**
Murine Aortic Smooth Muscle Cells (MSMCs)	Male	1	WT +TNF	57548
		17	WT +TNF	563.72
		22	WT +TNF	482.36
		13	*Mras* KO +TNF	603.28
		14	*Mras* KO +TNF	669.68
		15	*Mras* KO +TNF	761.12
	Female	11	WT +TNF	453.64
		21	WT +TNF	540.28
		16	*Mras* KO +TNF	576.12
		19	*Mras* KO +TNF	695.96

The samples were thawed in ice and 200µl of chloroform was added to each sample. The tube was mixed thoroughly for 15s and then left for incubation at room temperature for 2-3 min. The sample was centrifuged at 12000 rpm for 10 min by 4°C and three phases could be seen after the centrifugation step. The upper-watery phase was the RNA and the lower-red phase was Phenol-Chloroform with an interphase in between. The upper phase with RNA was carefully taken in a separate tube and equal volume of 70% ethanol was added. The contents of the tube were put in a RNeasy spin column and RNA isolation was performed with the RNeasy® Mini Kit according to its standard protocol. The RNA was eluted in 30 µl of DNase/RNase free water. The integrity of the RNA samples was checked with measuring the quality of the total RNA with the Agilent RNA 6000 Pico system in accordance to its standard protocol. A library was prepared to generate a sequenceable cDNA library. The standard protocol of Illumina Stranded mRNA Prep was conducted. The mRNA was purified and fragmented using oligo(dT) magnetic beads capturing the poly-A tailed mRNAs, followed by synthesis of the first and second strands of cDNA. The 3' ends of the blunt fragments were adenylated for prevention of ligation with each other. The pre-index anchors were ligated to the ends of the double-stranded cDNA fragments. The adapter-ligated fragments were cleaned up using magnetic beads and the library was amplified. Finally, the clean-up/purification of the library was performed using magnetic beads. The concentration and the quality of the final libraries was measured using the Agilent DNA 1000 Kit. The samples were proceeded to further analysis by Tobias Reinberger and Kristian Händler using the DeSeq2 (172) R package tool.

4.5 Cellular Assays/ Functional Assessment

4.5.1 Migration Assay

Material

Table 21 – Material, buffers, and devices for Migration assay

Category	Name	Manufacturer/Composition
Material	Reaction tubes (0.2, 0.5, 1.5, 2.0 and 50 ml)	Sarstedt
	Biosphere Filter Tips (10, 100 and 1000 µl)	Sarstedt
	Serological Pipettes (2, 5, 10 and 25 ml)	Sarstedt
	Culture flask 25 cm^2 – TC Flask T75	Sarstedt (#83.3911.002)
	Culture flask 75 cm^2 – TC Flask T175	Sarstedt (#83.3912.302)
	12- well plate (Nunclon^{TM} Delta Surface Multidish)	Thermo Scientific (#150628)
	Ibidi 4-well culture inserts for self- insertion	Ibidi GmbH (#80469)

Buffers	Cell culture medium (for human cells)- Human vascular SMC basal medium	M231 Gibco (#M-231-500), supplemented with SMGS (Smooth Muscle Growth Supplement) Cascade Biologics™ Gibco 20x (#S-007-25)
	Smooth Muscle Differentiation Supplement (SMDS)	Cascade Biologics™ Gibco (#S-008-5)
	Cell culture medium (for murine cells)- Dulbecco's modified eagle medium	DMEM 1x+GlutaMax™-I Gibco (#31966-021), supplemented with 10% FBS and 1% P/S
	FBS	Superiorstabil® Bio&Sell (#FBS.S 0615)
	P/S 10,000 U/ml	Penicillin/Streptomycin Biochrome (#A2213)
	Trypsin- EDTA	Capricorn Scientific (#TRY-1B10); for trypsinization → dilute 1:10 in PBS
	Trypsin neutralizer solution 1x	Cascade Biologics™ Gibco (#R-002-100)
	StemPro™ Accutase™ Cell Dissociation Reagent	Accutase/Biotase Bio and Sell (#BS.L 2193) with 0.5 mM EDTA; sterile filtered
Devices	CO_2-Incubator Hera cell	Heraeus
	Laminar Flow Clean Bench	CleanAir
	NucleoCounter® System NC-200™	Chemometec
	Centrifuge 5702R	Eppendorf
	Keyence Microscope BZ-X 810	Life Sciences

Method – Protocol

For Migration analysis, an assay similar to wound-healing was established at our Institute. Cells were seeded into each well of an ibidi 4-well culture insert inside a 12-well plate. Different concentration of cells was taken i.e., for humans aortic SMCs $1.09x10^5$ cells/ml and for mouse aortic SMCs 2.0-$2.5x10^4$ cells/ml. The cells were incubated at 37°C and 5% CO_2 in a CO_2- Incubator. In terms of human aortic SMCs, an additional step of siRNA transfection was performed after seeding of cells followed by incubation in M231 culture medium supplemented with Smooth Muscle Growth Supplement (SMGS) overnight. After 48h, the inserts were removed and the cells were washed with phosphate buffered saline (PBS) and cultured in serum-free media (SMDS). Murine aortic SMCs were cultured in DMEM culture medium.

Migration was assessed at 0h and 24h where images were captured with the Keyence Fluorescence microscope and positions were marked at all time points. All the time points included in the experiment were processed and confluency was analysed. The movement of the cells through the empty space generated by the silicone inserts was measured to determine the confluency. 7-9 independent technical replicates were analysed. Images were processed with a python script developed by Tobias Reinberger.

Moreover, different stimuli like PDGF, TNF, IL-6 and IL-1ß were added to the cell culture medium to show the difference in migration of human and mouse aortic SMCs when stimulated.

4.5.2 Proliferation Assay

Material

Table 22 – Material, buffers, and devices for Proliferation assay

Category	Name	Manufacturer/Composition
Material	Reaction tubes (0.2, 0.5, 1.5, 2.0 and 50 ml)	Sarstedt
	Biosphere Filter Tips (10, 100 and 1000 µl)	Sarstedt
	Serological Pipettes (2, 5, 10 and 25 ml)	Sarstedt
	96- well plate	Cellstar® Greiner Bio-one (#655180)
	BrdU colorimetric Kit	Roche (#11647229001)
Buffers	Hoechst 33342 dye	Merck (#14533)
	PBS	Capricorn Scientific Dulbeco's PBS w/o Ca & Mg, w/o Phenol Red (#PBS1A9)
Devices	CO_2-Incubator Hera cell	Heraeus
	Keyence Microscope BZ-X 810	Life Sciences
	Cell Counter Software	Keyence BZ-X810
	Synergy HT Microplate Plate Reader	Biotek

Method – Protocol

The cell proliferation assay was conducted to quantify the relative rates of cell division within the target tissues using divergent immunohistochemical staining techniques to detect proliferating cells.

4.5.2.1 Hoechst 33342 Staining of the Nuclei

The cells were plated into 96-well plates. The concentration for cells seeded in each well for humans was $1x10^4$ cells/well and for mice was $0.8\text{-}1.2x10^4$ cells/well. The cells were placed in the incubator and after 24h, the cell culture medium was replaced by serum-free medium. For quantification of proliferation, the cell nuclei were stained with Hoechst 33342 dye at several time points, and the numbers were assessed using the Cell Counter software. Six wells were taken for analysis for each condition. 7-9 technical replicate experiments were carried out.

4.5.2.2 BrdU- Assay

The BrdU- based proliferation assay is a non-isotopic immunoassay for the quantification of cell division in the S-Phase. Bromodeoxyuridine/5-bromo-2'-deoxyuridine (BrdU), a synthetic nucleoside is incorporated into newly synthesized DNA of actively proliferating cells as a thymidine and is detected through anti-BrdU antibodies. Detection of BrdU was performed in combination with the staining of DNA with the Hoechst 33342 dye.

The cells were seeded in a 96-well microplate at variable concentrations (for human in M231 culture medium and mice cells in DMEM) and left in the incubator for 24h at 37°C 5% CO_2. After 24h, 10 µl/well of BrdU labelling solution was added to the cells followed by incubation of cells at 37°C, 5% CO_2 for 7h. During this labelling period, the pyrimidine analogue BrdU is incorporated in place of thymidine into the DNA of proliferating cells. After removal of the labelling medium, 200 µl of FixDenat solution was added and the cells were fixed and the DNA denatured. The denaturation of DNA is important to improve the accessibility of the incorporated BrdU for detection by the antibody. After incubation with FixDenat for 30 min at room temperature, 100 µl/well of Anti-BrdU-POD working solution was added to the cells followed by incubation at room temperature for 90 min. The Anti-BrdU-POD binds to the BrdU incorporated in newly synthesized, cellular DNA. Subsequently, the antibody conjugate was eliminated by rinsing the wells three times with 300 µl/well of washing solution (1x PBS). 100 µl/well substrate solution was added to the wells until blue colour development was detected (15-20 min). The immune complexes were detected by the subsequent substrate reaction. The absorbance of the samples in an ELISA reader at 450 nm was measured. The samples were re-washed with washing buffer and distilled water three times each. The cells were stained with Hoechst and measurements at 370 nm were taken again. The difference between both the values was taken. The developed colour and the absorbance values directly correlate to the amount of DNA synthesis and the number of proliferating cells in each well. 4-6 independent technical replicates were analysed.

4.5.3 Apoptosis Assay

Material

Table 23 – Material, buffers, and devices for Apoptosis assay

Category	Name	Manufacturer/Composition
Material	Reaction tubes (0.2, 0.5, 1.5, 2.0 and 50 ml)	Sarstedt
	Biosphere Filter Tips (10, 100 and 1000 µl)	Sarstedt
	Serological Pipettes (2, 5, 10 and 25 ml)	Sarstedt
	6- well plate (Nunclon™ Delta Surface Multidish)	Thermo Scientific (#140675)
	Caspase-3 Assay Kit	Caspase-3 Assay Kit
Buffers	0.2% SMGS + M231	M231 Gibco (#M-231-500), supplemented with SMGS (Smooth Muscle Growth Supplement) Cascade Biologics™ Gibco 20x (#S-007-25); For starvation → 100 µl of SMGS in 50 ml M231 culture medium
	0.2% FBS + DMEM	DMEM 1x+GlutaMax™-I Gibco (#31966-021), supplemented with 10% FBS and 1% P/S; For starvation → 100 µl of FBS in 50 ml DMEM culture medium
	Trypsin- EDTA	Capricorn Scientific (#TRY-1B10); for trypsinization → dilute 1:10 in PBS
	Staurosporine (1 mM stock)	AAT Bioquest (#80050)
Devices	CO_2-Incubator Hera cell	Heraeus
	Nanophotometer N60 Touch	Implen GmbH (#T62326)
	Synergy HT Microplate Plate Reader	Biotek

Method – Protocol

The apoptosis assay used, was the Caspase-3 (colorimetric) Assay. Caspase 3, being an executioner caspase, carried out the mass proteolysis leading to apoptosis. The assay is mainly based on spectrophotometric detection of the chromophore p-nitroaniline (p-NA) after cleavage from the labelled substrate DEVD-p-NA. The p-NA light emission is quantified using a microtiter plate reader at 400 or 405 nm.

Apoptosis was induced in cells (human or mice) by seeding 6 x 10^4 cell/well in a six-well plate in culture media (M231 for humans or DMEM for mice) for 24 h supplemented with their respective growth factors (SMGS and 10% FBS). After 24 h, the cells were made quiescent by incubation in DMEM containing only 0.2% FBS. Additionally, the cells were treated with TNF (10 ng/mL) as stimuli to observe the change in rate of apoptosis. The cells, at this point, started starving and were left for starvation for two additional days (48 h). Simultaneously, a control culture without induction of apoptosis was also taken. A positive control with cells treated with Staurosporine (apoptosis inducer) was also taken. The cells were then detached from the six-well plates by incubation with Trypsin-EDTA in PBS or StemPro™ Accutase™ Cell Dissociation Reagent, and a pellet with concentration varying from 1-5 x 10^6 cells was obtained. These cells were resuspended in 50 µl of chilled cell lysis buffer and incubated on ice for 10 min, followed by a centrifugation step of 1 min/ 10,000rpm. The cytosolic extract (supernatant) was preserved, and the protein concentration was measured with a nanodrop machine. The optimal protein concentration to proceed was 50-200 µg per 50µl of cell lysis buffer. A 96-well plate was taken, and a sample well of 20 µl was prepared. A caspase reaction mix was made with 20 µl of DTT in 2 ml 2x reaction buffer. 5 µl of 4 mM DEVD-p-NA substrate was added to the samples and incubated at 37°C for 120 min. The colorimetric release of p-nitroaniline from the Ac-DEVD-p-nitroaniline substrate was monitored at OD 400-405 nm on a microplate reader. The fold increase in the caspase-3 activity was determined by the absorbance of p-NA from an apoptotic sample compared to an untreated control sample. 4-6 independent technical replicates were analysed.

4.6 Mouse Plaque Staining

The role of *Mras* in atherogenesis using *Mras* -knockout (KO) mice in the atherogenic *ApoE* KO background revealed no differences in plaque formation size and lipids levels of the wild type (*B6.ApoE*$^{-/-}$) and *Mras*$^{-/-}$*ApoE*$^{-/-}$ double knockout (dKO) mice. But the macrophage infiltration in plaques was less extensive in the dKO mice than in *ApoE* KO mice. It was concluded that *Mras* is also critical for plaque stabilization. In this case, *Mras* mice's plaque contents were thoroughly analysed. Four different stainings were conducted according to their respective standard protocols.

Material

Table 24 – Material, buffers, and devices for different Plaque staining

Category	Name	Manufacturer/Composition
Material	Reaction tubes (1.5, 2.0, 15 and 50 ml)	Sarstedt
	Biosphere Filter Tips (10, 100 and 1000 µl)	Sarstedt
	Microslides SuperFrost® Plus	epredia (#J800AMNZ)

	Dako Pen	Dako (#S2002)
	Cover Slips 24x50 mm, #1	Menzel (#9161050)
Buffers	Tissue freezing medium	Leica Biosystems (#14020108926)
	Oil red O Stock solution	Sigma (#O0625), 0.5 g oil red in 100 ml 100% Isopropanol
	Oil red O Staining solution	60% ORO Stock solution, in distilled water, filtered
	60% Isopropanol	Carl Roth, diluted in distilled water
	Mayer's Haematoxylin	Roth (#T865.1)
	Aquatex	Merck (#1.08562.0050)
	Masson's Trichrome Staining Kit	Sigma (#HT15-1KT)
	Bouin's solution	Sigma (#HT10132)
	Weigert's Haematoxylin solution	Weigert A (Ferric-Haematoxylin, Carl Roth, #X906.1), Weigert B (Ferri-Haematoxylin, Carl Roth, #X907.1) (1:1)
	1% Acetic acid	J. T. Baker, in distilled water
	Ethanol abs.	J.T. Baker (64-17-5)
	Cytoseal XYL	Thermo Scientific (#8312-4)
	0.3% H_2O_2	Sigma (#216763), 30%; diluted 1:100 in distilled water
	Block Buffer for MoMa	5% (w/v) skimmed milk powder (Carl Roth, #T145.3), 0.05% Tween 20 (Merck, #8.22184.1000), in PBS
	Tween 20	BioRad Labs (#1706531)
	PBS	Capricorn Scientific Dulbeco's PBS w/o Ca & Mg, w/o Phenol Red (#PBS1A9)
	Immpact NovaRed HRP Substrate	Vector (#SK-4805)
	DAPI Staining solution	Sigma (#D9542)
Devices	Keyence Microscope BZ-X 810	Life Sciences
	Leica Biosystems Cryostat	Thermo Scientific Cryostar NX50 HOVP (#S16071164)

Method – Protocol

All animal experiments were performed in accordance with the German animal studies committee of Schleswig- Holstein. For the analysis of the plaques, 49 mice hearts (males: 26, females: 23) with two different genotypes i.e., WT (*B6.ApoE*$^{-/-}$) (n= 32) and dKO (*Mras*$^{-/-}$*ApoE*$^{-/-}$) (n= 17) were provided by the animal care unit of the Institute for Cardiogenetics, Lübeck.

The aortic root was cut into slices by the Leica Biosystems Cryostat (cryo-sectioning machine) forming heart cross area-sections with three aortic cusps where the plaque was majorly formed.

Four dye staining were carried out i.e., Oil red O- staining (lipid content), Collagen staining (collagen content), macrophages and monocytes staining (MoMa) (macrophages and monocytes content) and Acta2+ staining (SMC content).

4.6.1 Oil Red O Staining

The dye, Oil Red O (ORO), basically stained the neutral lipids (triglycerides and diacylglycerols), in addition to the cholesterol esters. The cryostat sections were first thawed and then dried for an hour or two at room temperature. Then, they were dipped 10x in 60% isopropanol, and then incubated for 15 min in the ORO staining solution. Excess oil red o solution was removed by dipping the slides in 60% isopropanol and rinsing of slides with running tap water for further 5 min. The slides were counterstained with Mayer's Haematoxylin for 3 min followed by rinsing with running tap water for an additional 5 min. Finally, the slides were mounted with Aquatex, covered with cover slips and left overnight at 4°C to ensure an even polymerization of the mounting medium.

4.6.2 Collagen Staining

In collagen staining, the trichrome (Masson's trichrome) staining protocol was implemented. The collagen dye differentiated between the smooth muscle and collagen and verified the presence of collagen. In this staining, the muscle was stained red, collagen fibres blue, the erythrocytes red and nuclei were stained black.

First the cryostat sections were thawed and dried for 1 to 2h at room temperature. Then, the cryostat sections were incubated in a water bath at 56°C for 20 min in the Bouin's solution. To remove the excess yellow colour, the slides were left under running tap water for 15 min and further placed in the Weigert's Haematoxylin solution for 5 min. Furthermore, the sections were stained in Biebrich Scarlet-Acid Fuchsin Solution, in Phosphomolybdic/ Phosphotungstic acid (1:1:2 in distilled water), and Aniline blue solution for 5 min each, and then in 1% Acetic acid for 2 min with an alternative washing step in between all steps for 5 min with running tap water. The slides were further fixed in

70%, 96% and 100% ethanol and Roti-histol and then finally mounted with Cytoseal. The slides were further proceeded to analysis.

4.6.3 MoMa Staining

The MoMa staining was a monoclonal antibody staining (MOMA-2) which recognized the monocytes and macrophages in the mouse. Intracellular antigen of the mouse macrophages and monocytes were recognized by this antibody. This staining was intense and the antibody was very useful for defining tissue macrophages (mostly in the lymphoid organs in mouse strains) by immunohistochemistry. The cryostat sections were fixed in ice cold Methanol: Acetone for 10 min, airdried for 2-3 min and then circled with Dako Pen. To block endogenous peroxidase activity, sections were mounted in 0.3% H_2O_2 for 20 min at room temperature. After three times washing in PBS for 5 min, slides were incubated in pre-warmed 0.025% Trypsin solution for 5 min at 37°C followed by washing three times for 5 min in PBS. After the unblocking of unspecific binding sites with blocking buffer (1 g skimmed milk, 10 µl Tween, 20 ml PBS) for 1 h at room temperature, the slides were incubated with the MOMA antibody (1:500 in Block buffer) overnight at room temperature. The next day, the slides were washed three times with PBS and incubated with a secondary antibody (polyclonal rabbit anti Rat/ HRP-linked) for 1 h at room temperature, and washed again three times in PBS. The antibody staining was visualized using the ImmPACT NovaRed Peroxidase Substrate Kit (5ml Diluent, 3 drops Reagent 1, 2 drops Reagent 2, 2 drops Reagent 3 and 2 drops Reagent 4) for 5:30 min. Subsequently, a washing step with running tap water was carried out followed by counterstaining of the slides with Mayer's haematoxylin for 3 min. The slides were washed for additional 7 min under running tap water followed by fixation in 70%, 96% and 100% ethanol and Xylene and finally mounted with Cytoseal.

4.6.4 Acta2+ Staining

The Acta2+ staining involved an antibody that was specific for smooth muscle actin. It reacted specifically with α-smooth muscle actin in immunoblotting assays and was highly restricted to SMCs, pericytes and myofibroblasts. This monoclonal anti-actin antibody, α-smooth muscle specifically recognized the α-smooth muscle isoform of actin (42 kDa).

The cryosections were fixed in ice-cold Methanol: Acetone for 10 min at room temperature, dried for 2-3 min and then circled with Dako Pen. The sections were incubated in the primary Acta2+ antibody (1:100 dilution in PBS) for 2 h and 30 min or overnight (24 h). The next day, the sections were washed 3x for 5 min in PBS, and then visualized with DAPI (1:10000 dilution in distilled water) for 10 min at room temperature. After washing with distilled water, sections were mounted with Aquatex. All the stained tissues samples were then analysed with the software GIMP 2.10.22 version

(GNU Image Manipulation Program) and then proceeded to a python script where the amount of each plaque was calculated.

Table 25 – List of antibodies used in Acta2+ staining

Antibody	Description	Dilution	Manufacturer
MOMA primary antibody	Rat monoclonal anti- Monocyte + Macrophage	1 :500 in block buffer	ab33451, Abcam
MOMA secondary antibody	Rabbit polyclonal anti-rat IgG, HRP-linked	1:2000 in PBS	P0450, Dako
Acta2^{+}	Mouse monoclonal, Anti-actin, α-smooth muscle FITC antibody (clone 1A4)	1:100 in PBS	F3777, Sigma

4.7 Statistical Analysis

All the data is presented as column charts and regression curves showing all points, unless otherwise stated including the mean and standard deviation represented by horizontal bars. Unpaired t-tests using a Welch's correction, paired t-tests, student t-test, linear regression analysis were performed using GraphPad Prism vs. 9.5.1. Two way -analysis of variance (ANOVA) was also performed for all charts having more than two groups using GraphPad Prism vs.9.5.1. $P < 0.05$ was considered statistically significant. For all tests, *P <0.05, **P <0.01, ***P <0.001, ****P <0.0001, ns = not significant unless stated otherwise. Statistic outliers were identified using GraphPad outlier test and excluded from all the analysis. All the bars indicate n≥3 of independent experiments. Python scripts used in this research study are available on request by tobias.reinberger@uni-luebeck.de.

5. Results

The following section will comprehensively cover the outcomes and findings derived from the conducted research, providing a detailed exploration of the results obtained throughout this thesis. According to eQTL data, *MRAS* risk variants for coronary artery disease increase *MRAS* mRNA levels primarily in the arterial tissue (106). Thus, *MRAS* risk variants are specific to VSMCs. Therefore, the function of *MRAS* in vascular SMCs, one of the key cell types in etiology of atherosclerosis and plaque stabilization, was investigated. SMCs isolated from the aorta in humans and mice were used in the following experiments.

5.1 Human Vascular Aortic Smooth Muscle Cells

The role of the *MRAS* gene was investigated in HSMCs. The gene was silenced via RNA interference to observe the difference in cellular movement (migration), proliferation of cells and cell viability (apoptosis) with multiple stimuli.

5.1.1 RNA Interference causing effective siRNA Knockdown of MRAS in HSMCs

To test the most efficient siRNA for silencing the *MRAS* gene, three divergent siRNA for *MRAS*, targeting three separate positions on the mRNA transcript were used in the following experiments. Approximately 3.5 x10^4 cells/ml in one well of a 48-well plate was taken and transfected with siRNA concentrations varying from 10 – 40 nM. The experiments were replicated with the *MRAS* 13.2 and 13.3 siRNA resulting in 80.6% and 87.0% knockdown efficiency respectively (Figure 7).

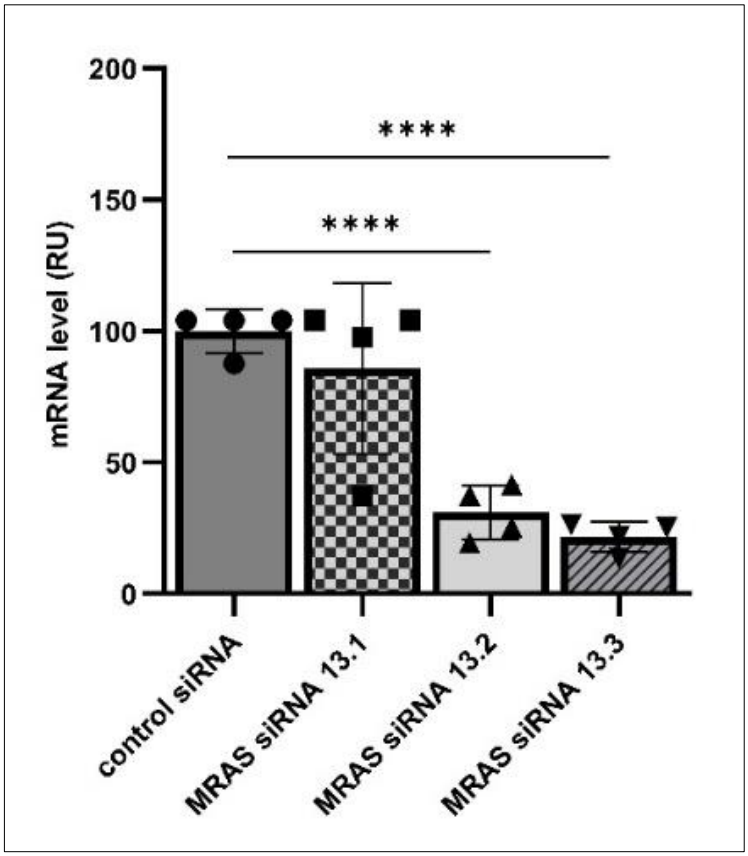

Figure 7 – siRNA knockdown validation in HSMCs

Shown here are the mean values of four technical replicates for each siRNA knockdown validation (n=4). mRNA expression levels were assessed by measuring the percentage of siRNA knockdown in each sample for control siRNA, *MRAS* siRNA 13.1, 13.2, and 13.3. Each point represents the mean of mRNA level per sample for each condition. The horizontal bars show the standard deviation of the data. Student's two-sided t-test and two-way ANOVA was carried out to determine the significance (****$p<0.0001$). This experiment was technically repeated 4 times.

5.1.2 *MRAS* Deficiency leads to increased SMC Migration

Migration was analysed using an ibidi 4-well culture insert setup inside a 12-well plate (similar to wound-healing). For each experiment, two wells in a 12-well plate with two inserts were taken for each condition, yielding eight values per condition per replicate. The cells were transfected with siRNA for 24h and the insert removed, and pictures were taken with the bright field contrast (Figure 8) of the Keyence microscope where the points were fixed at 0h and then at 24h, the same marked points were photographed to assess the distance travelled by the SMCs. All the time points included in the experiment were processed and confluency was analysed.

The optimized number of cells for human SMCs was $1.2x10^4$ cells/well taken in each well and transfected with 20 nM siRNA (13.2 & 13.3). The experiment was technically repeated for 7-9 times and some wells were excluded based on contamination in the wells, the cells being not confluent enough for assessment, or the cells were detached from the wells. The medium was changed from growth (SMGS) to differentiation (SMDS) after the removal of the inserts to avoid

doubling/replication of the cells. For optimization purposes, pictures were also taken at 6h and 16h to assess the rate of migration. Cellular confluence, as a parameter for migration ability, was determined by measuring the density of SMCs that had migrated into the empty space defined by the silicone inserts after removal.

MRAS siRNA transfected aortic SMCs showed a significantly increased migration rate, reaching the highest confluency percentage after 24h (76.3%; n = 7-9). Control siRNA aortic SMCs do not reach full confluency within this time and have a lower migration rate (52.1%) (Figure 9). As *MRAS* is involved in cell differentiation, proliferation and cell adhesion signalling pathways, 5 ng/ml of PDGF-BB (growth factor for cell division and proliferation) and 10 ng/ml of TNF were added to the assess the difference of migratory affect in cells. There was no significant difference observed between the control siRNA and *MRAS* siRNA transfected cells when treated with PDGF-BB (Figure 9). The concentration of PDGF-BB was increased up to 10 ng/ml, still no difference was observed. Higher concentrations of PDGF-BB were cytotoxic for the experiments. On the other hand, there was an elevated significant difference observed between the control siRNA transfected cells and *MRAS* siRNA treated with TNF. Addition of TNF to *MRAS* siRNA treated SMCs resulted in rapid migration reaching up to 80.4% confluency (n = 7-9) after 24h (Figure 9).

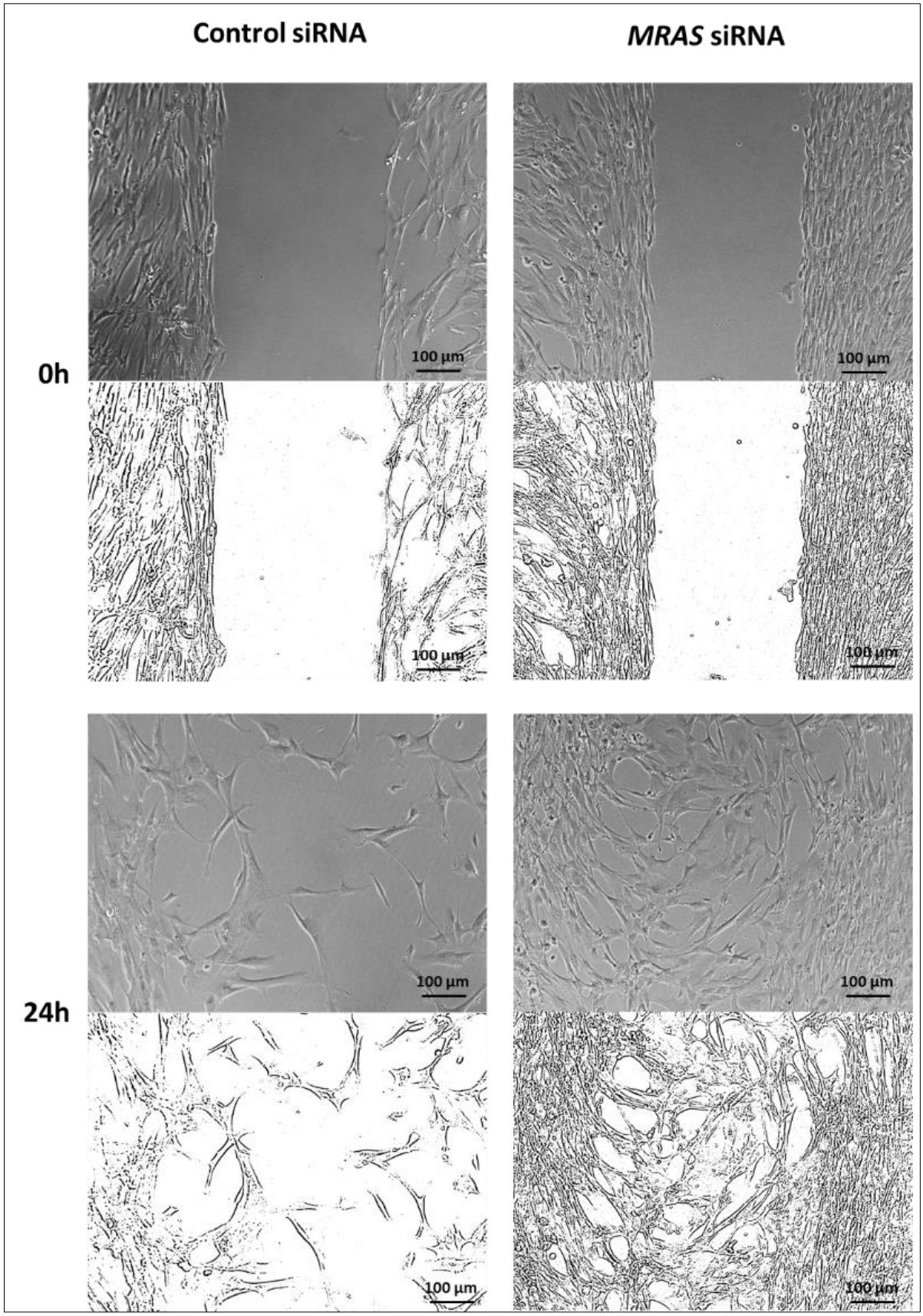

Figure 8 – Migration of HSMCs

Exemplary bright field and corresponding contour images of control and *MRAS* siRNA transfected SMCs. Knockdown cells show strong migration within 24h. Scale bars represent 100 µm.

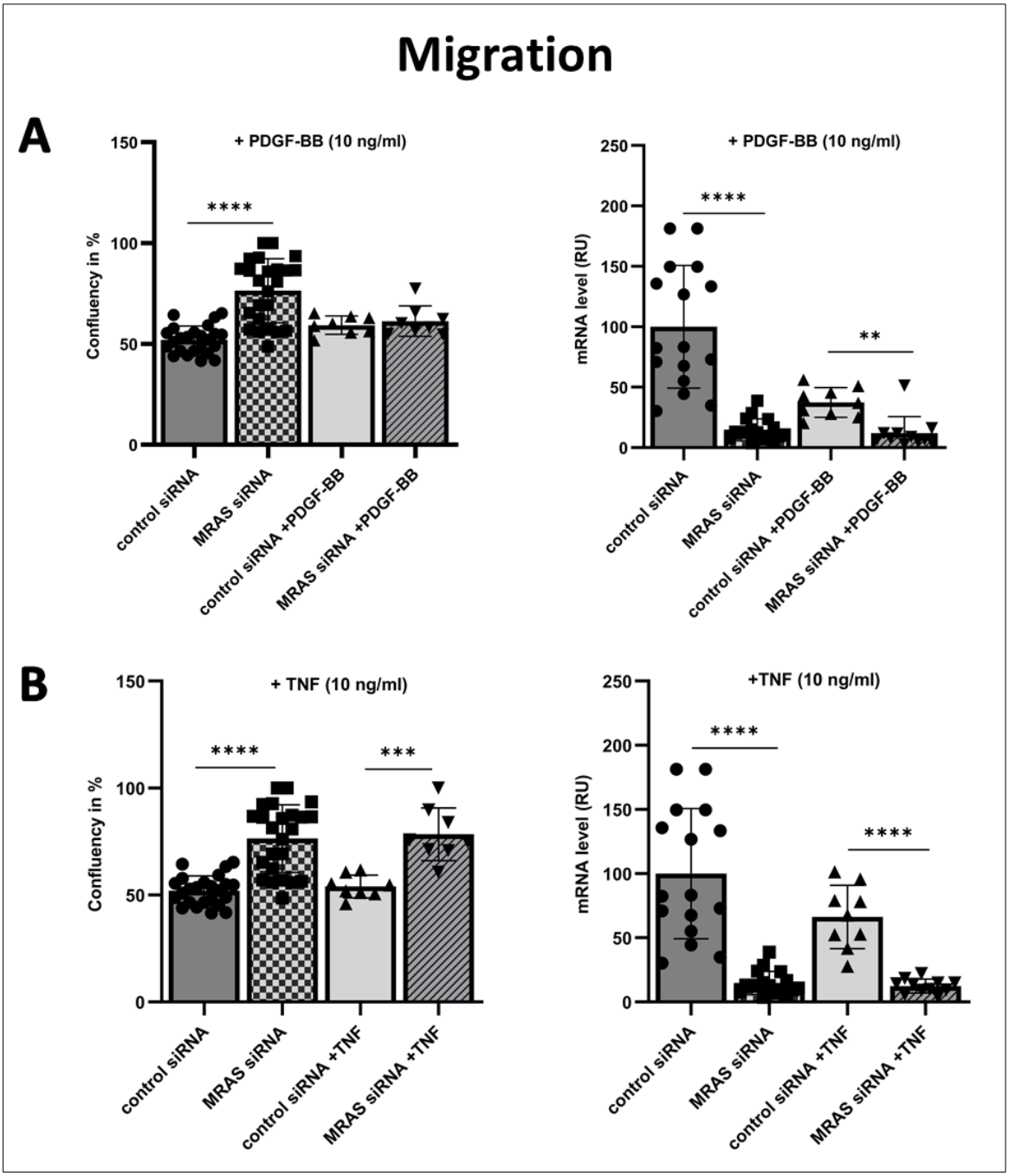

Figure 9 – Migration and mRNA expression level of HSMCs with stimulation of PDGF-BB (A) and TNF (B)

A (left): *MRAS* siRNA transfected aortic SMCs migrate faster than the control siRNA transfected cells without any stimulus, reaching about 76.3% after 24 h ($p = 4.18E-09$). There was no difference in migration observed between the control and *MRAS* siRNA transfected cells when stimulated with PDGF-BB 10 ng/ml ($p = 0.53$). **A (right):** mRNA levels of cells treated with PDGF-BB and no stimulus treated cells were assessed by measuring the percentage of siRNA knockdown in each sample. **B (left):** *MRAS* siRNA transfected aortic SMCs stimulated with TNF (10 ng/ml) migrate faster than the control siRNA cells with TNF, reaching about 80.4% after 24h ($p = 0.00015$). **B (right):** mRNA levels of TNF stimulated and non-stimulated SMCs were assessed by measuring the percentage of siRNA knockdown in each sample. **All figures continued:** The box plot for control and *MRAS* siRNA transfected cells without any stimulus in the migration assays contain more data points compared to each stimulus- (PDGF-BB, and TNF) treated sample because the data represents an average from all experiments. Each point represents the mean of the migration rate/ confluency in % per well analysed. The horizontal bars show the standard deviation of the data. The experiment was technically repeated 7-9 times. Student's two-sided t-test and two-way ANOVA was carried out to determine the significance (**$p<0.01$; ***$p<0.001$; ****$p<0.0001$).

Besides TNF, IL-6 and IL-1ß are proinflammatory cytokines involved in chronic inflammation, atherosclerosis and cellular processes like proliferation and survival. These were also added to assess the change in the cellular migration rate. For both cytokines (IL-6 and IL-1ß), 10 ng/ml was too cytotoxic, thus 5 ng/ml of both were added separately to the cells and migration was determined. *MRAS* siRNA transfected aortic SMCs stimulated with IL-6 depicted a significantly raised migration rate, reaching the highest confluency percentage after 24h (73.4%; n = 7-9) (Figure 10). Control siRNA aortic SMCs with IL-6 do not reach full confluency within this time, and have a lower migration rate (48.8%). Moreover, there was a significant difference also observed between the control siRNA (57.7%) and *MRAS* siRNA transfected cells (73.0%) stimulated with IL-1ß as well (n = 7-9) (Figure 10).

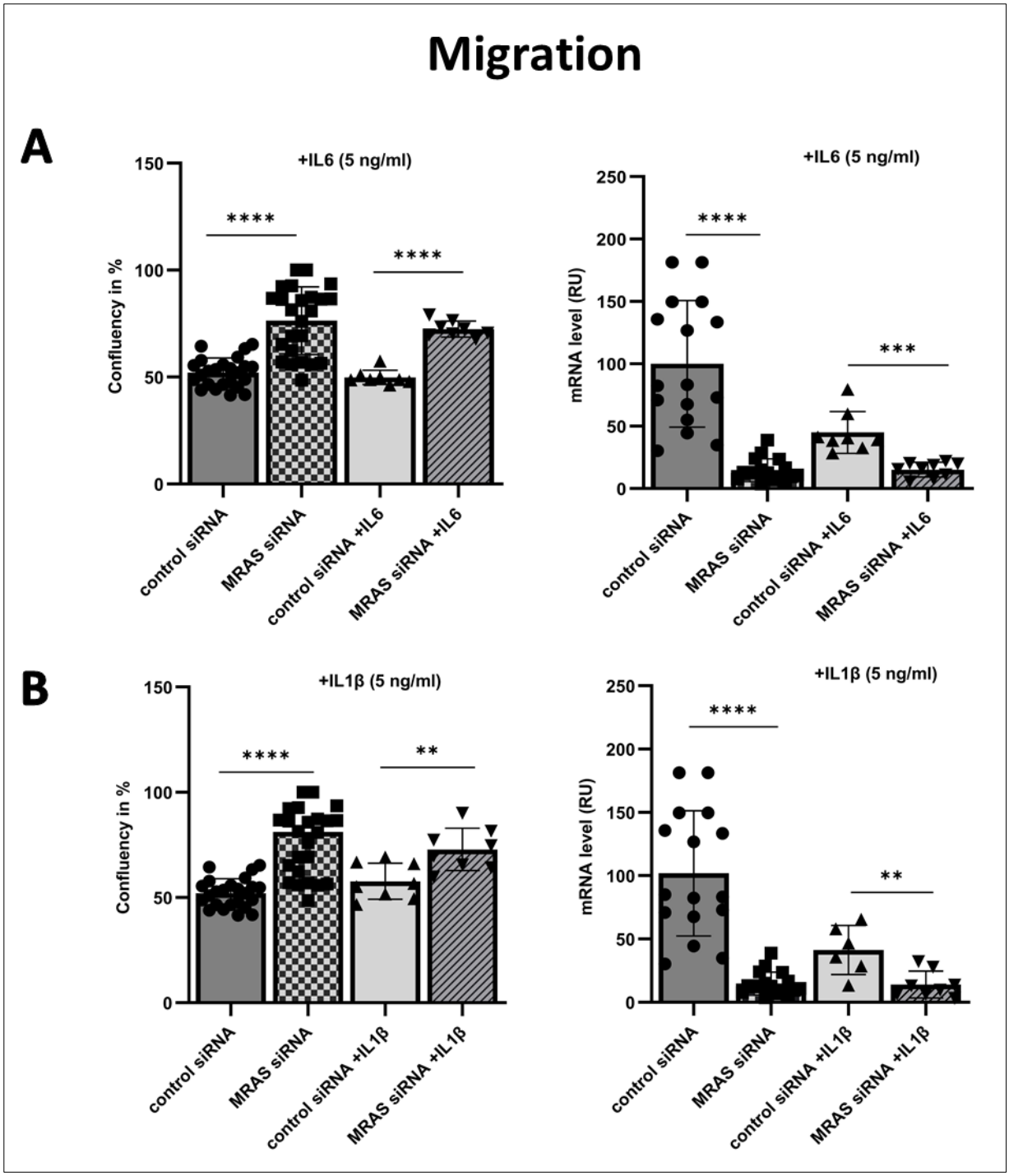

Figure 10 – Migration and mRNA expression level of HSMCs with stimulation of IL-6 (A) and IL-1ß (B)

A (left): *MRAS* siRNA transfected aortic SMCs stimulated with IL-6 migrate faster than the control siRNA transfected cells with IL-6 (5 ng/ml), reaching about 73.4% after 24h ($p = 4.606E-09$). **A (right):** mRNA levels of IL-6 treated and non-treated cells were assessed by measuring the percentage of siRNA knockdown in each sample. **B (left):** *MRAS* siRNA transfected aortic SMCs stimulated with IL-1ß (5 ng/ml) migrate faster than the control siRNA transfected cells with IL-1ß, reaching about 72.8% after 24h ($p = 0.005$). **B (right):** mRNA levels of IL-1ß treated and no stimulus treated cells were assessed by measuring the percentage of siRNA knockdown in each sample. The box plot for control and *MRAS* siRNA transfected cells without any stimulus in the migration assays contain more data points compared to each stimulus- (IL-6 or IL-1ß) treated sample because the data represents an average from all experiments. Each point represents the mean of the migration rate/ confluency in % per well analysed. The horizontal bars show the standard deviation of the data. The experiment was technically repeated 7-9 times. Student's two-sided t-test and two-way ANOVA was carried out to determine the significance (**$p<0.01$; ***$p<0.001$; ****$p<0.0001$).

5.1.3 Downregulation of *MRAS* in Human SMCs increases Proliferation

Smooth muscle cells increase in number through cell division. Excessive SMC proliferation contributes effectively to the formation of atherosclerotic plaques. SMCs migrate to the intima and proliferate, leading to plaque build-up and potentially vessel occlusion. SMC proliferation helps repairing the damaged blood vessel walls, promoting health and restoration of normal function.

Proliferation was analysed by seeding a defined cell number and counting the cells at different time points. 0.7-1x10^4 cells/well were taken in each well and transfected with 20 nM siRNA (13.2 & 13.3). After 24h transfection, the media was changed to SMGS (growth medium) with additional stimuli and propagation of cells was observed along the days (24, 48, 72 and 96h).

For each experiment, at each timepoint, three wells were photographed after Hoechst 33342 dye staining with the Keyence microscope (Figure 11). The nuclei were then counted manually with the Olympus cell count software. The knockdown effect lasts up to 5 days. *MRAS* siRNA knockdown cells depicted a higher proliferation rate when compared to control cells. The assay was conducted until 96h and pictures were taken after every 24h. After 96h, the *MRAS* siRNA knockdown cells were 37.4% more confluent compared to controls (p = 8.65E-07) (Figure 12). A similar trend was observed with the BrdU assay, which was a validation experiment to obtain the proliferation rates by quantifying the incorporation of BrdU into the DNA during DNA replication in the S-phase. Different stimuli like PDGF-BB, TNF, IL-6 and IL-1ß were added to the cells to assess the divergent proliferating rates.

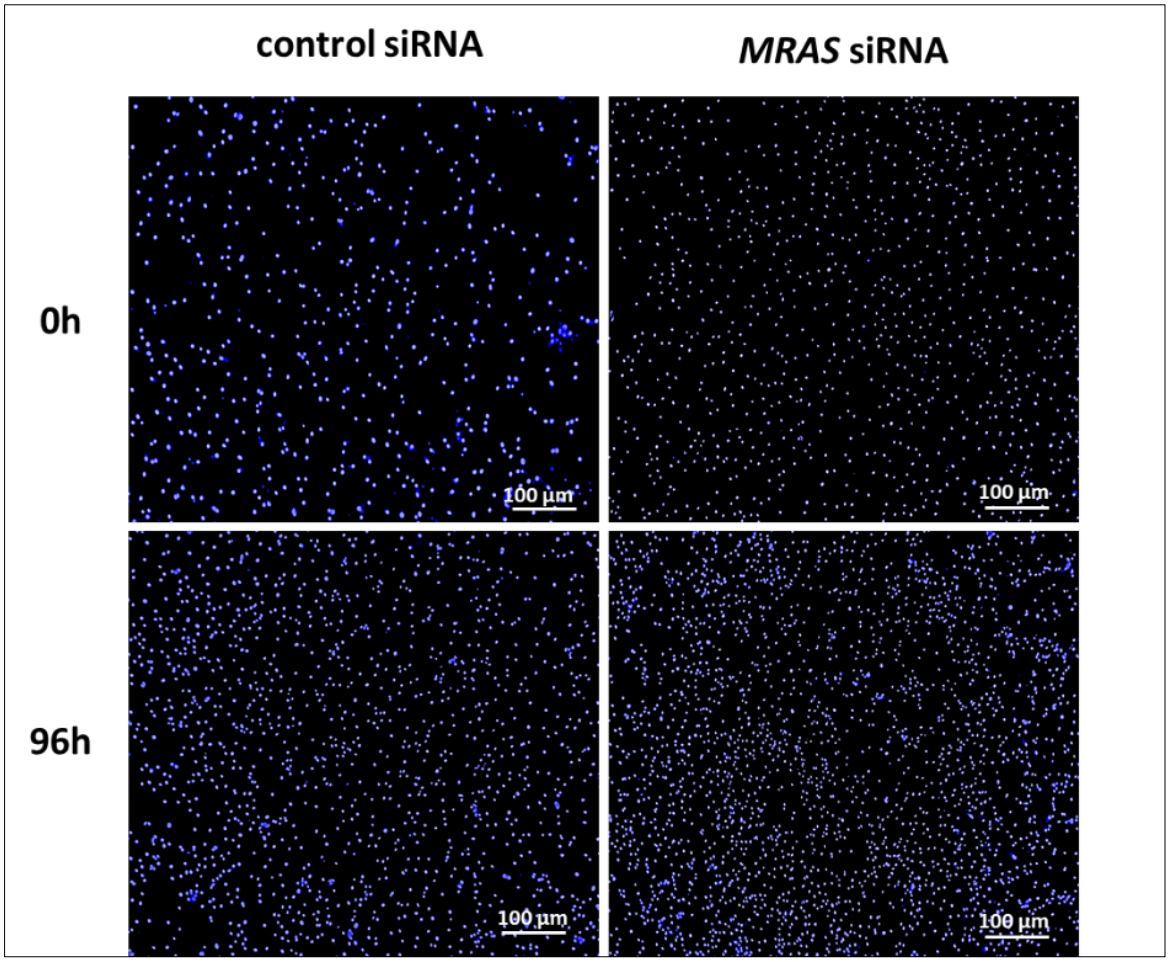

Figure 11 – Proliferation of HSMCs without any stimulus

Exemplary fluorescent images of cells stained with Hoechst 33342 dye are seen. The nuclei are stained blue. Knockdown cells show enhanced proliferation within 96h compared to control. Scale bars represent 100 µm.

Being a key regulator of SMC proliferation, PDGF-BB was added to the cells with concentrations varying between 5-10 ng/ml. There was no effect observed, thus the concentration was elevated to 30 ng/ml. No significant difference was observed in the proliferation rates after 96h between cells transfected with *MRAS* siRNA or control siRNA when treated with PDGF-BB (Figure 12). Furthermore, elevated rates of proliferation were observed by the addition of 10 ng/ml of TNF. The *MRAS* siRNA knockdown cells stimulated with TNF proliferated 88.2% more than the control cells with TNF (Figure 12).

Parallel to Hoechst staining, the BrdU assays were also carried out for additional validation (Figure 12). For each BrdU experiment, at each timepoint, six wells with anti-BrdU antibody were measured through a microplate reader at 450 nm, followed by readings with Hoechst 33342 dye staining. The difference of both the absorbance values was taken.

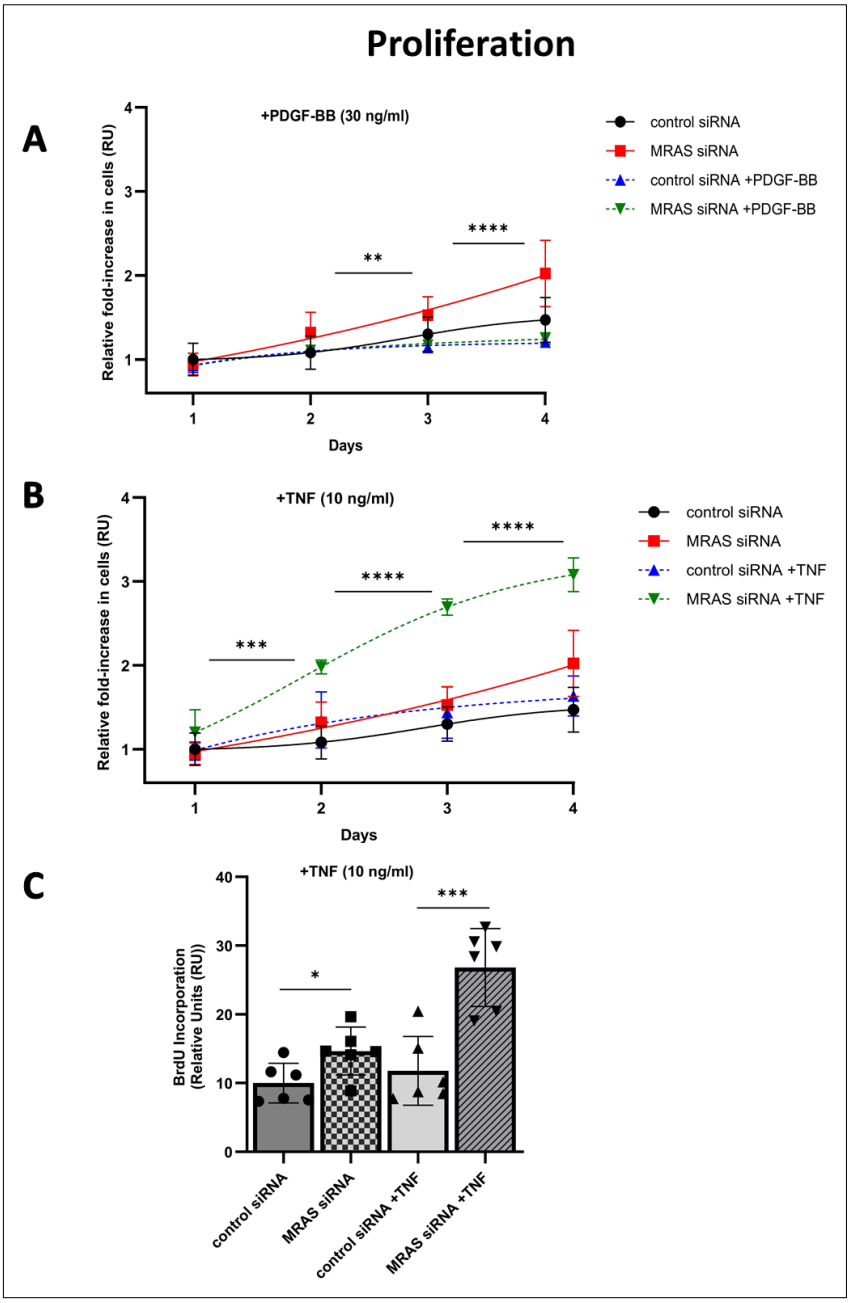

Figure 12 – Proliferation of HSMCs stimulated with PDGF-BB (A), or TNF (B+C)

A: *MRAS* siRNA transfected aortic SMCs proliferate faster than the control siRNA transfected cells, reaching about 37.4% after 96h (p = 8.65E-07). There was no significant difference observed between the *MRAS* siRNA transfected aortic SMCs stimulated with PDGF-BB (30 ng/ml) and the control siRNA transfected cells with PDGF-BB even after 96h (Day 4) (p = 0.105). Significance asterisks shown correspond to the difference between control and *MRAS* siRNA transfected cells at day 2 and day 4. **B:** *MRAS* siRNA transfected aortic SMCs stimulated with TNF (10 ng/ml) proliferate extra faster than the control siRNA transfected cells with TNF, reaching about 88.2% after 96h (p = 2.47E-10). Significance asterisks shown correspond to the difference between control siRNA + TNF cells and *MRAS* siRNA cells + TNF at day 2, 3 and 4. Linear regression analysis was performed resulting in formation of lines connecting all the values. Each dot is the mean value of values per well per day. The experiment was technically repeated 7-9 times. **C:** BrdU assay validation of cells showing *MRAS* siRNA transfected aortic SMCs stimulated with TNF proliferate faster than the control siRNA transfected cells with TNF, reaching about 26.8% (p = 0.0006). The box plot for control and *MRAS* siRNA transfected cells with stimulation by TNF in the BrdU assay has data points representing an average of all experiments. Each point represents the mean of the proliferation rate per condition per well in a technical replicate experiment. The horizontal bars show the standard deviation of the data. The experiment was technically repeated 4-6 times. Student's two-sided t-test and two-way ANOVA was carried out to determine the significance (*p<0.05; **p<0.01; ***p<0.001; ****p<0.0001).

Besides TNF, pro-inflammatory cytokines that play an important role in regulating inflammation, apoptosis and cell proliferation, IL-6 and IL-1ß were also separately added to the cells with concentrations varying between 1-10 ng/ml. The optimal concentration for proliferation assay for both the cytokines was 10 ng/ml. IL-6 treated *MRAS* siRNA transfected cells proliferated 60.0% (Figure 13) more than control cells after 96h (n = 7-9, p = 2.43E-18). *MRAS* siRNA transfected cells stimulated with IL-1ß had a proliferation rate of 30.0% after 96h more than control siRNA transfected cells with IL-1ß (n = 7-9, p = 0.00062) (Figure 13).

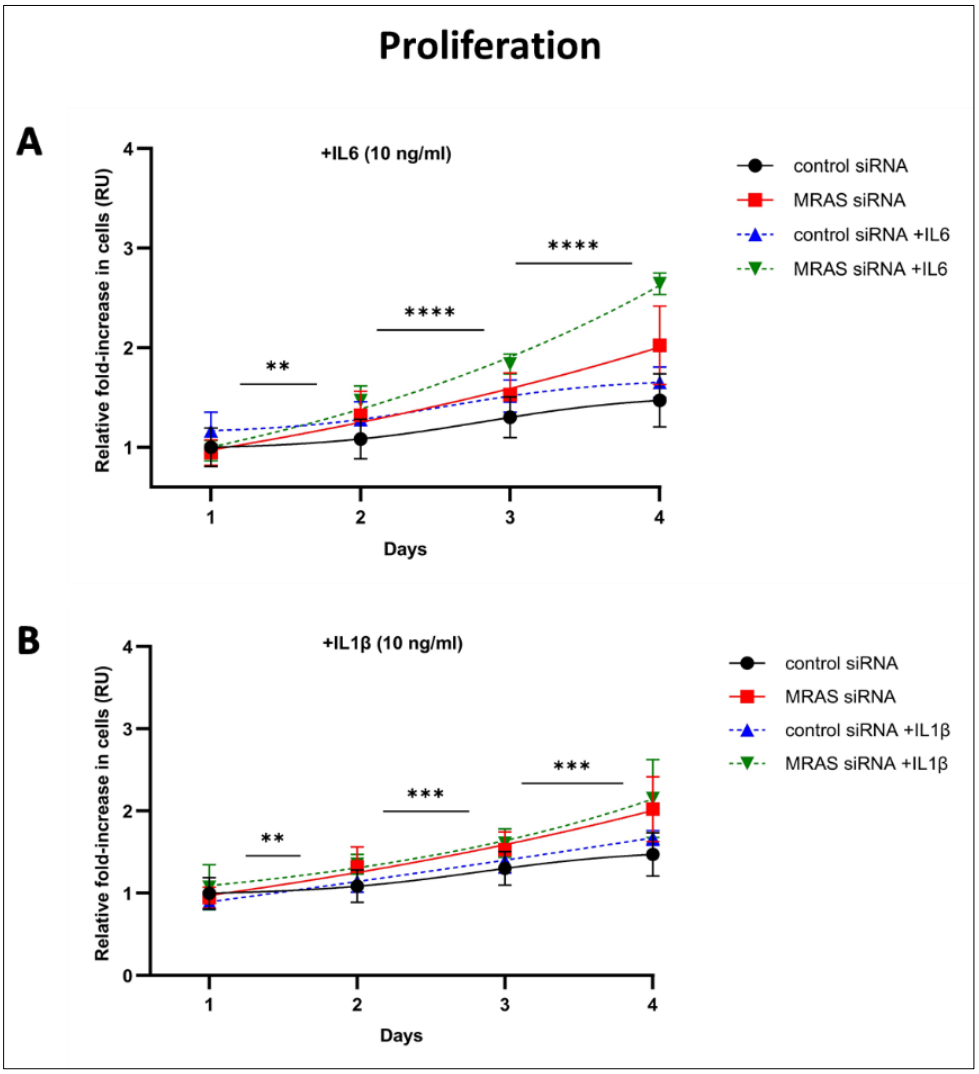

Figure 13 – Proliferation of HSMCs stimulated with IL-6 (A) and IL-1ß (B)

A: *MRAS* siRNA transfected aortic SMCs stimulated with IL-6 (10 ng/ml) proliferate faster than the control siRNA cells with IL-6, reaching about 60.0% after 96 h (p = 2.43E-18). Significance asterisks shown correspond to the difference between control siRNA + IL-6 cells and *MRAS* siRNA cells + IL-6 at day 2, 3 and 4. **B:** *MRAS* siRNA+ IL-1ß (10 ng/ml) proliferate slightly faster than the control siRNA transfected cells with IL-1ß, reaching about 30.0% after 96 h (p = 0.00062). Significance asterisks shown correspond to the difference between control siRNA + IL-1ß cells and *MRAS* siRNA cells + IL-1ß at day 2, 3 and 4. Linear regression analysis was performed resulting in formation of lines connecting all the values. Each dot is the mean value of values per well per day. The experiment was technically repeated 7-9 times. The horizontal bars show the standard deviation of the data. Each dot represents a technical replicate, and is the mean value of values per well. Student's two-sided t-test and two-way ANOVA was carried out to determine the significance (**p<0.01; ***p<0.001; ****p<0.0001).

5.1.4 Knockdown of *MRAS* leads to lower Apoptosis

Besides, migration and proliferation, a cell senescence assay like apoptosis was also performed to assess the effect of siRNA knockdown in cells on programmed cell death. Apoptosis and proliferation are opposing but complementary process in SMCs; thus, these assays are used together to understand the balance between cell death and growth in SMCs under different conditions. Both processes contribute to the maintenance of healthy blood vessels, and any imbalance between them can cause development of vascular diseases.

The SMCs were seeded into 6-well plates, starved with media containing 0.2% FBS, and left to grow for 48 h. Then, $2x10^6$ cells/well were lysed resulting in 1-4 mg/ml of protein. For each experiment, six wells with DTT and DEVD-p-nitroaniline treatment were measured through an microplate reader at 405 nm, followed by readings for control samples (no apoptosis). The difference of both the absorbance values was taken, thus the Caspase-3 activity was measured in each sample.

Lower caspase-3 activity (0.05-fold) was observed in *MRAS* siRNA transfected SMCs compared to control siRNA transfected samples (0.21-fold) (Figure 14).

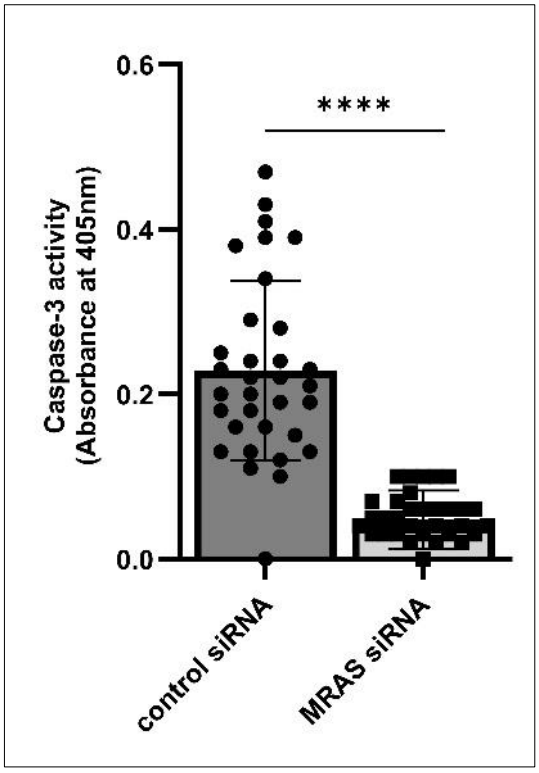

Figure 14 – Apoptosis of siRNA mediated knockdown HSMCs without any stimulus

MRAS siRNA knockdown aortic SMCs have less apoptotic activity as compared to the control cells (p = 3.66E-13). Each dot represents a readout, and is the mean value of two values per technical experiment. This experiment was repeated technically 4-6 times. The horizontal bars represent the standard deviation of the data. A two-sided Student's t-test was carried out to determine the significance (****p<0.0001).

5.1.5 Protein Expression Levels of *MRAS* in Human SMCs

The gene expression of *MRAS* and the successful siRNA knockdown was confirmed with qPCR and western blot analysis. In addition, the protein levels of the *MRAS* gene with and without TNF stimulation was quantified using western blot analysis (Figure 15). This experiment was technically repeated for three times.

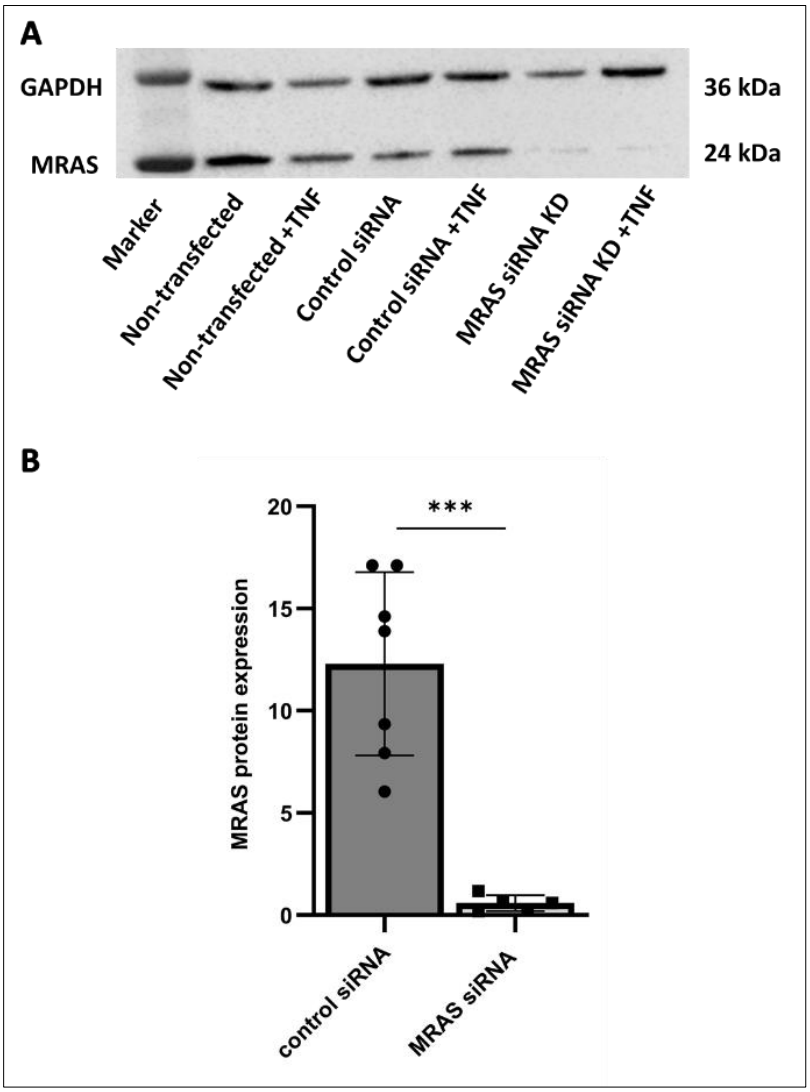

Figure 15 – Protein expression of TNF stimulated SMCs with and without MRAS siRNA transfection

A: Shown here is an exemplary western blot image used for analysis of total protein extract from SMCs from a non-transfected sample, a control siRNA transfected sample, an *MRAS* siRNA transfected sample, a non-transfected treated with TNF, a control siRNA stimulated with TNF, and an *MRAS* siRNA +TNF sample. GAPDH was used as an internal standard (house-keeping gene). *MRAS* siRNA transfected samples show less protein expression of MRAS. **B:** Quantification of western blot was performed. Values from SMCs stimulated with TNF and SMC without stimulation were combined as TNF had no obvious effect on MRAS protein expression. Data is presented in bar diagrams mean ± SD; (n=3, ***$p<0.001$).

5.2 Overexpression of *MRAS*

To confirm the effects of siRNA- mediated knockdown on SMC proliferation and migration, experiments to overexpress *MRAS* were conducted. This approach showed the reverse effect providing a clear understanding of the *MRAS* gene.

GFP plasmid was used as a control to detect immunofluorescence in the cells (Figure 16) and the intensity and percentage of efficient transfection of the plasmid into the cells via Amaxa Nucleofection. Geneticin was used as a selection marker to enhance the survival and efficiency of only those cells that were containing the plasmid (Figure 16).

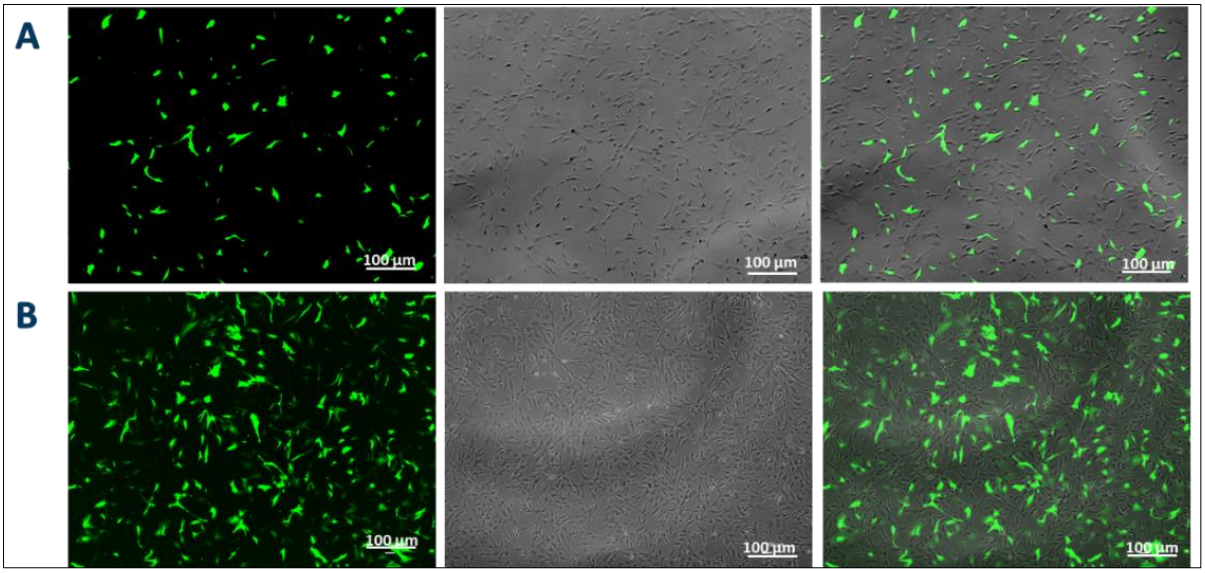

Figure 16 – Immunofluorescent and bright field images of day 1 (A) and day 5 (B) of overexpression with GFP

A: Exemplary immunofluorescent and bright field images of SMCs overexpressing the GFP plasmid at day 1 (24h). **B:** Addition of 0.6 mg/ml selection marker (Geneticin G418) increases the number of GFP- positive cells at day 5.

5.2.1 Overexpression of *MRAS* reduces SMC Migration

Approximately $1.2x10^4$ cells/well were taken in each well and transfected with (1-5 µg) of each plasmid (pCMV6-GFP, pCMV6-empty, pCMV6-MRAS; clone 1 or 2). GFP plasmid was used as control to visually depict the overexpression of the plasmid into the cells. Migration assays were performed as described above for *MRAS* knockdown experiments (5.1.2 *MRAS* Deficiency leads to increased SMC Migration. SMCs overexpressing *MRAS* had the lowest migration rate (34.4%) and were very slow whereas the empty plasmid overexpressing cells had the highest migration rate (91.5%) (Figure 17). Similar to the siRNA-mediated knockdown experiments, PDGF-BB (10 ng/ml) was added to test the different conditions and effect on the overexpressed SMCs. With addition of this stimulus, cells overexpressing *MRAS* were migrating slower than cells expressing empty and GFP plasmids (Figure 17).

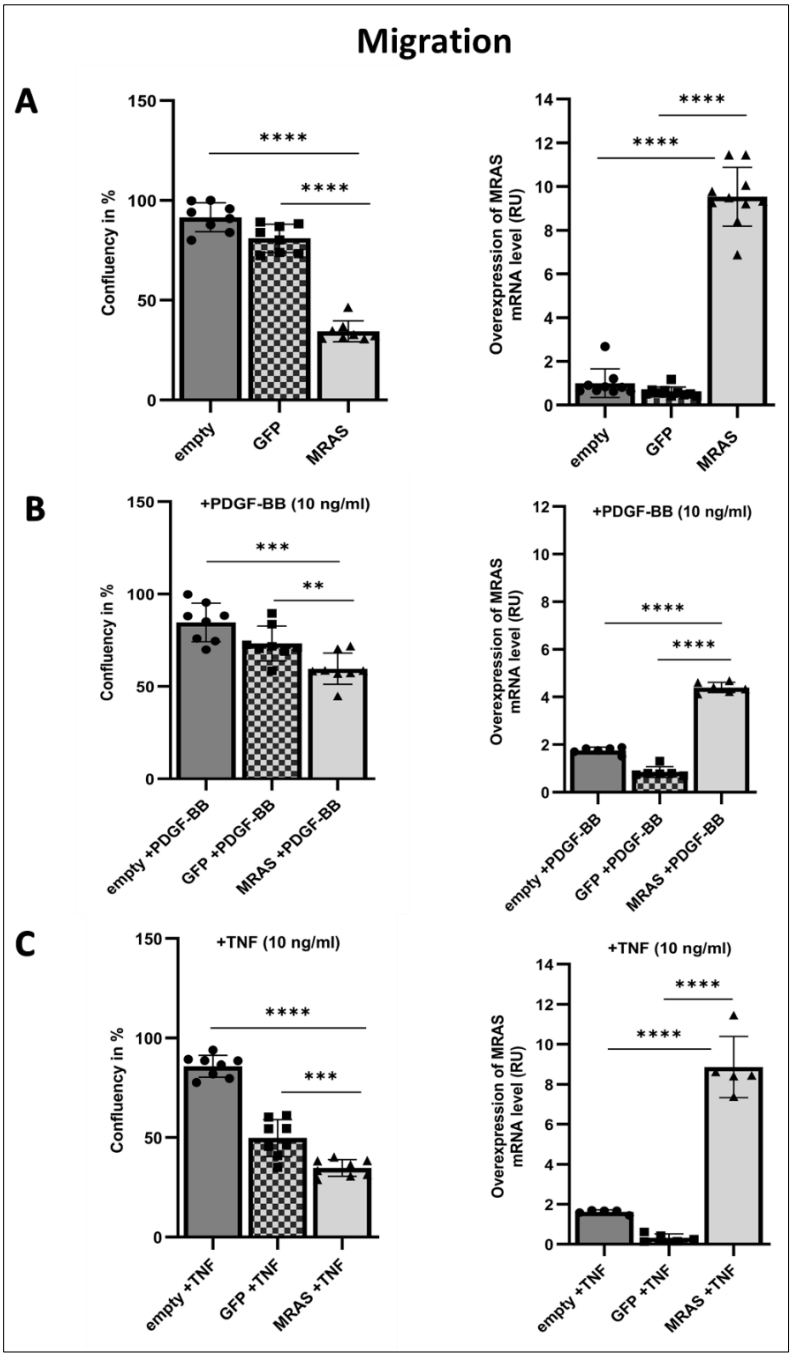

Figure 17 – Migration and mRNA expression level of overexpressed HSMCs without stimulus (A), stimulation of PDGF-BB (B) and TNF (C)

A (left): Cells with overexpressed MRAS plasmid migrated very slowly (34.4%) compared to empty (91.5%) and GFP expressed cells (81.02%) after 24h (p = 4.49E-11). **A (right):** mRNA levels of empty, GFP and *MRAS* cells without any stimulus were assessed by measuring the percentage of gene expression in each sample. **B (left):** Cells with overexpressed *MRAS* treated with PDGF-BB (10 ng/ml) migrated less (59.6%) compared to empty (84.6%) and GFP expressed cells (73.25%) after 24h (p = 0.0001). **B (right):** mRNA levels of GFP, *MRAS* and empty plasmid stimulated with PDGF-BB were assessed by measuring the percentage of gene expression in each sample. **C (left):** Cells with overexpressed MRAS plasmid treated with TNF (10 ng/ml) migrated gradually (34.7%) compared to empty (85.7%) and GFP expressed cells (49.7%) after 24 h (p = 5.88E-12). **C (right):** mRNA levels of all three plasmids treated with TNF were assessed by measuring the percentage of gene expression in each sample. The box plot represents the data as an average of all experiments. Each point represents the mean of the migration rate/ confluency in % per well analysed. The horizontal bars show the standard deviation of the data. The experiment was technically repeated 7-9 times. Student's two-sided t-test and two-way ANOVA was carried out to determine the significance (*p<0.05; **p<0.01; ***p<0.001; ****p<0.0001).

Furthermore, TNF playing a significant role in the biology of SMCs, in context of vascular diseases and inflammation, was also added to the overexpressed cells to observe the effect of TNF on migration of cells. SMCs overexpressed with *MRAS* stimulated with TNF migrated with the lowest rate (34.7%) compared to SMCs with overexpressed GFP (49.7%) and empty plasmid (85.7%) ($p = 5.88E-12$) (Figure 17).

5.2.2 Overexpression of *MRAS* in Human SMCs reduces Proliferation Rates

Transfection of SMCs and cellular proliferation was obtained via nuclei counting, as described above **(**5.1.3 Downregulation of *MRAS* in Human SMCs increases Proliferation and **(**4.5.2 Proliferation Assay.

Overexpression of *MRAS* in human SMCs displayed a significant decrease in cell proliferation rates. *MRAS* thus acted as a negative regulator of the cell cycle progression in SMCs. $0.4x10^4$ cells/well were taken in each well and transfected with 1-5 µg of each plasmid (pCMV6-GFP, pCMV6-empty, pCMV6-MRAS; clone 1 or 2). GFP plasmid was used as control to visually depict the overexpression of the plasmid into the cells.

MRAS overexpressing cells depicted slow proliferation rates without any stimulus (Figure 18) and with addition of PDGF-BB (30 ng/ml) or TNF (10 ng/ml). SMCs overexpressing *MRAS* stimulated with TNF declined in cell number (10.5%) and those cells that were treated with PDGF-BB proliferated only 20% (Figure 18). On the other hand, SMCs overexpressing empty plasmid cells with TNF had 60.2% proliferation (Figure 18) and with PDGF-BB, 72.0% proliferation was depicted respectively ($n = 4-6$).

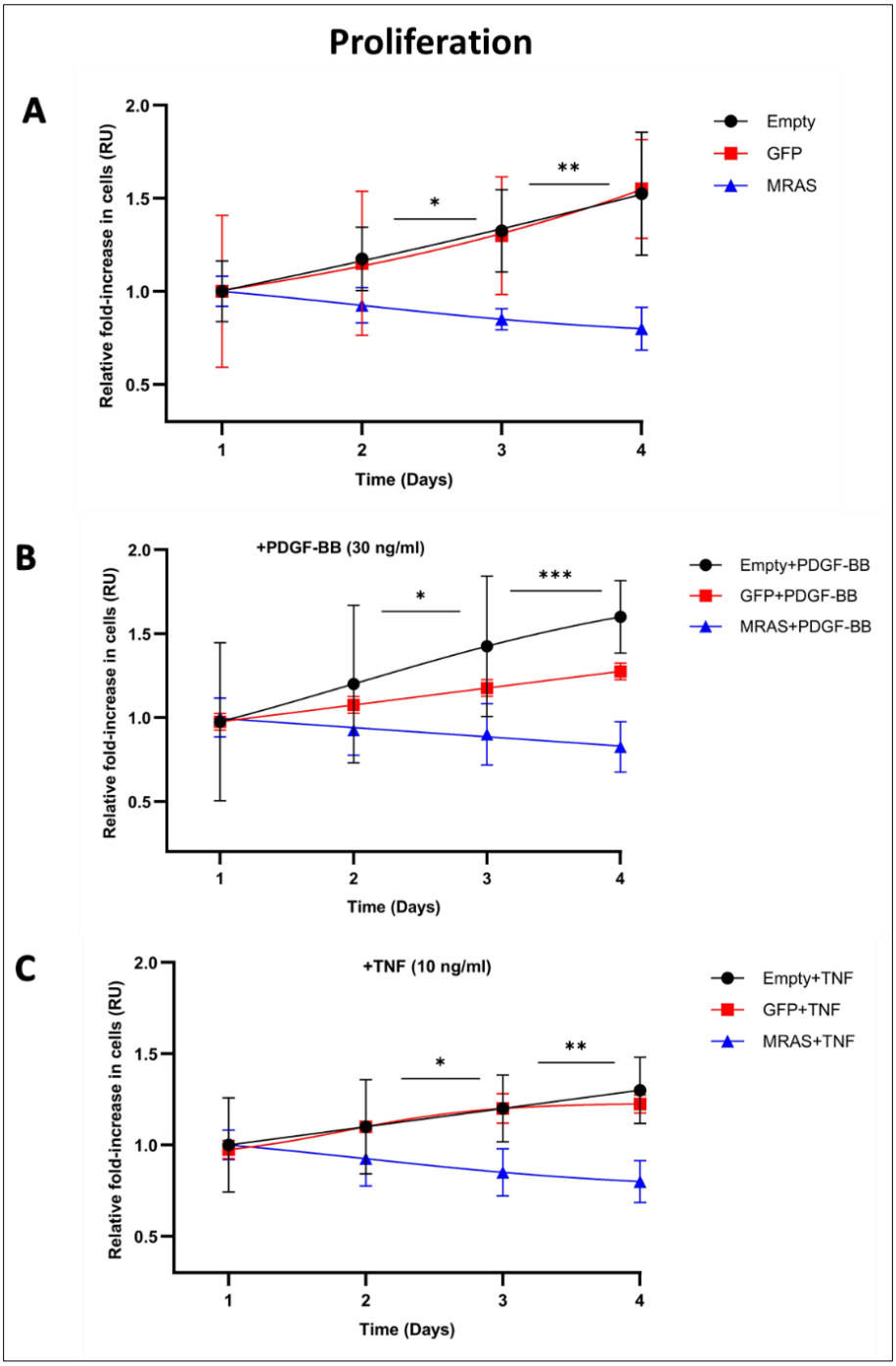

Figure 18 – Proliferation of overexpressed HSMCs without stimulus (A) & stimulation of PDGF-BB (B), & TNF (C)

A: SMCs overexpressing *MRAS* cells proliferated very slowly (10.5%) compared to empty (60.8 %) and GFP expressed cells (58.8%) after 96 h ($p = 0.004$). Significance asterisks shown correspond to the difference between empty and MRAS plasmid at day 2 and 4. **B:** There was strong difference between the proliferation rate of cells with overexpressed empty plasmid +PDGF (84.0%) and GFP expressed cells (73.0 %) compared to *MRAS* (50.0%) after 96 h ($p = 0.001$). Significance asterisks shown correspond to the difference between empty and MRAS plasmid, both stimulated with PDGF-BB at day 2 and 4. **C:** SMCs overexpressing empty plasmid +TNF (70.7 %) and GFP expressed cells (65.2 %) proliferated highly compared to *MRAS* (44.0 %) after 96 h ($p = 0.002$). Significance asterisks shown correspond to the difference between empty and MRAS plasmid, both stimulated with TNF at day 2 and 4. Linear regression analysis was performed resulting in formation of lines connecting all the values. Each dot is the mean value of values per well per day. The experiment was technically repeated 4-6 times. The horizontal bars show the standard deviation of the data. Each dot represents a technical replicate, and is the mean value of values per well. Student's two-sided t-test and two-way ANOVA was carried out to determine the significance (*$p<0.05$; **$p<0.01$; ***$p<0.001$; ****$p<0.0001$).

5.2.3 Overexpression of *MRAS* leads to higher Apoptosis

Analogous to siRNA knockdown experiments **(Section 5.1.4)**, apoptosis was carried out for the overexpressed cells as well. The caspase-3 colorimetric assay was conducted to check the effect of overexpression on apoptosis of SMCs.

The SMCs overexpressing *MRAS* and empty were seeded separately into 6-well plates, starved with 0.2% FBS media and grown for 48h. Approximately $2x10^6$ cells/well were lysed resulting in 1-4 mg/ml protein yield, which was further subjected to DTT and DEVD-p-nitroaniline treatment. Measurements were taken with a microplate reader at 405 nm. Control samples with no apoptosis were also measured and the difference of both the absorbance values was taken to measure the Caspase-3 activity in each sample.

Elevated caspase-3 activity (0.25-fold) was observed in SMCs overexpressing *MRAS* compared to SMCs overexpressing empty (0.05-fold) (Figure 19).

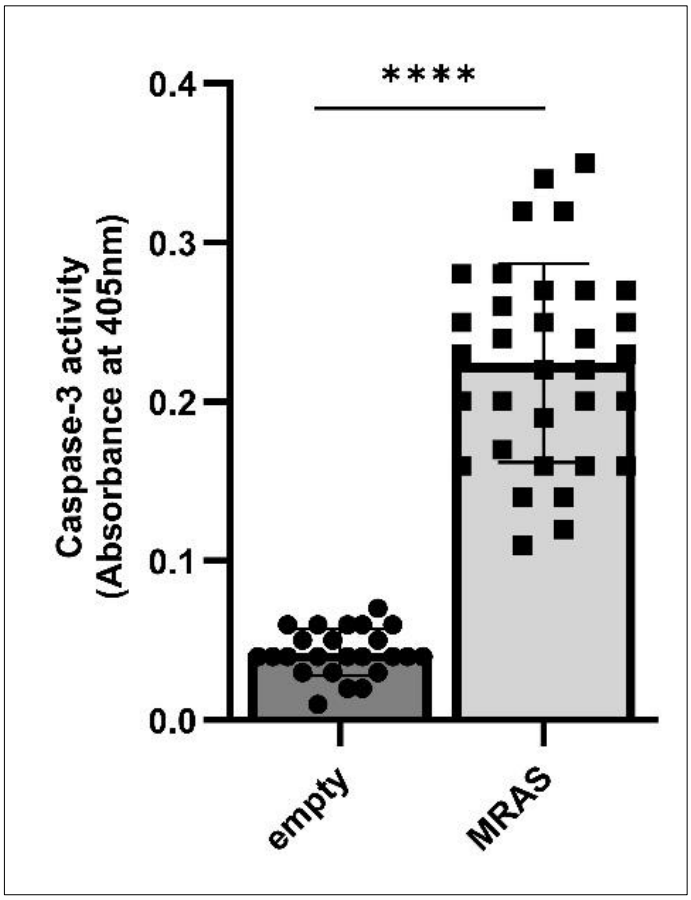

Figure 19 – Apoptosis of overexpressed HSMCs without any stimulus

SMCs overexpressing *MRAS* have higher apoptotic activity as compared to the SMCs overexpressing empty plasmid (p = 1.10E-19). Each dot represents a readout, and is the mean value of two values per technical experiment. This experiment was repeated technically 4-6 times. The horizontal bars represent the standard deviation of the data. A two-sided Student's t-test was carried out to determine the significance (****p<0.0001).

5.3 *Mras* Knockout Mice

Murine SMCs isolated from *Mras* and *ApoE* double knockout mice and *B6.ApoE*$^{-/-}$ wild-type controls mice were subjected to migration, proliferation and apoptosis assays to confirm the findings from the experiments with human SMCs.

5.3.1 Knockout of *Mras* promotes SMC migration in Mice

Mras's role as a key regulator of cellular motility is evident when murine cells exhibit enhanced migratory behaviour following the knockout of *Mras*. *B6.ApoE*$^{-/-}$ were wild-type and *Mras*$^{-/-}$*ApoE*$^{-/-}$ double knockout mice (dKO) were the knockout type.

Cellular migration was observed in murine SMCs similar to the human SMCs migration assays as stated above **(Sections 5.1.2 & 5.2.1).**

As SMC migration is regulated by several signalling pathways including the TNF-adhesion signalling, PI3K/Akt and MAPK/ERK pathways, pro-inflammatory cytokines like TNF, IL-6 and IL-1ß were added to the murine SMCs to determine the effect of these stimuli on the migration of cells. These cytokines enhance SMC migration particularly in inflammatory conditions associated with vascular diseases.

As murine cells were smaller in size compared to human cells, approximately 2.2×10^4 cells/well were taken in each well with controls (no stimulation) and samples stimulated with divergent stimuli like TNF (10 ng/ml), IL-6 (5 ng/ml) and IL-1ß (5 ng/ml) respectively.

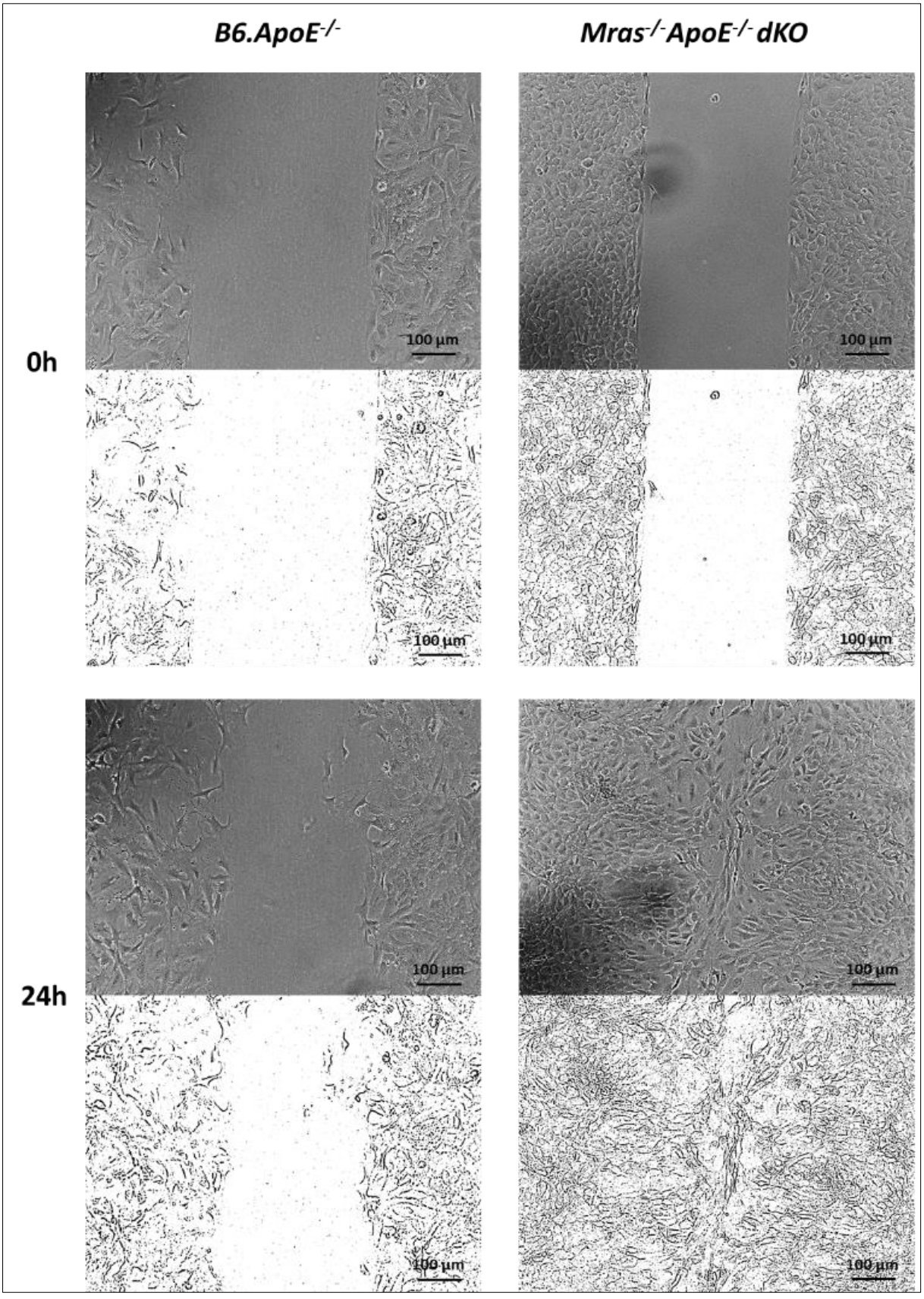

Figure 20 – Migration of MSMCs

Exemplary bright field and corresponding contour images of *B6.ApoE*$^{-/-}$ wild-type and *Mras*$^{-/-}$*ApoE*$^{-/-}$ double knockout SMCs. Knockout cells show strong migration within 24h. Scale bars represent 100 µm.

qPCR validation was performed to validate the complete knockout of gene. mRNA expression level was assessed by measuring the gene expression of *Mras* in each sample (Figure 21). Knockout of *Mras* promotes migration in SMCs, no matter, in every condition. Stimulation of knockout with TNF resulted in 76.9% migratory rate of SMCs (Figure 21) compared to wild type cells with TNF (23.2%). Significantly elevated migration rates were observed in response to stimulation with IL-6 (95.2%) (Figure 21) and IL-1ß (90.1%) (Figure 21) in knockout SMCs, indicating the crucial role of these pro-inflammatory cytokines in the behaviour of SMCs. In wild-type cells stimulated with IL-6 and IL-1ß, 88.3% and 76.0% migratory rates were observed respectively.

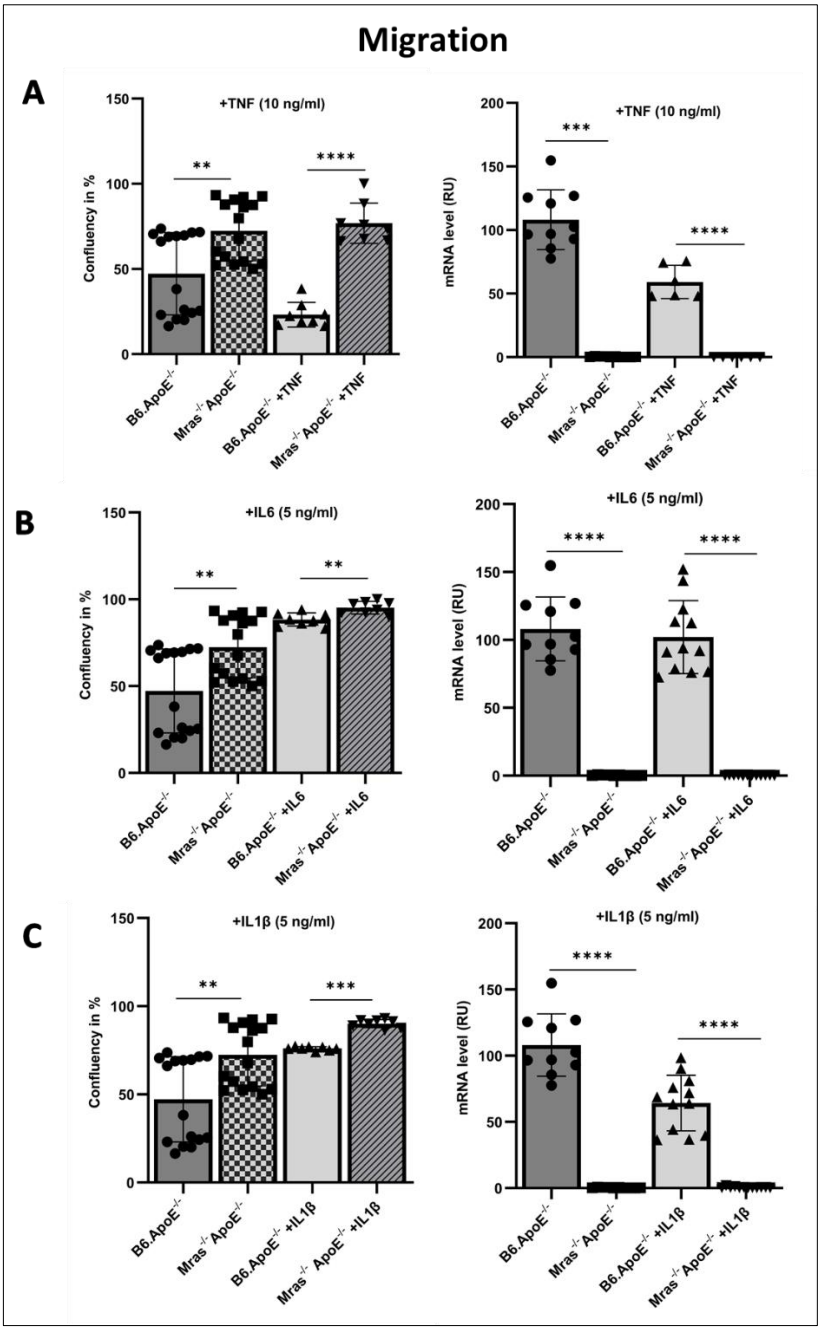

Figure 21 – Migration and mRNA expression level of MSMCs stimulated with TNF (A), IL-6 (B), and IL-1ß (C)

A (left): *Mras*$^{-/-}$*ApoE*$^{-/-}$ dKO aortic SMCs stimulated with TNF (10 ng/ml) migrate rapidly than the *B6.ApoE*$^{-/-}$ wild-type murine cells with TNF (23.2%), reaching about 76.9% after 24h (p = 3.07E-08). **A (right):** mRNA levels of SMCs for both genotypes stimulated with TNF were assessed by measuring the percentage of gene expression level in each sample. **B (left):** *Mras*$^{-/-}$*ApoE*$^{-/-}$ dKO SMCs stimulated with IL-6 (5 ng/ml) migrate quickly than the *B6.ApoE*$^{-/-}$ murine cells with IL-6, reaching about 95.2% after 24h (p = 0.002). **B (right):** mRNA levels of cells stimulated with IL-6 were assessed by measuring the percentage of gene expression level in each sample. **C (left):** *Mras*$^{-/-}$*ApoE*$^{-/-}$ dKO SMCs stimulated with IL-1ß (5 ng/ml) tend to migrate quicker than the *B6.ApoE*$^{-/-}$ control cells with IL-1ß, reaching about 90.1% after 24h (p = 3.19E-10). **C (right):** mRNA levels of IL-1ß treated murine SMCs were assessed by measuring the percentage of gene expression level in each sample. The box plot for *B6.ApoE*$^{-/-}$ wild type cells and *Mras*$^{-/-}$*ApoE*$^{-/-}$ dKO SMCs without any stimulus in the migration assays contain more data points compared to each stimulus- (TNF, IL-6 and IL-1ß) treated sample because the data represents an average from all experiments. Each point represents the mean of the migration rate/ confluency in % per well analysed. The horizontal bars show the standard deviation of the data. The experiment was technically repeated 7-9 times. Student's two-sided t-test and two-way ANOVA was carried out to determine the significance (**p<0.01; ***p<0.001; ****p<0.0001).

5.3.2 Knockout of *Mras* elevates Rate of Proliferation

In murine cells, proliferation was also conducted through Hoechst 33342 staining by visualizing and counting cell nuclei analogous to human cellular proliferation assays as stated above **(**5.1.3 Downregulation of *MRAS* in Human SMCs increases Proliferation & 5.2.2 Overexpression of *MRAS* in Human SMCs reduces Proliferation RatesApproximately 0.9-1.2x10^4 cells/well were taken in each well for the Hoechst 33342 staining assay (Figure 22) with controls (no stimulation) and samples stimulated with TNF (10 ng/ml), IL-6 (10 ng/ml) and IL-1ß (10 ng/ml) separately.

Mras$^{-/-}$*ApoE*$^{-/-}$ dKO SMCs proliferated rapidly in comparison to *B6.ApoE*$^{-/-}$ wild-type cells. When stimulated with TNF (10 ng/ml), IL-6 (10 ng/ml) and IL-1ß (10 ng/ml), the proliferation rates of knockout SMCs were highly elevated (Figure 23). The highest proliferation rate was observed in knockout cells stimulated with TNF (78.7%), followed by IL-6 (50.6%) and lastly IL-1ß (14.8%).

Alternatively, BrdU incorporation was also assessed by measuring DNA synthesis during the S phase of the cell cycle by incorporating bromodeoxyuridine (BrdU) into newly synthesized DNA. 0.9x10^4 cells/well were taken in each well. Six wells with BrdU staining were measured for each timepoint, followed by measurement with a microplate reader at 450 nm. The same wells were stained additionally with Hoechst 33342 dye and fluorescence intensity measured with a microplate reader at 360 nm. The difference of both the absorbance values was taken (Figure 24).

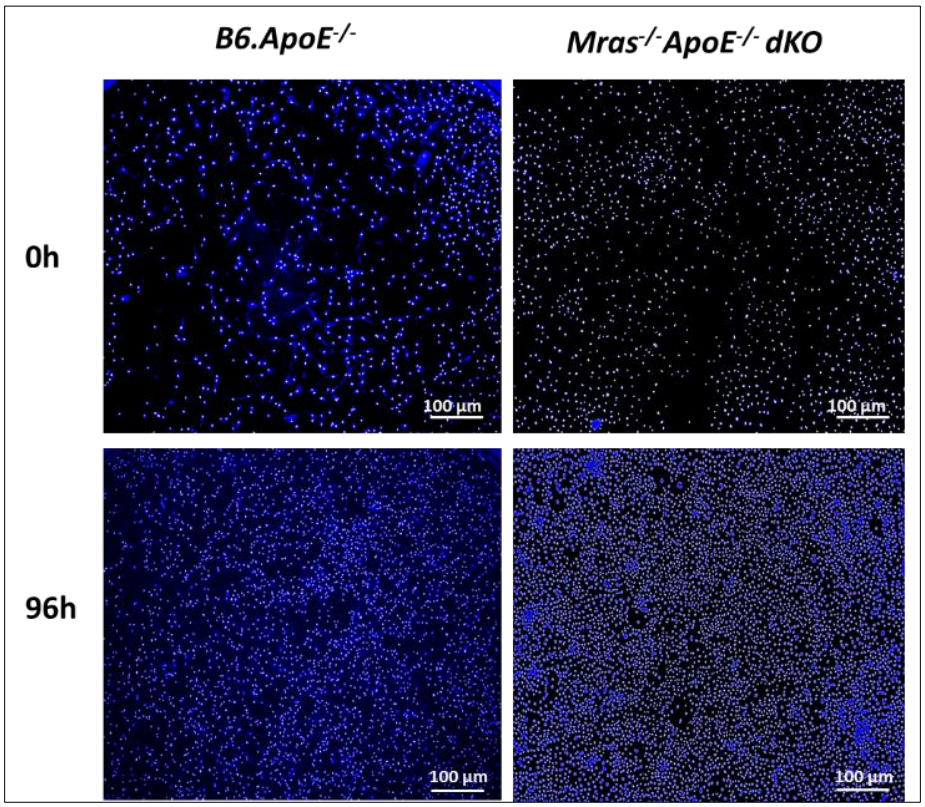

Figure 22 – Proliferation of MSMCs

Exemplary fluorescent images of cells stained with Hoechst 33342 dye are seen. The nuclei are stained blue. Knockout cells show enhanced proliferation within 96h compared to control. Scale bars represent 100 µm.

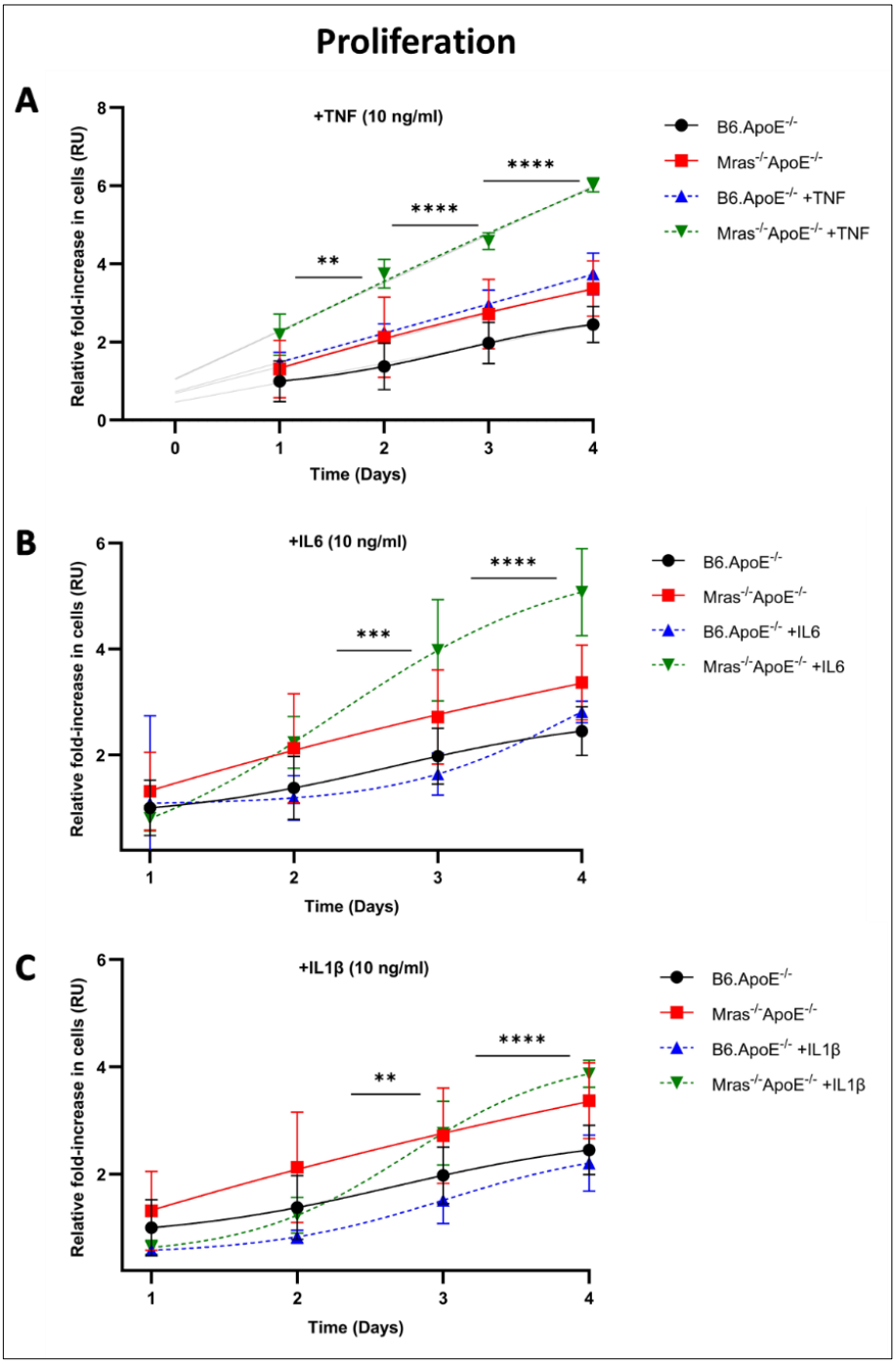

Figure 23 – Proliferation of MSMCs stimulated with TNF (A), IL-6 (B) and IL-1ß (C)

A: *Mras*$^{-/-}$*ApoE*$^{-/-}$ dKO SMCs stimulated with TNF (10 ng/ml) proliferate extra quicker than the *B6.ApoE*$^{-/-}$ cells with TNF, reaching about 78.7% after 96 h (p = 1.95E-13). The grey lines in the figure indicate that equal number of cells were seeded on day 0 of proliferation assay. Significance asterisks shown correspond to the difference between *B6.ApoE*$^{-/-}$ cells +TNF and *Mras*$^{-/-}$*ApoE*$^{-/-}$ dKO SMCs + TNF at Day 2, 3 and 4. **B:** *Mras*$^{-/-}$*ApoE*$^{-/-}$ dKO SMCs stimulated with IL-6 (10 ng/ml) proliferate rapidly than *B6.ApoE*$^{-/-}$ cells with IL-6, reaching about 50.6% after 96 h (p = 4.77E-09). Significance asterisks shown correspond to the difference between *B6.ApoE*$^{-/-}$ cells +IL-6 and *Mras*$^{-/-}$*ApoE*$^{-/-}$ dKO SMCs + IL-6 at Day 2 and 4. **C:** *Mras*$^{-/-}$*ApoE*$^{-/-}$ dKO SMCs stimulated with IL-1ß (10 ng/ml) proliferate slightly higher than the *B6.ApoE*$^{-/-}$ control cells with IL-1ß, reaching about 14.8% after 96 h (p = 1.33E-09). Significance asterisks shown correspond to the difference between *B6.ApoE*$^{-/-}$ cells +IL-1ß and *Mras*$^{-/-}$*ApoE*$^{-/-}$ SMCs + IL-1ß at Day 2 and 4. Linear regression analysis was performed

resulting in formation of lines connecting all the values. Each dot is the mean value of values per well per day. The experiment was technically repeated 7-9 times. The horizontal bars show the standard deviation of the data. Student's two-sided t-test and two-way ANOVA was carried out to determine the significance (**p<0.01; ***p<0.001; ****p<0.0001).

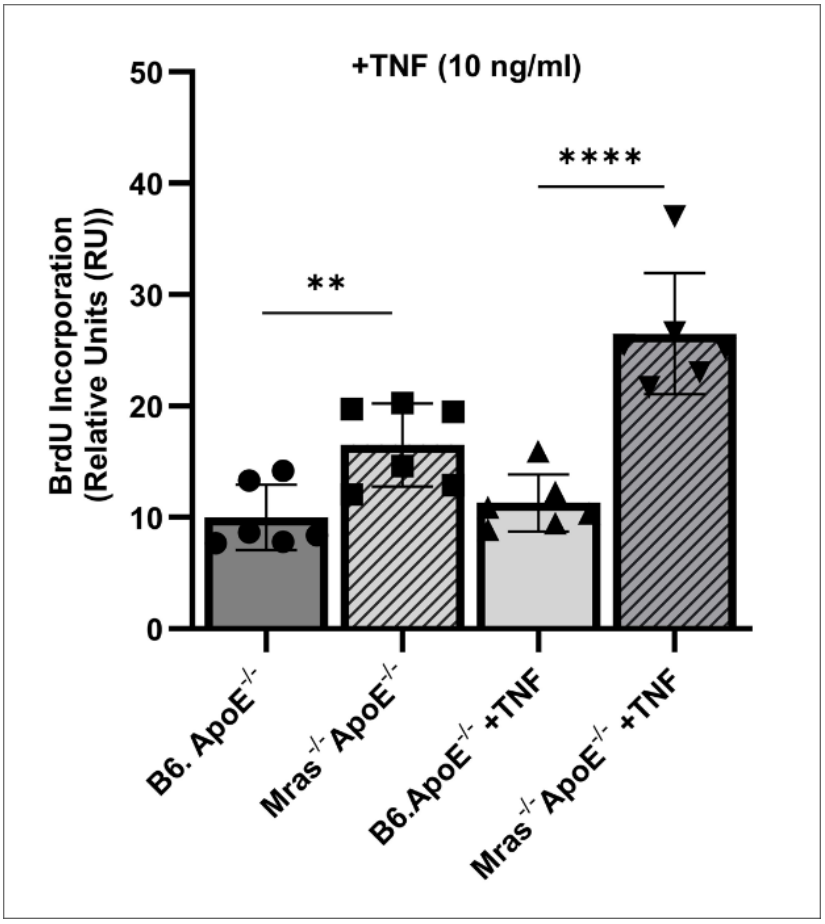

Figure 24 – BrdU proliferation assessment of MSMCs stimulated with TNF

BrdU assay resulting in *Mras*$^{-/-}$*ApoE*$^{-/-}$ dKO aortic SMCs stimulated with TNF (10 ng/ml) proliferating faster than the *B6.ApoE*$^{-/-}$ wildtype control cells with TNF, reaching about 26.49% (p = 0.0001). This experiment was technically repeated six times (n=6).

5.3.3 Knockout *Mras* SMCs reduces Caspase-3 Activity

The caspase-3 apoptosis assay was conducted to measure programmed cell death in the MSMCs similar to (5.1.4 Knockdown of *MRAS* leads to lower Apoptosis5.2.3 Overexpression of *MRAS* leads to higher Apoptosis). This colorimetric assay measured the enzymatic activity of caspase-3 using substrates release a colorimetric product upon cleavage at 405 nm. The enzyme activity between the treated and control samples was measured to determine the level of apoptosis.

The SMCs were seeded into 6-well plates, starved with media containing 0.2% FBS, and left to grow for 48h. Then, $2x10^6$ cells/well were lysed resulting in 1-4 mg/ml of protein. For each experiment, six wells with DTT and DEVD-p-nitroaniline treatment were measured through an microplate reader

at 405 nm, followed by readings for control samples (no apoptosis). The difference of both the absorbance values was taken, thus the Caspase-3 activity was measured in each sample.

Lower caspase-3 activity (0.05-fold) was observed in knockout SMCs compared to wild-type samples (0.2-fold) (Figure 25).

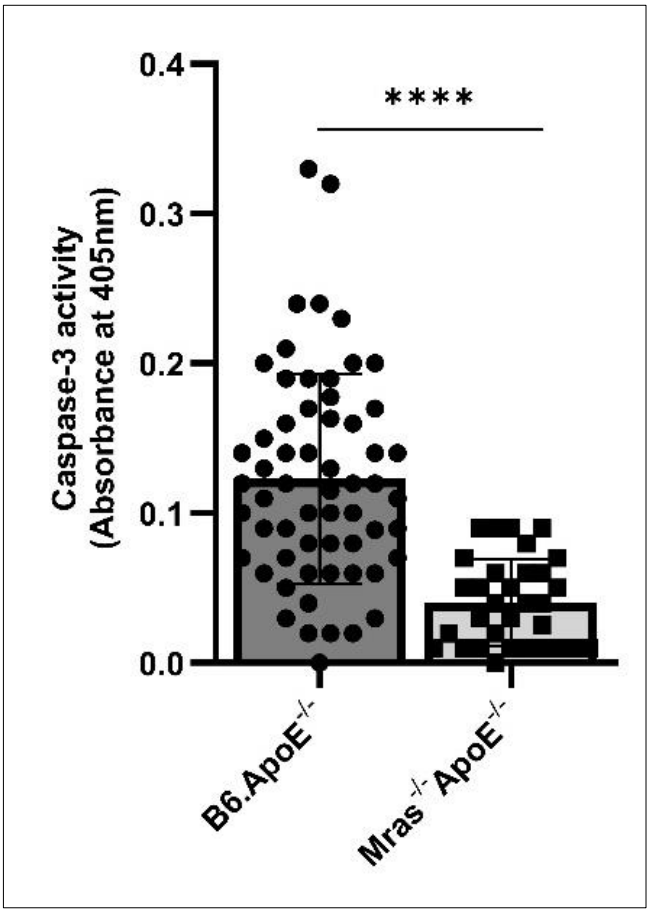

Figure 25 – Apoptosis of MSMCs

Mras$^{-/-}$*ApoE*$^{-/-}$ dKO aortic SMCs have less apoptotic activity as compared to the control cells (p = 3.47E-09). Each dot represents a readout, and is the mean value of two values per technical experiment. This experiment was repeated technically 4-6 times. The horizontal bars represent the standard deviation of the data. A two-sided Student's t-test was carried out to determine the significance (****p<0.0001).

5.3.4 Protein Expression Level of MRAS in Mice

The protein expression of MRAS in mice and the successful knockout of the complete gene was firstly confirmed through qPCR and western blot analysis. Additionally, the protein levels of the *Mras* gene with and without TNF, IL-6 and IL-1ß stimulation was quantified using western blot analysis (Figure 26). The data could not be quantified because knockout of *Mras* displayed no band. Only the wild-type samples with and without stimulation showed protein quantity and band intensity.

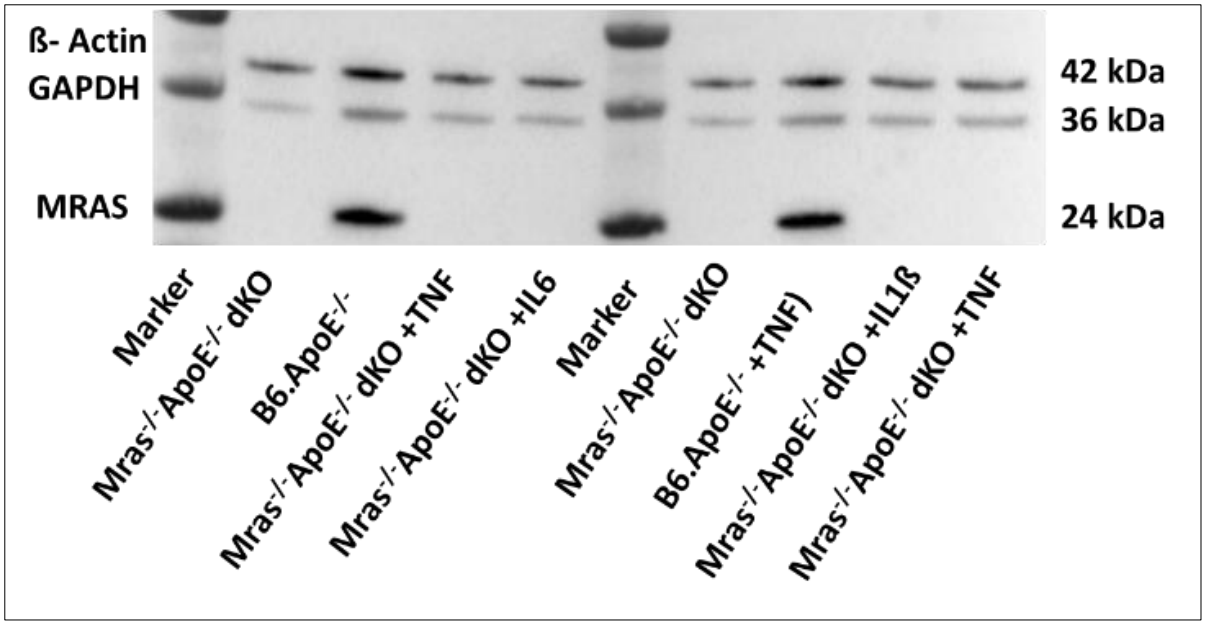

Figure 26 – Protein expression of MRAS in murine cells

Shown here is the analysis of total protein extract from SMCs from a wild-type sample, a knockout murine sample, a wild-type sample stimulated with TNF, a knockout murine sample with TNF, a knockout murine sample stimulated with IL-6, and a knockout murine sample stimulated with IL-1ß.

5.3.5 RNA Sequencing of *MRAS* in Murine SMCs

RNA sequencing was performed to study the transcriptome i.e., the complete set of RNA transcripts produced by the genome. To determine the precise quantification of gene expression levels and identify the downregulated and upregulated genes between the *B6.ApoE*$^{-/-}$ wild type samples stimulated with TNF and *Mras*$^{-/-}$*ApoE*$^{-/-}$ double knockout mice samples stimulated with TNF, RNA sequencing was performed. Ten samples (five for each condition) were sequenced using the Illumina platform and R analysis (DEseq2) (172) was performed to check for the differential gene expression in the samples.

Appropriate separation of both the groups can be seen in (Figure 27). The variation between both the groups (PC1- 90%) was higher than the variation within the groups (PC2 – 2%), indicating a higher number of differentially expressed genes (DEGs) between both the groups.

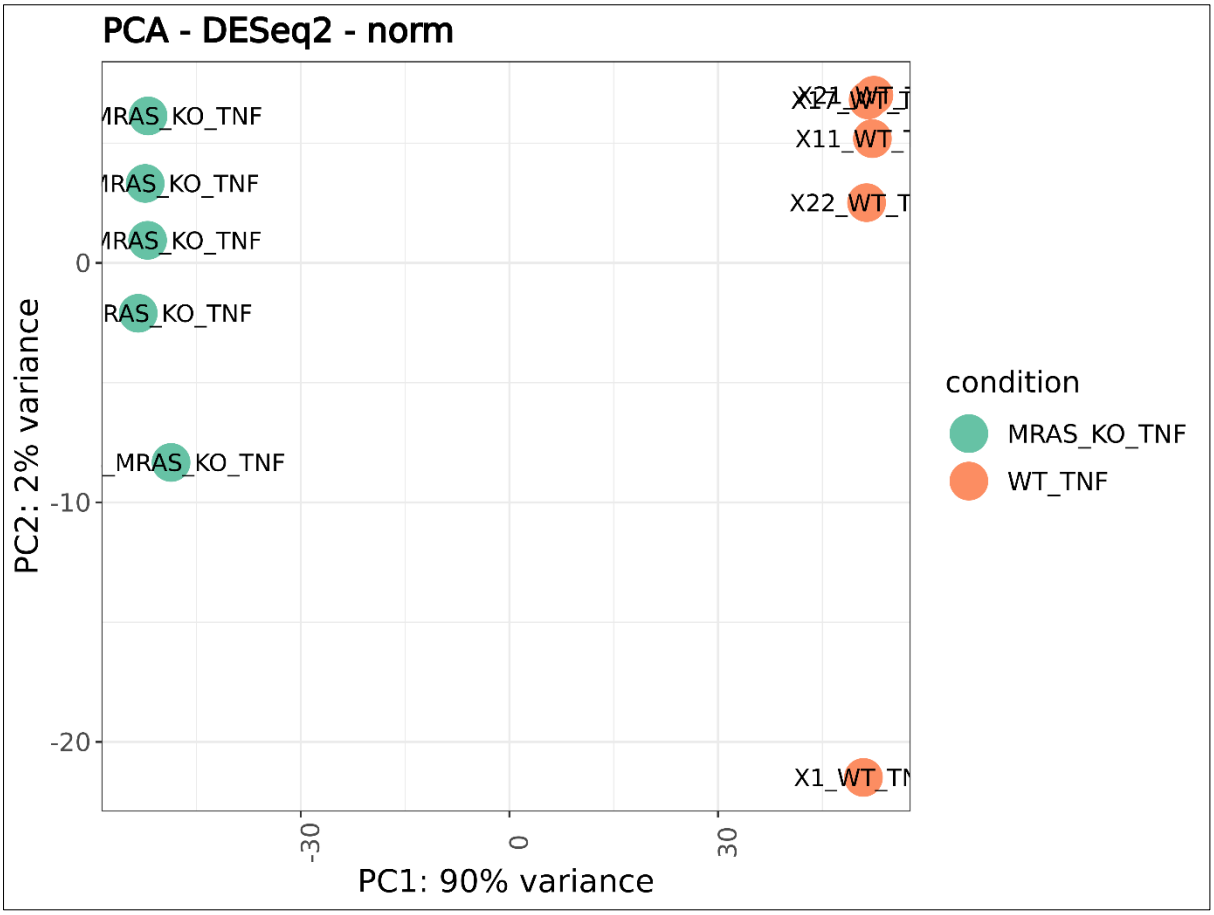

Figure 27 – Principal component analysis plot (PCA) of all samples

A: All 10 samples are plotted based on their PC1 and PC2, that are two variables displaying variance. Data points are labelled based on their conditions (green: *MRAS* knockout cells with TNF, orange: wild type murine cells with TNF).

Histograms of p values with and without adjustment (Figure 28) showed higher frequency of genes with the p value around 0 and flat distribution for higher p values. Conclusively, the data was normally distributed and indicated a large number of significant differentially expressed genes. The DEGs with adjusted p-values were 1847 and with non-adjusted p-values were 2112 in number.

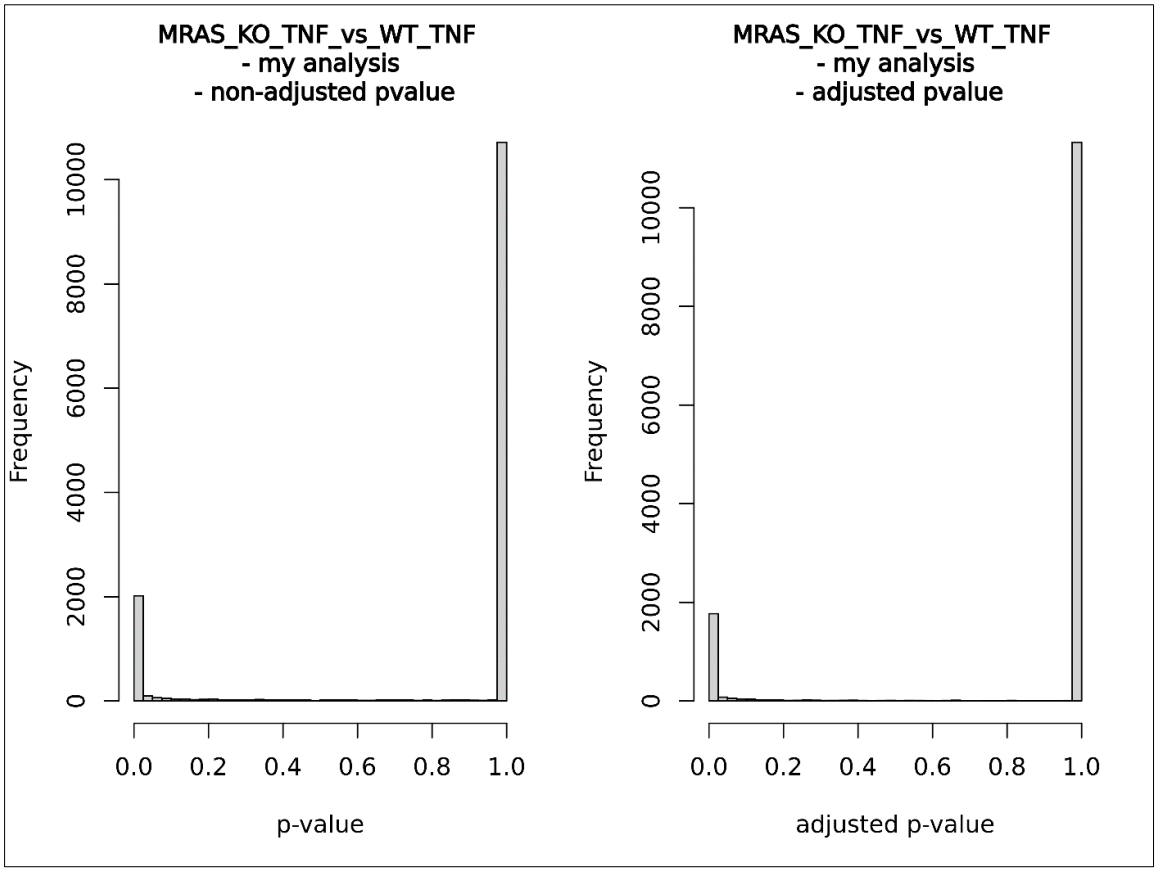

Figure 28 – Histograms of p values with and without adjustment

Two plots display the distribution of the non-adjusted p-values **(left)** and adjusted p-value for all genes **(right)**. The p value distribution towards 0 means that there are numerous significant DEGS.

Initial enrichment analysis of gene expression profiling with the gene set enrichment tool (*WebGestalt*) (173) (https://www.webgestalt.org/)) was performed. Genes downregulated in *Mras* KO SMCs (log_2(fold change) < -2) had a ratio of enrichment (Figure 29) of ~1.8 for "immune response" and "defence response". In contrast, genes that were higher expressed in *Mras* KO SMCs were enriched for "cell adhesion" and "cell-cell signalling". This can be interpreted to mean that the absence of *Mras* makes murine SMCs more sensitive to "internal"/paracrine signals from neighbouring cells than to "external" stimuli, e.g., originating from bacteria (Figure 30).

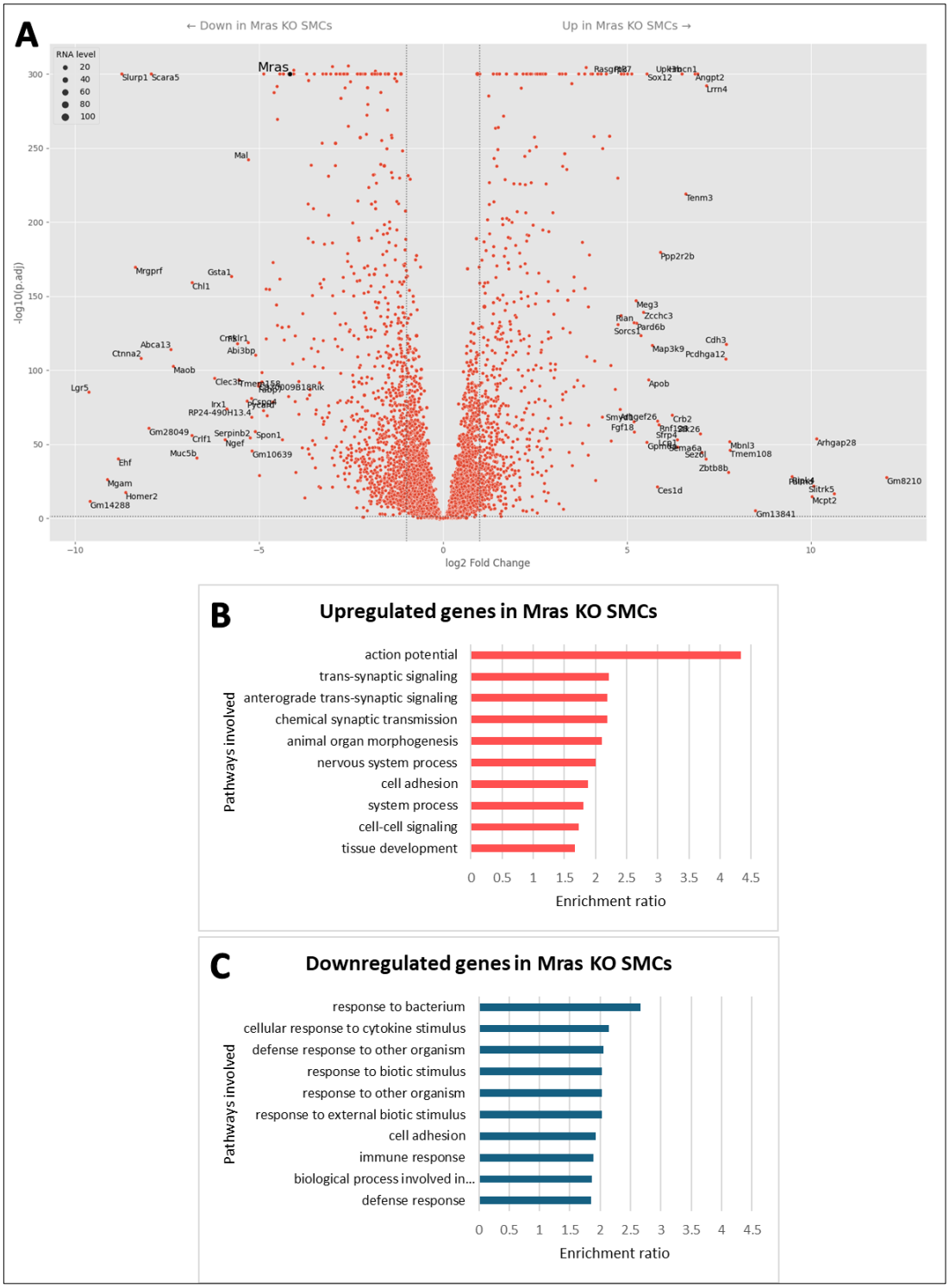

Figure 29 – Volcano plot (A), upregulated genes in *Mras* KO (B) & downregulated genes in *Mras* KO SMCs (C)

A: Scatter plot showing statistical significance (adjusted p-values) vs. magnitude of change (log2 fold change). Each point on the graph represents a gene. A positive fold change with upregulated genes in KO murine SMCs are illustrated to the right of the zero. A negative fold change with downregulated genes are located to the left of the zero on x-axis. Higher statistically significant genes are depicted at the top part along the y-axis (lower p-values). **B:** Bar chart plots the enrichment results vertically with the bar width equal to enrichment ratio. Ratio of enrichment = the number of observed genes divided by the number of expected genes from each KEGG category in the list (according to WebGestalt (173) or alternatively GSEA, or GOTM tools) . The signalling pathways/processes involving the upregulated genes in *Mras* KO SMCs and their enrichment ratios. **C:** The downregulated genes and their ratios of enrichment.

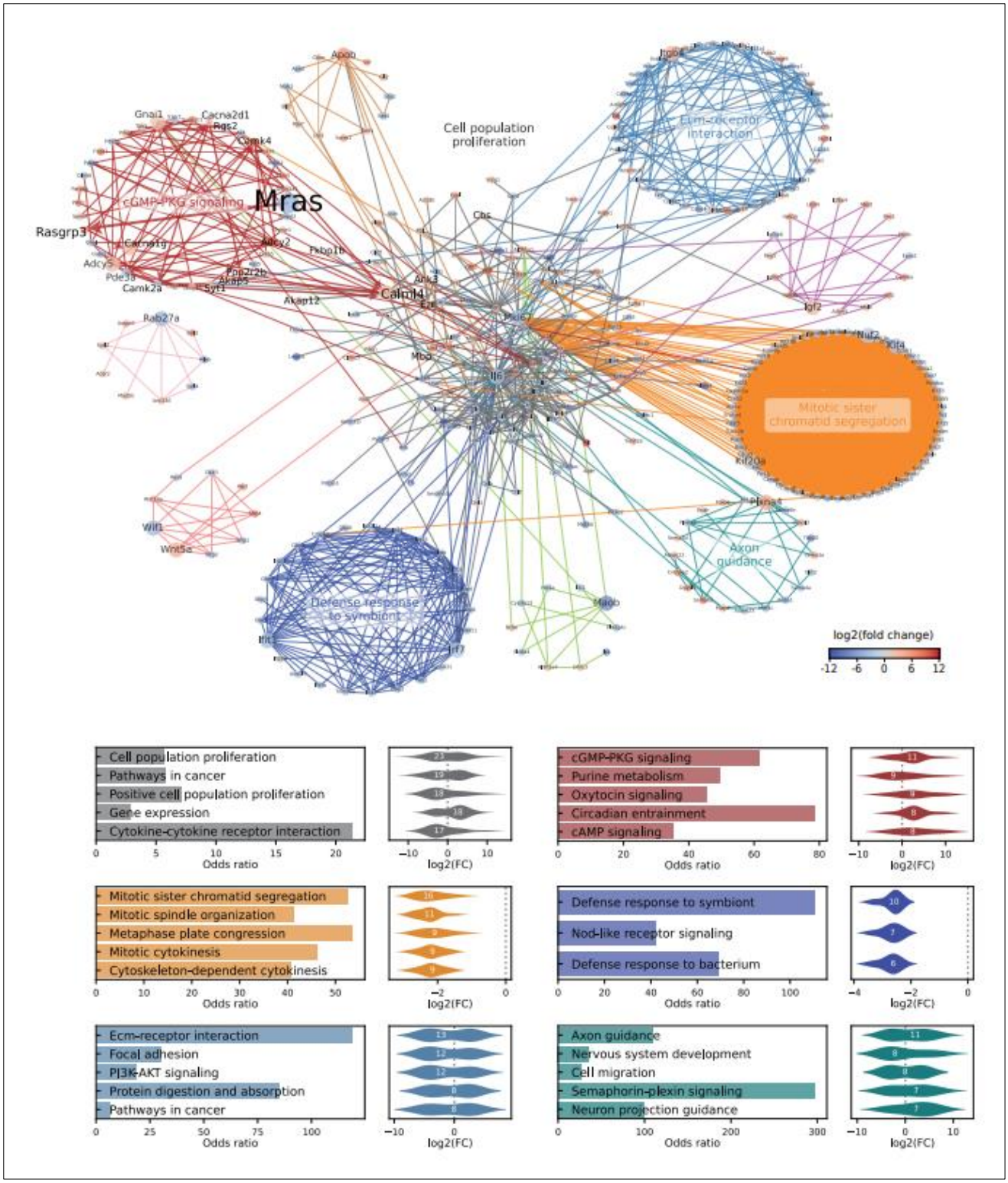

Figure 30 – STRING interaction network and gene set enrichment analysis of differentially expressed genes (DEGs) in murine *Mras*$^{-/-}$*ApoE*$^{-/-}$ SMCs vs. *B6.ApoE*$^{-/-}$ SMCs

DEGs were defined as adj<0.05, $\log_2$(fold change) > 2 or $\log_2$(fold change) < -2, and read count > $\log_2$ (5). The edges in the network represent STRING scores >0.6 which are calculated from co-expression scores, experimental scores, database scores, and text mining scores. The fold change in gene expression on the $\log_2$-scale is depicted by red and blue spheres, respectively. The network was created using the Python packages *networkx*. Gene clusters were defined using the *greedy_modularity_communities* module. The plots below show enriched terms and the corresponding distribution of $\log_2$(FC) values of gene sets. Gene set enrichment analysis of gene clusters was carried out using the *enrichr* API in Python. The number of matched genes for a gene set is depicted in the violine plots. This figure was created by Tobias Reinberger.

Both the *MRAS* transcript counts from the RNA sequencing data align with the *MRAS* transcript levels from qPCR analysis (Figure 31).

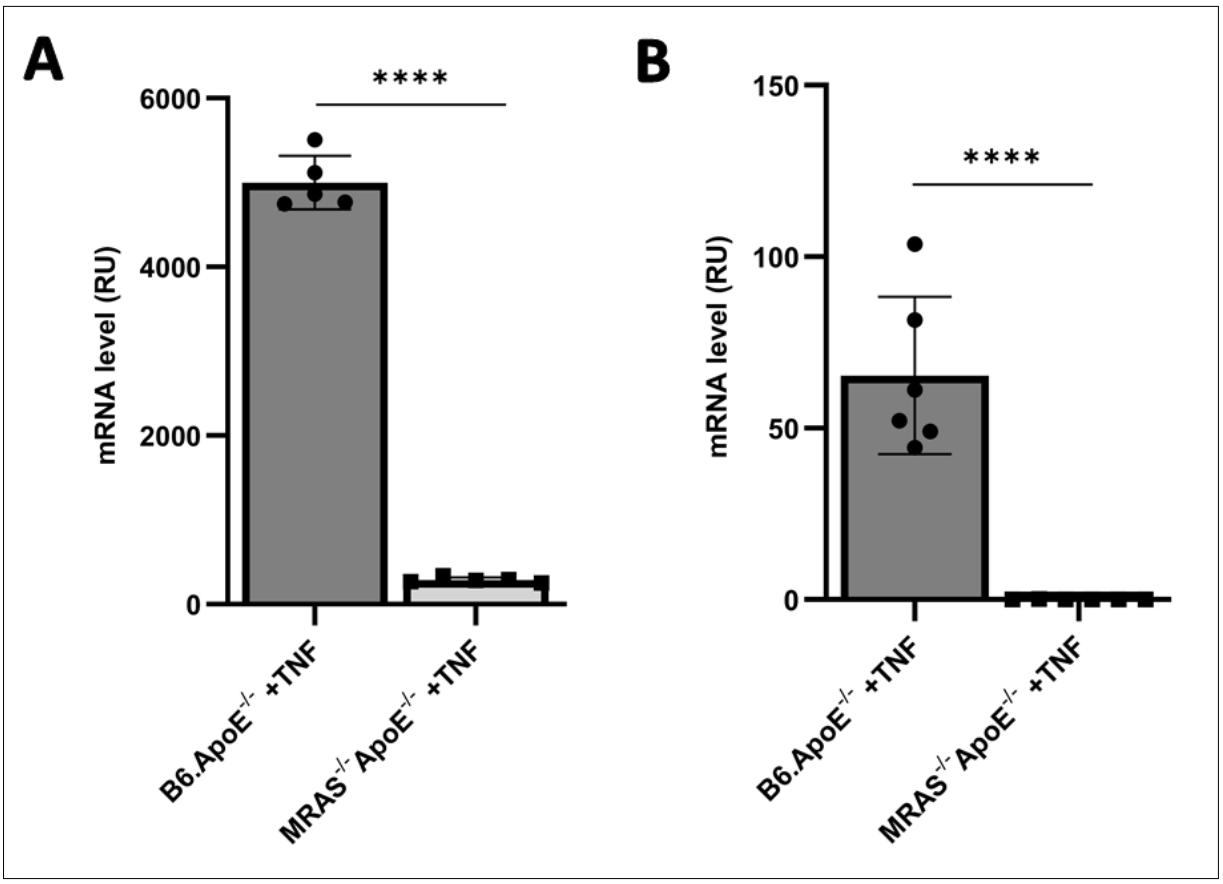

Figure 31 – *MRAS* transcript counts from RNA sequencing (A) vs. *MRAS* transcript level from qPCR analysis (B)

A: Bar plots of the normalized counts of the conditions i.e., *B6.ApoE*$^{-/-}$ SMCs with TNF (10 ng/ml) and *MRAS*$^{-/-}$*ApoE*$^{-/-}$ SMCs stimulated with TNF. The calculated mean of the samples (5 each) within each group is the height of the plots and the standard deviation of the samples is shown as error bars. **B:** Shown here are the mean values of twelve samples (6 per each condition). mRNA levels were assessed by measuring the percentage of mRNA levels in each sample. The horizontal bars show the standard deviation of the data. Student's two-sided t-test was carried out to determine the significance (****$p<0.0001$).

5.4 Quantitative Plaque Analysis

The progression and extent of atherosclerosis was analysed in sections of the aortic root. The plaque sizes were determined, followed by the analysis of the plaque composition by quantification the amount of Collagen, monocytes and macrophages, and SMCs, respectively, normalized to the plaque area. For this analysis, in total forty-nine (49) mice were used consisting of nine (n = 9) *Mras*$^{-/-}$ *ApoE*$^{-/-}$ dKO male mice, seventeen (n = 17) *B6.ApoE*$^{-/-}$ wild type male controls, eight (n = 8) *Mras*$^{-/-}$ *ApoE*$^{-/-}$ dKO female mice and fifteen (n = 15) *B6.ApoE*$^{-/-}$ wild type female controls. Overall, the consequences of *Mras* deficiency on plaque characteristics might be sex-specific as only in male

mice significant differences were observed in terms of plaque size, collagen content and macrophages staining.

5.4.1 Plaque Size

Aortic root sections, spaced 40 µm, ten in number, were taken for plaque size assessment. The sections were stained with ORO and the plaque area was normalized to the aorta area. Image processing (with the software GIMP) for the analysis of the aorta was conducted where the aorta area was selected, including the lumen and valves. The plaque area was then selected and calculated as percent of the aorta area. *Mras*$^{-/-}$ *ApoE*$^{-/-}$ dKO male mice (n = 9) had significantly reduced lipid content compared to *B6.ApoE*$^{-/-}$ wild type controls (n = 17) (36.0% vs. 45.3%, p = 0.04) whereas in females, there was no significant difference in the relative plaque size between both the groups (Figure 32).

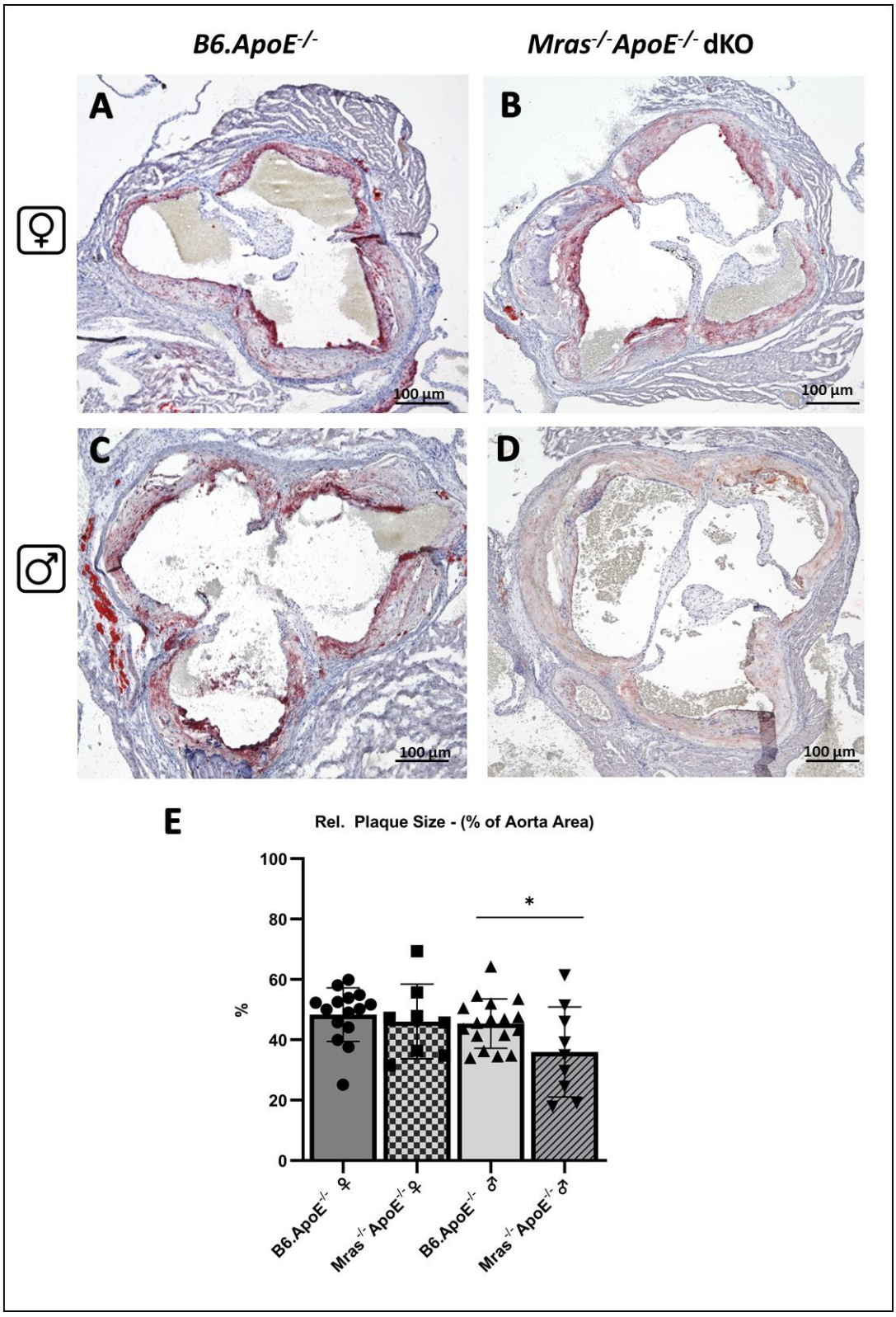

Figure 32 – Plaque Size

ORO-stained heart sections of **A:** *B6.ApoE*$^{-/-}$ WT female mouse, **B:** *Mras*$^{-/-}$*ApoE*$^{-/-}$ dKO female mouse, **C:** *B6.ApoE*$^{-/-}$ WT male mouse, and **D:** *Mras*$^{-/-}$*ApoE*$^{-/-}$ dKO male mouse. **E:** Box plot showing the distribution of relative plaque size in all four groups. Significant difference between male mice *Mras*$^{-/-}$*ApoE*$^{-/-}$ dKO and *B6.ApoE*$^{-/-}$ WT (36.0% vs 45.3%, p = 0.04). Whiskers: smallest/largest value; Box: first and third quartile, different colours & patterns depict different genders & genotypes respectively; Line: median; Dots: individual data points. The horizontal bars show the standard deviation of the data. Two-sided Student's t-test and two-way ANOVA were carried out to determine the significance (*p<0.05).

5.4.2 Collagen Content

The collagen content was analysed in five sections of the aortic root, where sections were stained with Masson's Trichrome to visualize collagen fibres. Collagen content was calculated as percentage % of plaque area. Plaque area was selected with the software GIMP, supported with the ORO-stained images, and cut out. The collagen fibres that were appearing blue in the staining, were selected with an image processing algorithm through python. Collagen area was then normalized to the plaque area. *Mras*$^{-/-}$*ApoE*$^{-/-}$ dKO male mice (n=9) had a slightly significantly higher collagen content than *B6.ApoE*$^{-/-}$ WT controls (n=17) (11.4% vs. 6.9%, p = 0.03). No difference was observed in the female mice (Figure 33).

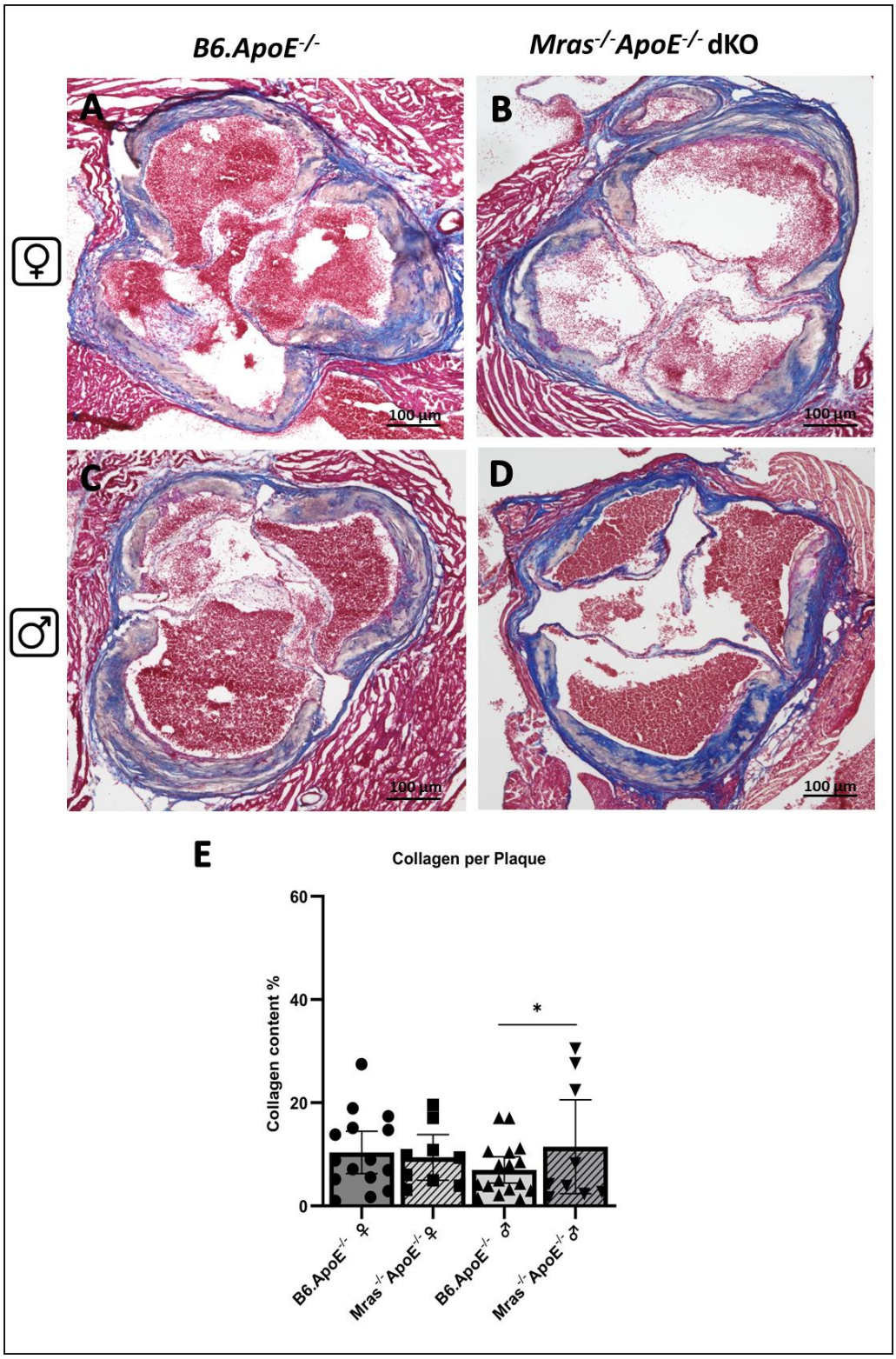

Figure 33 – Collagen Content

Masson's Trichrome staining of heart sections of **A:** *B6.ApoE*$^{-/-}$ WT female mouse, **B:** *Mras*$^{-/-}$*ApoE*$^{-/-}$ dKO female mouse, **C:** *B6.ApoE*$^{-/-}$ WT male mouse, and **D:** *Mras*$^{-/-}$*ApoE*$^{-/-}$ dKO male mouse. **E:** Box plot showing the distribution of collagen content in all four groups. A slight significant difference between male mice *Mras*$^{-/-}$*ApoE*$^{-/-}$ dKO and *B6.ApoE*$^{-/-}$ WT (11.4% vs 6.9%, p = 0.03). No difference was observed in the female mice. Whiskers: smallest/largest value; Box: first and third quartile, different colours & patterns depict different genders & genotypes respectively; Line: median; Dots: individual data points. The horizontal bars show the standard deviation of the data. Two-sided Student's t-test and two-way ANOVA were carried out to determine the significance (*p<0.05).

5.4.3 MoMa Content

Similarly, to the collagen content, the number of inflammatory Monocytes and Macrophages (MoMa) was determined. In five sections of the aortic root, monocytes and macrophages were stained with the anti-Monocyte + Macrophage (MoMa-2) antibody, and the positive MoMa-stained area was normalized to the plaque area. For the analysis, plaque area was selected with the software GIMP, supported with the ORO-stained images, and cut out. The brown area resembling the positive staining was then selected with an automated image analysis algorithm with Python. There was significant difference between the MoMA content of the *Mras*$^{-/-}$*ApoE*$^{-/-}$ dKO male mice (n = 9) and the *B6.ApoE*$^{-/-}$ WT controls (n = 17) (5.41% vs. 2.02%, p = 0.0001) (Figure 34).

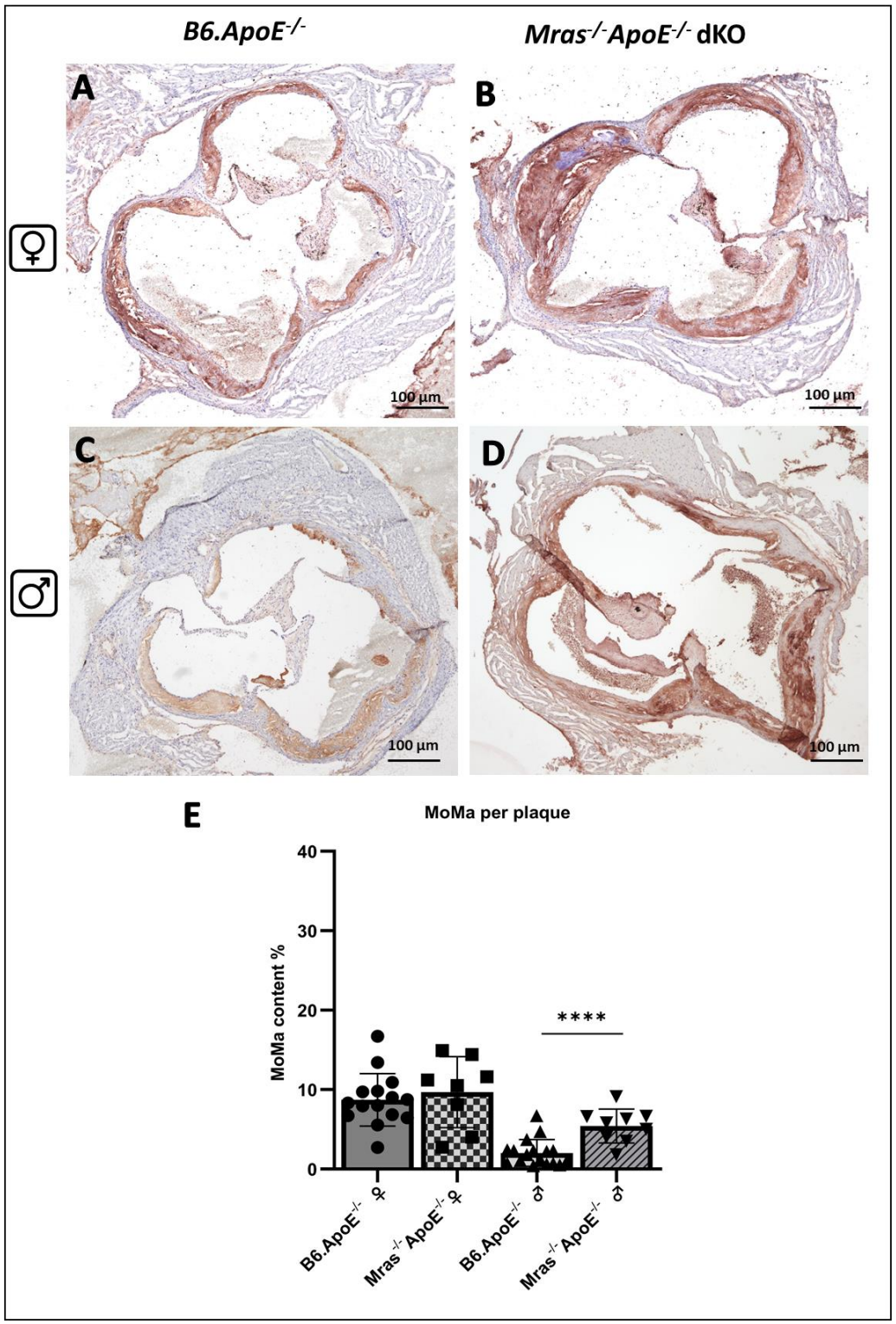

Figure 34 – Monocytes and Macrophages per plaque

Staining of the heart sections with the anti- Monocyte + Macrophage (MOMA-2) antibody of **A:** *B6.ApoE*$^{-/-}$ WT female mouse, **B:** *Mras*$^{-/-}$*ApoE*$^{-/-}$ dKO female mouse, **C:** *B6.ApoE*$^{-/-}$ WT male mouse, and **D:** *Mras*$^{-/-}$*ApoE*$^{-/-}$ dKO male mouse. **E:** Box plot showing the distribution of MoMa content in all four groups. Significantly elevated levels of MoMa-content were seen in *Mras*$^{-/-}$*ApoE*$^{-/-}$ dKO male mice in comparison to *B6.ApoE*$^{-/-}$ WT controls (5.41% vs. 2.02%, p = 0.0001). No difference was observed in the female mice. Whiskers: smallest/largest value; Box: first and third quartile, different colours & patterns depict different genders & genotypes respectively; Line: median; Dots: individual data points. The horizontal bars show the standard deviation of the data. Two-sided Student's t-test and two-way ANOVA was carried out to determine the significance (****p<0.0001).

5.4.4 SMC Content

The number of SMCs in the plaque were determined with this staining. In five sections, parallel to those that were used to quantify ORO, collagen and monocytes and macrophages, SMCs were stained with the α-smooth muscle FITC antibody. For the analysis, plaque area was selected with the software GIMP, supported with the ORO-stained images, and cut out. The green fluorescent area resembling the positive staining was then selected with an automated image analysis algorithm with Python. Positive SMC-stained area was then normalized to the plaque area. *Mras*$^{-/-}$*ApoE*$^{-/-}$ dKO male mice (n=9) had in average 15.5% SMCs per plaque, compared to 9.5% in the *B6.ApoE*$^{-/-}$ WT controls (n=17), where the difference was significant ($p = 0.04$) (Figure 35).

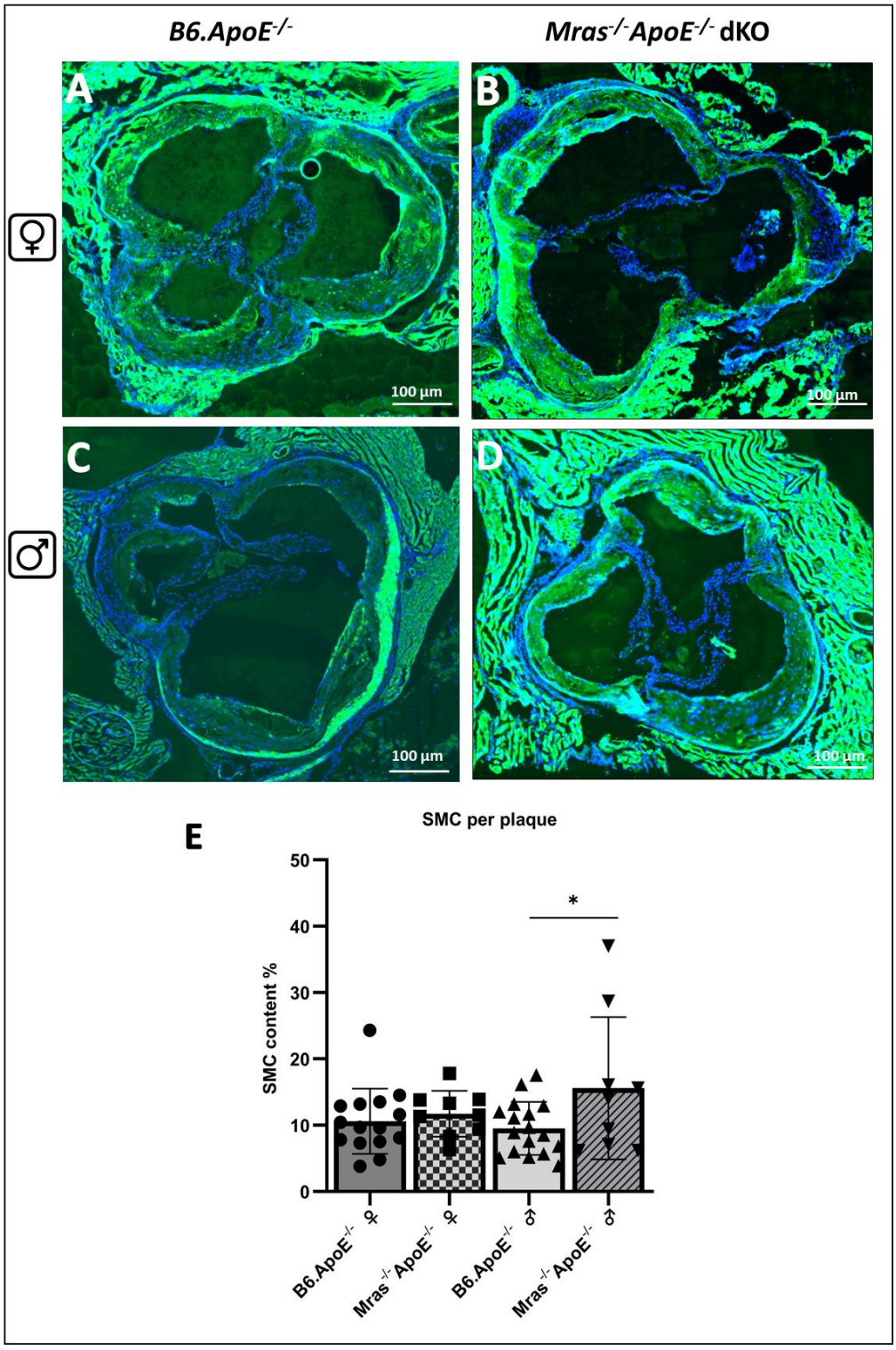

Figure 35 – Smooth muscle cell content in the plaque

Staining of the heart sections with the α- smooth muscle FITC antibody of **A:** *B6.ApoE*$^{-/-}$ WT female mouse, **B:** *Mras*$^{-/-}$ *ApoE*$^{-/-}$ dKO female mouse, **C:** *B6.ApoE*$^{-/-}$ WT male mouse, and **D:** *Mras*$^{-/-}$*ApoE*$^{-/-}$ dKO male mouse. **E:** Box plot showing the distribution of SMC content in all four groups. *Mras*$^{-/-}$ *ApoE*$^{-/-}$ dKO male mice showed a significant trend towards higher SMC-content compared with the *B6.ApoE*$^{-/-}$ WT controls (15.5% vs. 9.5%, p = 0.04). There was no difference observed between the female mice. Whiskers: smallest/largest value; Box: first and third quartile, different colours & patterns depict different genders & genotypes respectively; Line: median; Dots: individual data points. The horizontal bars show the standard deviation of the data. Two-sided Student's t-test and two-way ANOVA was carried out to determine the significance (*p<0.05).

6. Discussion

Coronary artery disease (CAD) and myocardial infarction (MI) are a major risk for death globally (1). Coronary artery disease, resulting from atherosclerotic lesions in the vascular walls, is marked by the narrowing and eventual blockage of the coronary arteries (174). This condition includes a range of clinical presentations, from ischemia to MI and sudden death (32). In addition, to smoking, hypertension, obesity, hyperlipidaemia, and diabetes, genetic predisposition significantly increases the risk of developing CAD (175, 176).

Divergent studies have linked numerous chromosomal regions called loci to disease (39, 45, 60, 63, 67, 72). Many regions contain genes of unknown contribution to development of CAD; these genes are likely acting as cis- or trans-regulators for proximal and distant genes. Statistical and fine mapping of these loci helps in the identification of causal genes– hints as eQTL effects (*i.e.*, variants that alter gene expression) or amino acid changes with direct impact on protein function (74) are strong indicators of promising candidate genes; making these genes worthy of further functional investigations.

Among those genes that were selected for further investigation is the *MRAS* gene. *MRAS* functions as a signal transducer for diverse signalling pathways like MAPK/ERK (105), PI3K (112), TNF (109) as well as acute response signalling (85, 115). The *MRAS* gene encompasses single nucleotide variants (SNVs) associated with increased risk of coronary artery disease *e.g.*, rs9818870, is located in the 3' untranslated region, causing modification in the structure of mRNA causing microRNA-mediated dysregulation of gene expression (81). Indeed, many intronic *MRAS* variants are in enhancer regions (Figure 2).

Knockdown experiments in human SMCs and knockout experiments in mice were performed resulting in elevated SMC migration and proliferation in both species. Less apoptosis was observed in *MRAS* deficient cells. Conversely, overexpression experiments were conducted to validate the results of the siRNA knockdown. The opposite effect was observed with reduced proliferation and migration, along with increased apoptosis in the knockdown and knockout cells.

6.1 Functional Assessment of *MRAS* in Human and Murine Cells

Vascular smooth muscle cells (VSMCs) are one of the key cell types in the etiology of atherosclerosis and plaque stabilization. According to GTEx Portal (https://gtexportal.org/home/), several *MRAS* risk variants for CAD increase *MRAS* mRNA levels primarily in the arterial and cardiac tissue, showing the strongest effect in the aorta (Figure 2). Therefore, we decided to use human SMCs as disease model to study the role of MRAS in CAD. As the function and structure of *MRAS* are highly conserved between human and mouse (177), studying *Mras* in mice also provided a good model to

investigate the functional role of this gene in atherosclerosis, in further elucidation of the observed human GWAS-CAD association.

SMC behaviour with respect to *MRAS* modulation is the prime focus of this research study. Functional assessment through migration, proliferation and apoptosis (Figure 6) were carried out using SMCs as the ideal cell type for *MRAS* gene expression.

The next two sections discuss the SMC experiments in detail, also pointing out the limitations of the methods used. After that the role of proliferation and migration will be discussed with respect to atherosclerosis. The second last part of the discussion addresses findings from RNA sequencing thereby speculating how SMC overcome the loss of *MRAS* by promoting cyclic guanosine monophosphate (cGMP)/ cyclic adenosine monophosphate (cAMP) signalling. Finally, the effects of loss of *Mras* on atherosclerosis in mice are discussed.

6.2 Influence of *MRAS* in Human Derived VSMCs

The role of *MRAS* in human derived aortic SMCs from three variable donors was investigated through siRNA knockdown experiments. To determine the function in various cellular processes, the *MRAS* gene was knockdown through RNA interference (RNAi). Three different siRNA were used for the experiments (hs.Ri. MRAS.13.1, 13.2, and 13.3). The 13.1 siRNA had the least transfection efficiency of 25% whereas 13.2 and 13.3 had transfection efficiencies of 75% and 80% respectively. Two *MRAS*-specific siRNAs were utilized since the usage of RNA interference has a variety of limitations including variability in knockdown efficiency affecting the experimental outcomes. Moreover, siRNAs can also target and silence genes that are similar in sequences leading to off-target effects. Incomplete knockdown could also be a consequence of RNAi leading to reduced gene expression but not complete silencing of the target gene. This partial knockdown could leave residual gene activity maintaining biological functions making it insufficient to analyse the gene function in SMCs. Transient effect of an siRNA knockdown is the issue faced by many researchers as the siRNA knockdown could be short-term *i.e.,* lasting only a few days. High concentrations of siRNA are cytotoxic for the cells inducing apoptosis. To avoid all these limitations, a control or scrambled siRNA was used and the experiments were validated with qPCR to show the divergent knockdown efficiency before every functional assay.

Different donors have distinct genetic backgrounds, leading to inherent differences in the behaviour of SMCs which can be a limitation of these experiments. Donor age and health status can significantly impact SMC function. SMCs from older donors show altered cellular response in comparison to young aged donors (178). The SMCs from older donors will automatically demonstrate increased senescence and reduced proliferation (178–180) which makes it ineffective to be used in experiments. Presence of atherosclerosis or cardiovascular diseases, diabetes or any kind

of metabolic disorders can highly influence the properties of their SMCs, affecting their response to experimental conditions. Besides age, sex-related differences highly influence the experimental data outcome as male and female donors may present biological differences in their SMCs. For improvement of experimental consistency and the reduction of variability, researchers should pool donor cells or use standardized protocols and large sample sizes.

MRAS deficiency led to elevated SMC migration and proliferation in human aortic SMCs. *MRAS* siRNA transfected SMCs were 76.3% confluent after 24h whereas the control siRNA was only 52.1%. After stimulation with PDGF-BB, no significance difference was observed between both the conditions. Addition of TNF, IL-6 and IL-1ß resulted in 80.4%, 73.4% and 73% confluency after 24h respectively. Conclusively, the latter cytokines basically pushed SMCs more towards migration. Similar trend was observed in proliferation assay as well. The downregulation of *MRAS* increased SMC proliferation after 96h. In contrast, reduced apoptosis (4 times less) was observed in *MRAS* siRNA mediated knockdown cells.

One speculation for this behaviour towards PDGF-BB is PDGF-BB signalling pathway has compensatory mechanisms that can bypass the need for *MRAS*, resulting in no observable difference when *MRAS* is knocked down. PDGF-BB acts primarily through PDGF receptor activation and downstream pathways like PI3K/AKT which may have a different effect on SMC behaviour in terms of migration and proliferation. VSMCs may express high levels of TNF, IL-6 and IL-1ß receptors compared to PDGF receptors allowing for a more robust response to these cytokines. TNF signalling may be more sustained compared to PDGF-BB leading to prolonged activation of proliferative pathways. TNF, IL-6 and IL-1ß activate different signalling cascades in VSMCs. *MRAS* may act as a negative regulator of TNF-induced proliferation and migration. When *MRAS* is knocked down, this negative regulation is removed, leading to enhanced responses to TNF stimulation. Moreover, TNF also activates NFκB signalling in VSMCs. This activation can lead to increased transcription of genes involved in inflammation and cell survival, contributing to proliferation under certain conditions (181).

Overexpression experiments were performed to validate the findings of siRNA knockdown. The overexpression of *MRAS* was highly cytotoxic for the cells when transfected with the plasmid through the divergent nucleofector programs. This may be due to overexpressed proteins disrupting the normal cellular processes and thus destabilizing the cell's machinery. After numerous experiments, optimization was achieved, and 4 million SMCs were pooled together from two nucleofection reactions and let grown for more than 4 days. These cells were cultured in the presence of antibiotics (*e.g.*, Geneticin G418) to maintain plasmid expression. The yield of cells was higher, and the experiments were conducted accordingly.

As expected, the result of *MRAS* overexpression was opposite to the result of siRNA knockdown. Reduced SMC migration and proliferation were observed when the gene was overexpressed. Elevated apoptosis was observed in SMCs overexpressing *MRAS*.

SMCs overexpressing *MRAS* had a decline in the cell number in the proliferation assay after 96h by 10.5% and the SMCs overexpressing empty and GFP had proliferation rates of 60.8 and 58.8% without any stimulus. Moreover, when stimulated with TNF and PDGF-BB, proliferation was increased in the empty and GFP plasmid, but the MRAS plasmid transfected SMCs were dying and could not proliferate anymore. A similar trend was observed in the migration assays where SMCs overexpressing *MRAS* had low migratory rates (34.4% confluency) after 24 h in comparison to empty (91.5% confluency) and GFP plasmid overexpressing SMCs (81.02% confluency). Elevated caspase-3 activity (0.25-fold) was observed in SMCs overexpressing *MRAS* compared to SMCs overexpressing empty (0.05-fold).

A limitation of overexpression is the activation of compensatory pathway by overexpressing cells leading to the masking of the true biological effects of the gene. Reproducibility in the experiments could also be a factor as every overexpression experiment is highly variable from the other one due to the impact of the plasmid transfection into the cells. Plasmid-based systems often drive gene expression at much higher levels than natural gene expression, under strong promoters like CMV that was used in these experiments. This can cause artificial phenotypes and exaggerated cellular responses that are not representative of the gene's normal function. Moreover, the overexpression samples were tested with qPCR, indicating high values of *MRAS* making it very hard to control the amount of protein produced by the SMCs.

Another limitation was also that many cells who were not transfected with the plasmid, died causing apoptosis in the cellular environment inducing cell death in the healthy cells. Mixed populations of transfected and un-transfected cells reduced the total yield of overexpressed cells by the end leading to less cell material for further functional assays.

SMCs overexpressing *MRAS* were dying in the proliferation assays indicating the cytotoxic effect of *MRAS* on SMCs. This effect would mask the real effect of proliferation in overexpressed SMCs. *MRAS* overexpression was 10-fold and significantly promoted apoptosis and inhibited proliferation of SMCs. The overexpression basically affected the cell cycle distribution and induced G1 phase arrest thus causing apoptosis.

6.3 Murine *Mras* KO SMCs are Proliferative

The role of *Mras* in atherosclerosis was determined in a knockout (KO) mice model. The *ApoE* KO mouse model is the best model to study the effect of atherosclerosis. *Mras*$^{-/-}$ *KO* and *ApoE*$^{-/-}$ *KO* mice

(both backcrossed more than seven times onto a *C57BL/J* background) were mated and heterozygous F1 progeny was crossbred to obtain the *Mras*$^{-/-}$*ApoE*$^{-/-}$ *(dKO)* and *B6. ApoE*$^{-/-}$ control mice.

To confirm the results from siRNA knockdown experiments in human SMCs, mouse SMCs were subjected to the same functional assays. A major limitation is that a gene knockout can lead to more extreme phenotypes than a gene knockdown, as the signalling pathways in which the gene product is involved can be severely disrupted.

SMCs were isolated from the aorta of these mice and further investigation focused on the characterization of *Mras KO* SMCs in term of proliferation and migration was carried out. Both the proliferation methods (cell counting and BrdU assay) revealed that *Mras* KO cells proliferated significantly more than *WT* cells reaching about 1.5-fold increase in cell number after 96h. When stimulated with variable stimuli, the confluency trends changed significantly i.e., *Mras* KO stimulated with TNF proliferated 3-fold and IL-6 and IL-1ß stimulation resulted in 2.5-fold increase of cells respectively. Notably, in both the proliferation assays, both genotypes have comparable cell counts until 24h and begin to diverge from 48h onwards.

When migration was analysed in murine cells, the experiments showed that *Mras* KO SMCs have a higher migration rate in comparison to wild type cells. The cells were migrating at a confluency rate of 76.3% after 24h without any stimulus. When stimulated with TNF, IL-6 and IL-1ß, the confluency rates were elevated to 80.4%, 73.4% and 72.8% respectively. PDGF had no influence on the migration rate.

Most research studies have shown that phenotypical changes of SMCs usually encompass proliferation and migration to be modified in similar directions – meaning higher proliferation aligns with higher migration and vice versa (159, 182–184). A cell's ability to migrate is cell-cycle dependent providing a functional link between the CAD-risk gene *Mras* and the consequences of its knockout.

6.4 SMC Proliferation and Migration in Atherosclerosis

SMC proliferation and migration are important characteristics to analyse as these processes are crucial in response to physiological and pathological stimuli (169) and important in atherosclerosis in which it can be beneficial for mature lesions, but detrimental in early stages. Therefore, it is a target for therapeutic interventions.

In a healthy state, SMCs exhibit a low proliferative rate, maintaining vascular and organ integrity (185). However, in disease, SMCs switch to a synthetic phenotype, marked by increased proliferation, migration, and ECM production (Figure 36) (186). Intracellular signalling pathways like MAPK and PI3K/Akt pathway are mediators for these responses.

Homogenous population of VSMCs in plaques, distinct from macrophages, can aberrantly proliferate and contribute to plaque formation (169), but are also beneficial for stabilizing the fibrous cap and prevention in rupture. These VSMCs are known as athero-protective plaque- stabilizing VSMCs (169).

Conversely, VSMC senescence, apoptosis and macrophage-like VSMC derivatives can drive inflammation (187). VSMCs from older rodents exhibit higher proliferation rates compared to younger animals (188–190). However, VSMCs from aged human vessels and advanced atherosclerotic plaques show decreased proliferation and prolonged population doubling times (191, 192). In culture, plaque VSMCs exhibit decreased S-phase and increased G_1 phase percentages, indicating G_1 growth arrest (191).

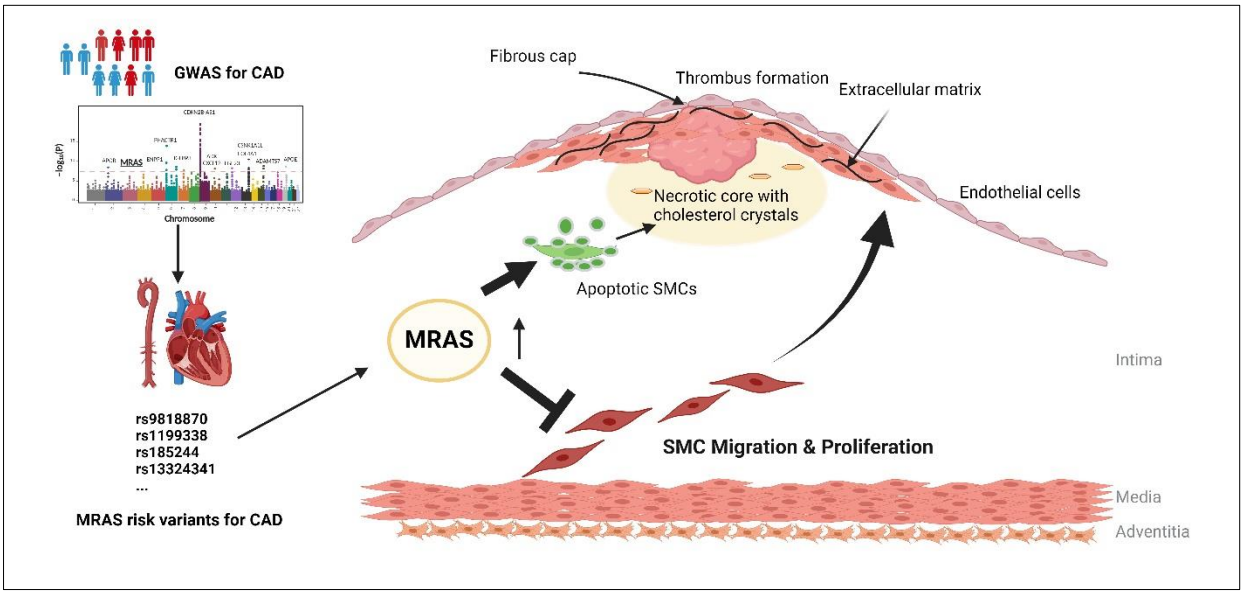

Figure 36 – Graphical representation of the hypothesis of this research study

MRAS risk variants for CAD increased *MRAS* levels primarily in the arterial tissue leading to high levels of *MRAS*, thereby promoting apoptosis and inhibiting SMC migration and proliferation. This figure was created by Biorender.com.

This arrest is linked to changes in the cell cycle regulators (involved in G_1-S transition) despite reduced responses to mitogens like IGF-1 (insulin-like growth factor 1) (193). Increased cyclin-dependent kinase inhibitors (194), and decreased cyclins D and E (195) expression levels, are observed in both normal VSMCs and plaque VSMCs in humans. These findings suggest that VSMC proliferation contributes to plaque stability and progression.

Furthermore, VSMC migration also plays an important role in atherogenesis where large number of intimal VSMCs form the fibrous cap (Figure 36) (169). In rodents, VSMCs arise from the intima by migration and invasion of myeloid cells from the lumen by transdifferentiation (196). In human vessels, VSMCs can only migrate by stimulating with various stimuli in culture and the contribution

of VSMC migration to mature atherosclerotic plaque is still ambiguous. It is also vague if migration occurs independently or is dependent on cell proliferation in human SMCs (169).

Isolated primary VSMCs quickly also lose their phenotypic traits *in vitro*, making them difficult to be used for long term experiments (166). Their proliferative ability also decreases with increasing donor age, and isolating these cells requires surgical intervention, posing risks to donors (163).

Cell apoptosis indices are low in early lesions but increase with lesions development in the necrotic core and the fibrous cap. Plaque rupture occurs mostly in the area of the plaque which has reduced VSMCs and increased number of macrophages. VSMC apoptosis thus occurs through death ligand/ death receptor interactions induced by macrophages (197). Stable lesions have less apoptosis than symptomatic plaques that have increased level of VSMC apoptosis (198). Chronic VSMC apoptosis expedites atherogenesis and progression of established lesions. VSMC apoptosis is a primary initial event in diseases like Marfan syndrome (199, 200).

Apoptosis can be characterized in stages of necrosis i.e.; primary necrosis refers to dying VSMCs releasing IL-1 and the necrotic core releasing IL-1α. Secondary necrosis releases both IL-1α and IL-1ß (148). VSMCs have the ability to efficiently clear the apoptotic VSMCs from the vessel wall within 48 hours (201, 202). However, in hyperlipidaemia and enhanced cardiovascular disease, phagocytosis is delayed because of the defective phagocytosis induced by phenotypic switching of VSMCs into macrophage-like cells resulting in inflammation dependent on IL-1 (148). Another research study linked the 9p21 human gene locus (58), which is strongly associated with increased cardiovascular disease risk, to reduced expression of cyclin-dependent kinase inhibitor 2B (203) and calreticulin. Apoptotic bodies lacking cyclin-dependent kinase inhibitor 2B were resistant to efferocytosis and not effectively cleared by neighbouring macrophages (203). Thus, loss of cyclin-dependent kinase inhibitor 2B contributes effectively to atherosclerosis by increasing the size and complexity of the lipid-laden necrotic core through impaired efferocytosis (169).

Bone marrow-derived cells may migrate to the atherosclerotic plaques or the neointima after injury and thus express SMC markers. VSMC apoptosis releases stromal cell-derived factor 1α after injury, potentially recruiting SMC progenitors to arterial injury sites (204). The bone marrow-derived SMC-like cells apoptosis reduced atherosclerosis and plaque inflammation (205). Their proatherogenic effect depends on release of cytokines like IL-6 and CXCL-16 and monocyte chemoattractant protein-1, consequently reducing plaque inflammation (205). Apoptosis depends on the origin of cells, if cells are vessel wall- derived cells and undergo apoptosis, then they promote inflammation whereas bone marrow- derived SMC like cells have proinflammatory phenotype and apoptosis in these cells reduce inflammation (169).

The role of VSMCs proliferation and migration has beneficial perspectives. SMCs contribute to the formation of a protective fibrous cap over atherosclerotic lesions. This involves the migration of

VSMCs from the media into the intima, where they proliferate and produce ECM thereby stabilizing the plaque and preventing rupture (206, 207). When vascular injury occurs, VSMCs undergo phenotypic switching enhancing their synthetic capacity, allowing repair of damaged tissue. This response is crucial for maintaining vascular integrity (206, 208). Pathways involving PDGF-BB, TNF, and IL-6 promote VSMC proliferation and migration generally, and are essential for normal vascular remodelling to counteract the effects of atherosclerotic damage (206, 209).

Apoptosis is reduced in SMCs when proliferation and migration are elevated. The local microenvironment plays a crucial role in determining VSMC fate. During atherosclerosis, inflammatory cytokines and growth factors create a milieu that favors cell survival. The signaling pathways activated by these factors can suppress pro-apoptotic signals while promoting cell proliferation and migration (210). When apoptosis occurs, it can lead to efferocytosis, where macrophages or other phagocytic cells clear the apoptotic VSMCs. In conditions where proliferation and migration are high, the overall cellular turnover may favour survival over apoptosis, leading to fewer apoptotic cells being present for efferocytosis (211).

6.5 RNA Sequencing of Human and Murine Cells

Bulk RNA sequencing (RNA-seq) was conducted to measure the average expression levels of individual genes to obtain a transcriptome prolife of *Mras*$^{-/-}$*ApoE*$^{-/-}$ dKO murine SMCs in comparison to *B6.ApoE*$^{-/-}$ WT SMCs.

In the murine cells, the knockout of the gene showed differentially expressed genes and the samples were very well separated (Figure 27). There was appropriate separation between both the groups and the variation between the groups was much higher than the variance within the groups. The RNA-seq data was normally distributed. Initial enrichment analysis of the gene expression profiling with the gene enrichment tool (*WebGestalt* (https://www.webgestalt.org/)) was performed. Genes downregulated in *Mras* KO SMCs ($\log_2$(fold change) < -2) had a ratio of enrichment of ~1.8 for "immune response" and "defence response". In contrast, genes that were higher expressed in *Mras* KO SMCs were enriched for "cell adhesion" and "cell-cell signalling". This can be interpreted to mean that the absence of *Mras* makes murine SMCs more sensitive to "internal"/paracrine signals from neighbouring cells than to "external" stimuli, e.g., originating from bacteria.

In order to obtain a more detailed insight into pathways affected by the deficiency of *Mras* in SMCs, an interaction network of differentially expressed genes (DEGs) were created using STRING database (https://string-db.org/) (Figure 30). The MRAS subnetwork indicates that both cGMP/cAMP signalling is modulated when *Mras* is absent in murine KO SMCs. cGMP signalling

directs vascular tone and smooth muscle cell proliferation and differentiation (212). cGMP signalling is dysfunctional in cardiovascular diseases (212).

Additionally, this pathway is also regulated by phosphodiesterases (PDEs). PDEs are enzymes that convert cAMP and cGMP to their inactive forms 5'AMP and 5'GMP, respectively, thus regulating cellular levels of cAMP/cGMP and terminating the signalling pathways (213–215). There are 11 distinct families of PDEs identified in mammals differing in properties and substrate specificities. For example, PDE-4 has been identified for its role in the heart where it regulates cAMP levels critical for cardiac function (216). Additionally, cGMP regulates the activity of PDE-2, -5, and -9. PDE-3 and -5 are expressed in VSMCs. PDE-3 is involved in regulating smooth muscle contractility as well as VSMC phenotype switch and stress response.

RNA-seq indicates**,** that adenylate cyclases (*Adcy2* and *Adcy5*) and guanylate cyclases (*Gucy1a1* and *Gucy1b1*) are highly expressed. At the same time, several PDEs (*i.e.*, Pde1a, Pde3a, Pde3b, Pde5a, Pde7b, Pde8b and Pde10a) are downregulated in *Mras* KO SMCs (Figure 30 and Table 26). When PDE activity is reduced or PDE levels are low and levels of adenylate/ guanylate cyclases are high, levels of cGMP and cAMP can increase (Figure 37). Elevated cGMP and cAMP normally suppresses VSMC proliferation and migration through activation of cGMP/cAMP-dependent protein kinases (PKG/PKA), which inhibit cell cycle progression and promote cell quiescence (217, 218). In contrast, it has been demonstrated that inhibition of PDEs, particularly those that hydrolyse cAMP or cGMP, can facilitate this transition by altering the signalling landscape within the cells (217, 219). Moreover, in pathological conditions like atherosclerosis, downregulation of PDEs has been associated with increased VSMC proliferation and migration, contributing to vascular remodelling and occlusion (218, 220).

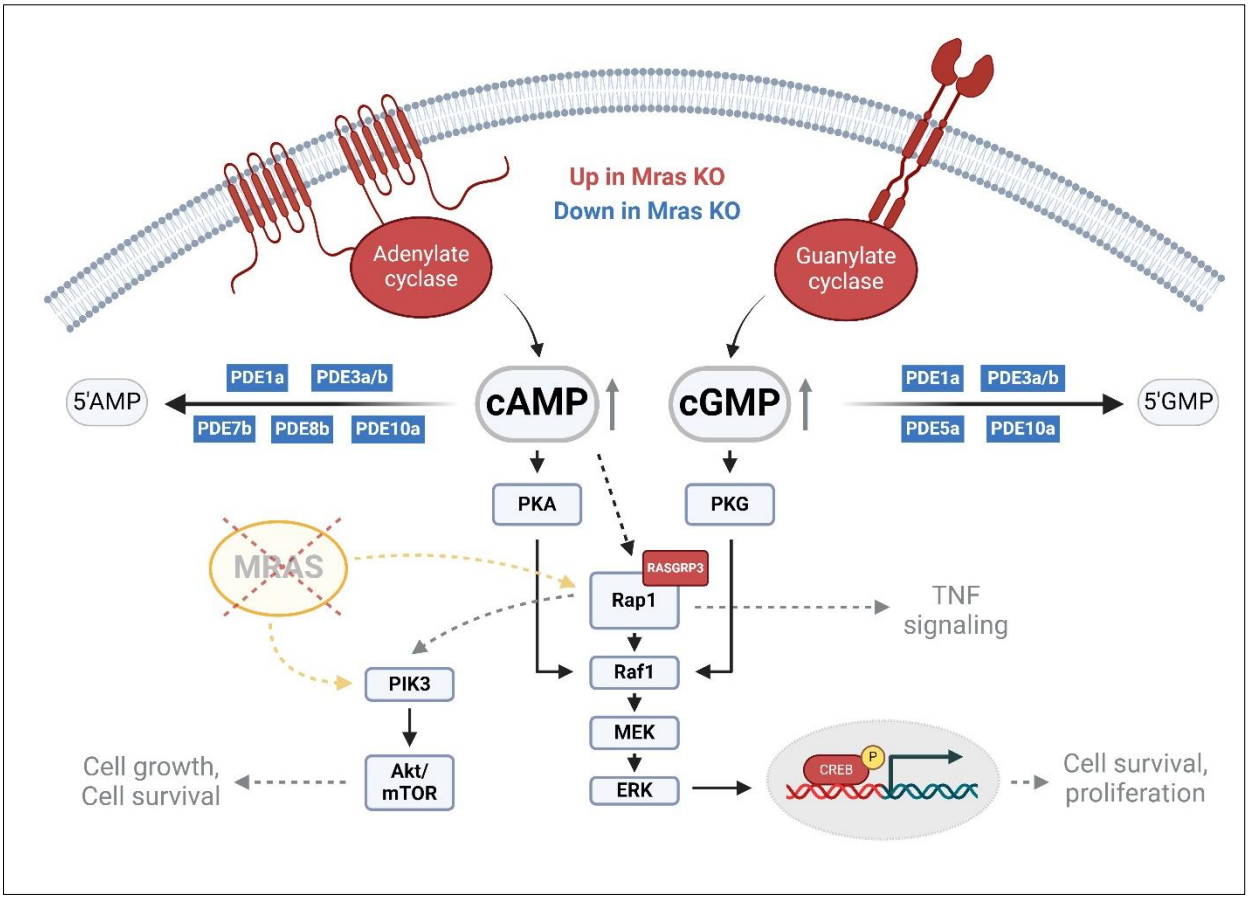

Figure 37 – Schematic representation of regulation of cAMP synthesis by Adenylate Cyclases (AC) and cGMP synthesis by guanylate cyclases (GC)

Degradation of cAMP and cGMP is catalysed by various PDEs depicted in the figure. cAMP and cGMP are hydrolysed by PDEs. PDEs catalyse the hydrolysis of the 3′ phosphate bond of cAMP and cGMP to generate 5′ AMP and 5′ GMP. Up regulation is depicted by red in *Mras* KO cells and down regulation is depicted by blue in *Mras* KO cells. cAMP/cGMP can activate the ERK and AKT/mTOR pathways which leads to proliferation and cell growth and survival. This figure was created by biorender.com

Furthermore, cGMP regulates the cytosolic free calcium level within VSMCs through removal of intracellular calcium through calcium pump mechanisms and directly inhibits the influx of extracellular calcium via voltage-gated calcium channels (212). Our data shows that Calml4 and Camk4 (genes that enable the binding of calcium ions) are upregulated in *Mras* KO SMCs, indicating compensatory mechanisms that might counteract the reduction of intracellular calcium.

Moreover, the cGMP-PKG-MAPK/ERK signalling axis plays a critical role in cellular proliferation and migration. The balance between cGMP levels and thus PKG activity can determine if cells should migrate or proliferate. The interplay between cGMP-PKG signalling and calcium influx pathways also influences VSMC behaviour. Increased cGMP levels can lead to decreased intracellular calcium concentrations, which are necessary for contraction and can affect migration (221).

Although cGMP and cAMP signalling generally inhibit SMC proliferation, chronic elevation of these cyclic nucleotides can disrupt the balance between pro- and anti-proliferative signals within SMCs and desensitize its signalling pathways. Therefore, lower PDE levels and hence higher cGMP/cAMP

levels can paradoxically lead to enhanced SMC proliferation under chronic inflammatory conditions (222). Additionally, the involvement of cGMP in the nitric oxide cGMP-dependent protein kinase 1 pathway promotes VSMCs growth and survival under certain conditions. This pathway can stimulate SMC growth in the context of vascular remodelling associated with atherosclerosis (223, 224). Moreover, the Exchange Protein Directly Activated by cAMP 1 (Epac1) has been identified as a crucial mediator of cAMP signalling in SMCs. It promotes foam cell formation by upregulating oxidized low-density lipoprotein receptor 1 (LOX-1), facilitating the uptake of ox-LDL, which is central to the development of atherosclerotic lesions (225). In certain scenarios, such as during inflammatory responses or when mediated by Epac1, cAMP can promote SMC growth and contribute to the pathogenesis of atherosclerosis (226).

Interestingly, cAMP and cGMP signalling share common pathways as MRAS signalling leading to the suggestion that SMCs compensate for the loss of *MRAS* by increasing cAMP and cGMP levels. However, further studies that focus on analysis of proteins involved in cAMP/cGMP pathways are needed to underpin this hypothesis. In addition to that, cAMP and cGMP levels should be determined in *Mras* KO SMCs.

6.6 MRAS Pathways relevant to Atherosclerosis

MRAS plays a distinct role in cell differentiation and proliferation and modulates cell polarity regulation (83). The mammalian small GTPase superfamily consists of six subfamilies: ARF, RAB, RAN, RAS, RHO and SAR1. The RAS superfamily, named after the Rat sarcoma virus, includes guanosine triphosphate binding proteins encoded by the prototypic RAS oncogenes – *NRAS*, *KRAS*, and *HRAS* – as well as *MRAS* (107). While *MRAS* shares functional similarities with the classical RAS family members, it also has unique roles, by acting through specific effectors that dephosphorylate Raf, to activate the extracellular signal-regulated kinase (ERK) pathway (Figure 4).

Although, it is conceivable that elevated basal levels of MRAS enhance MAPK/ERK signalling or PI3K/AKT/mTOR signalling in vascular SMCs, leading to diffuse intimal thickening, a characteristic feature of early atherosclerosis (227), a recent article suggested that *MRAS* mediates the suppression of proliferation by inhibition of MAPK/ERK and PI3K-AKT signalling in breast cancer cells when interacting with G- Protein Subunit Gamma 2 (GNG2) (228) (Figure 38). In the ERK and AKT activity pathways, the *MRAS* forms a binary complex with SHOC2 (112), followed by the complex associating with PP1 (229). However, when MRAS-SHOC2 binds to SCRIB, forming the MRAS-SHOC2-SCRIB complex, ERK and AKT activity is inhibited, suggesting *MRAS* having a bidirectional effect on these pathways (112, 229, 230). It is speculated that GNG2 overexpression increases *MRAS* expression (228) promoting the formation of MRAS-GNG2 binary

complexes which can then form ternary complexes with SCRIB or PI3K, leading to the inhibition of ERK/AKT activity (Figure 38).

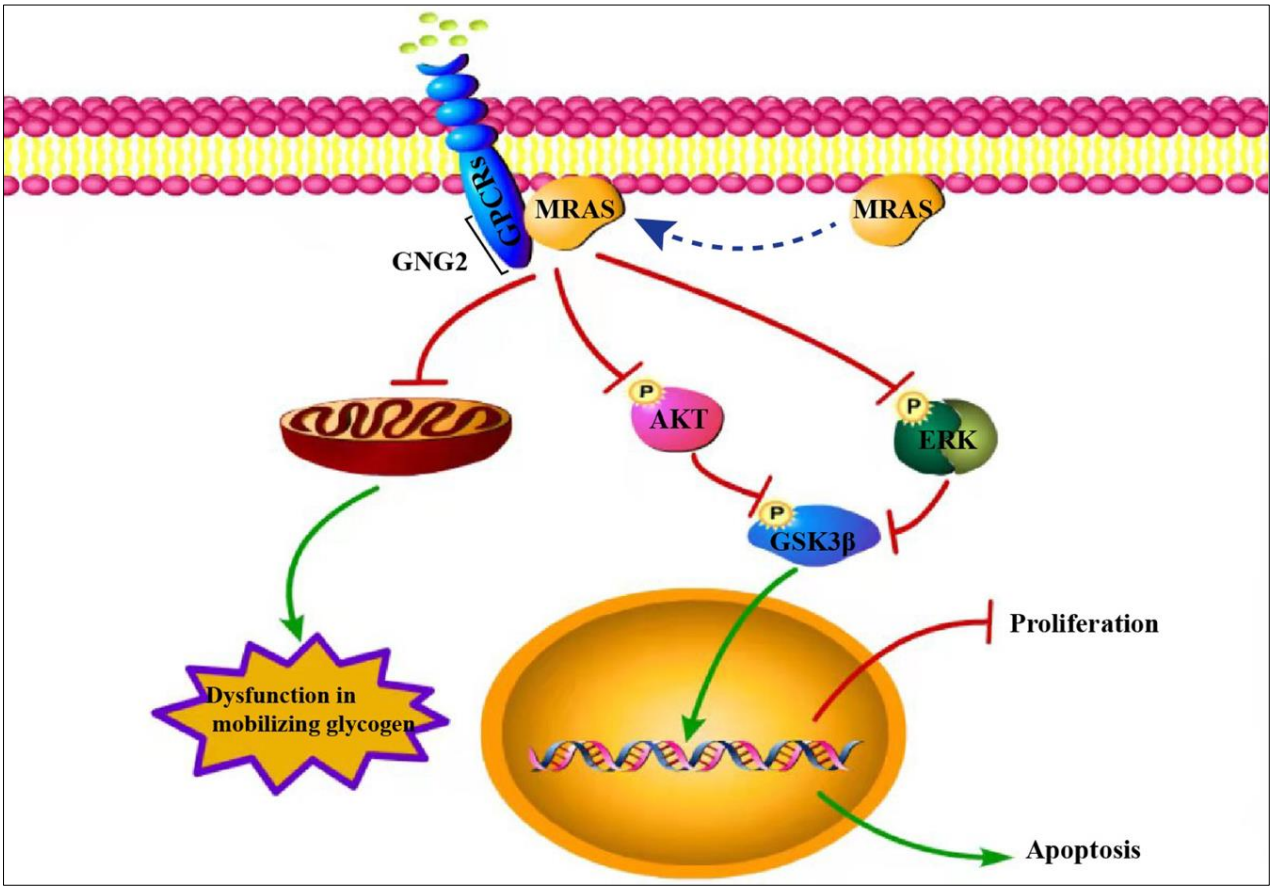

Figure 38 – GNG2 acts a tumour suppressor in breast cancer through stimulating MRAS signalling

GNG2- MRAS mediated inhibition of AKT/ERK activity causes more apoptosis and inhibits proliferation in breast carcinoma cells. This figure is taken from (228).

Moreover, enhanced *MRAS*-mediated acute phase response signalling, including TNF-stimulated adhesion signalling can also be a mechanism contributing to *MRAS* variants influencing atherosclerosis development. Macrophages bind to ICAM-1 and other adhesion molecules expressed by vascular endothelial cells through TNF/*MRAS*-induced activation of LFA-1. This enables immune cells to migrate from the circulating blood into the arterial intima, thereby exacerbating the inflammatory burden of the atherosclerotic plaque (119).

On the other hand, *MRAS* risk variants increase *MRAS* level in the cardiac tissue consequently causing left ventricular hypertrophy (LVH) (231). LVH independent of CAD, results in myocardial ischemia which increases morbidity and mortality due to MI (231). This is supported by the fact that the gain-of-function variant, p.Gly23Val, identified in patients with Noonan syndrome is accompanied by cardiac hypertrophy and a 40-fold increase in *MRAS* activation (113).

Additionally, *MRAS* is also involved in the MAPK-mediated adipocyte hypertrophy, which might explain the association of the gene with obesity (232, 233). The elevated accumulation of

macrophages in adipose tissue due to obesity (234), along with their secretion of TNF, is clinically significant, as it is directly linked to the development of insulin resistance and vascular endothelial dysfunction (235, 236).

Hypertrophy is characterized by an increase in the volume or organ or tissue due to the enlargement of its component cells. This process occurs in muscle and adipose tissues. Hypertrophic smooth muscle cells exhibit reduced proliferation compared to their non-hypertrophic counterparts. This is evident in the context of vascular smooth muscle cells, where hypertrophy occurs with minimal or no accompanying hyperplasia (an increase in cell number). During hypertension, smooth muscle cells enlarge without significant cell division, leading to predominance of hypertrophic responses over proliferative ones (237). When there is vascular injury, smooth muscle cells proliferate significantly but not in stable hypertrophic states.

Taken together, *MRAS* could play a diametrical role in different cell types and in the configuration of their signalling pathways. While *MRAS* promotes hypertrophy in cardiac and adipose tissue, we and others have shown that in hyperplasic conditions, lower *MRAS* levels promotes cellular proliferation. Therefore, MRAS pathways seem to be highly cell-specific and dependent on the microenvironment and inflammatory signalling. This is supported by the fact that PDGF stimulation had almost no effect, whereas TNF and IL-6 treatment markedly enhanced the effect of *MRAS* knockdown with respect to increased SMC proliferation.

6.7 Plaque Characteristic in *B6. ApoE*$^{-/-}$ and *Mras*$^{-/-}$*ApoE*$^{-/-}$ dKO Mice

The plaque composition was analysed in both mouse genotype groups with regard to SMC/collagen, monocyte/macrophages (MoMa), and lipid content. SMCs are a key component that contribute to the architecture of plaques, SMCs migrate to form a protective cap structure over the plaque, synthesizing collagen to enhance its stability, and also play a role in clearing lipids within the plaque.

Collagen, a structural component and marker of plaque stability, is primarily produced in plaques by the SMCs. The amount and distribution of collagen in plaque significantly impacts its vulnerability, or likelihood of rupture. Monocytes and macrophages serve as markers for the immunological state of a plaque, playing a role throughout its development – from the initial fat deposits in the vessel wall to the final stages of a plaque rupture.

Male *Mras*$^{-/-}$*ApoE*$^{-/-}$ dKO mice showed significantly higher levels of collagen content (Figure 33), MoMa content (Figure 34) and SMC content (Figure 35) as compared to *B6.ApoE*$^{-/-}$ mice. These findings support the hypothesis that *Mras* deficiency increases SMC proliferation and migration that seem to be accompanied with higher level of collagen in a plaque.

To have a clearer conclusion in terms of plaque stability, it might be necessary to analysis the distribution of collagen in a plaque in more detail as a thick fibrous cap and dense collagen network spanning the lesions are indicators for more stability. A limitation of the Acta2+ staining to detect the SMC content was the autofluorescence caused by the surrounding collagen tissue in the plaque.

Overall, the effects of *Mras* deficiency on plaque characteristics may be sex-specific, as significant differences in plaque size, collagen content and macrophage staining were only observed in male mice. In general, the *Mras*$^{-/-}$*ApoE*$^{-/-}$ mouse model supports the assumption that lower *Mras* levels in the vessel wall, especially in SMCs, protect against CAD by stabilizing the atherosclerotic plaque and thus reducing the likelihood of plaque rupture and hospitalization.

7. Conclusion & Outlook

Further experiments are required to build a better understanding of the association between the CAD-risk gene *MRAS* and atherosclerosis.

Deficiency of *MRAS* protruded an effect on the proliferation and migration of primary aortic smooth muscle cells, a cell type that is relevant to atherosclerosis, in humans and mice consecutively. To gain a deeper understanding of the role of the CAD-risk gene *MRAS* in these processes, it might be beneficial to further characterize the ability of SMCs to undergo phenotype switching or to examine the impact of SNV rs9818870 on the cell cycle in more detail.

The role of the lead SNV rs9818870 at *MRAS* risk locus on *MRAS* gene expression should have been studied in depth. By employing gene editing, GWAS variants can be introduced into iPSCs to study their effects. Cell genomes are altered using CRISPR/Cas based- methods. Prime editing enables precise base changes, while the classical CRISPR/Cas system generates knockout cell lines by removing entire exons. These cells could be further utilized in functional assays

Luciferase reporter gene assay could be performed to study the critical role of microRNA at post-translation levels. The effect of the miRNA and cellular factors on the luciferase coding sequence shall be demonstrated to obtain the specific impact of the miRNA on the 3' UTR target.

Additional research focusing on the analysis of proteins involved in the cAMP/cGMP pathways could be performed. Measurement of cAMP and cGMP levels through a colorimetric assay in SMCs in *Mras* KO and WT should be determined.

Approaches like single-cell RNA sequencing or spatial transcriptomics could be a future perspective to check the overall gene expression profile for *MRAS* for other cell populations beside SMCs with more cellular heterogeneity and spatial resolution.

The results from the *in vivo* study suggests the impact of *MRAS* on plaque stability. Therefore, a thorough analysis of plaque composition and architecture with particular emphasis on the distribution of collagen and SMCs within the plaque may offer further insights. Another important factor could be assessing *MRAS* levels in stable and unstable plaques in humans.

8. References

[1] GBD 2013 Mortality and Causes of Death Collaborators (2015) Global, regional, and national age-sex specific all-cause and cause-specific mortality for 240 causes of death, 1990-2013: a systematic analysis for the Global Burden of Disease Study 2013. Lancet (London, England) 385, 117–171.

[2] Al Hasani, J. (2017) Functional analysis of the CAD-Risk gene Zc3hc1. Doctoral dissertation, University of Lübeck.

[3] Lusis, A. J. (2000) Atherosclerosis. Nature 407, 233–241.

[4] Koenig, W., and Khuseyinova, N. (2007) Biomarkers of atherosclerotic plaque instability and rupture. Arteriosclerosis, Thrombosis, and Vascular Biology 27, 15–26.

[5] Aqel, N. M., Ball, R. Y., Waldmann, H., and Mitchinson, M. J. (1984) Monocytic origin of foam cells in human atherosclerotic plaques. Atherosclerosis 53, 265–271.

[6] McGill, H. C., McMahan, C. A., and Gidding, S. S. (2008) Preventing heart disease in the 21st century: implications of the Pathobiological Determinants of Atherosclerosis in Youth (PDAY) study. Circulation 117, 1216–1227.

[7] Tuzcu, E. M., Kapadia, S. R., Tutar, E., Ziada, K. M., Hobbs, R. E., et al. (2001) High prevalence of coronary atherosclerosis in asymptomatic teenagers and young adults: evidence from intravascular ultrasound. Circulation 103, 2705–2710.

[8] Björkegren, J. L. M., Hägg, S., Talukdar, H. A., Foroughi Asl, H., Jain, R. K., et al. (2014) Plasma cholesterol-induced lesion networks activated before regression of early, mature, and advanced atherosclerosis. PLoS genetics 10, e1004201.

[9] Libby, P. (2002) Inflammation in atherosclerosis. Nature 420, 868–874.

[10] Libby, P., and Theroux, P. (2005) Pathophysiology of coronary artery disease. Circulation 111, 3481–3488.

[11] Schoenhagen, P., Ziada, K. M., Kapadia, S. R., Crowe, T. D., Nissen, S. E., et al. (2000) Extent and direction of arterial remodeling in stable versus unstable coronary syndromes : an intravascular ultrasound study. Circulation 101, 598–603.

[12] Witztum, J. L. (1994) The oxidation hypothesis of atherosclerosis. Lancet (London, England) 344, 793–795.

[13] Wilcox, J. N., Smith, K. M., Schwartz, S. M., and Gordon, D. (1989) Localization of tissue factor in the normal vessel wall and in the atherosclerotic plaque. Proceedings of the National Academy of Sciences of the United States of America 86, 2839–2843.

[14] Ross, R., Masuda, J., Raines, E. W., Gown, A. M., Katsuda, S., et al. (1990) Localization of PDGF-B protein in macrophages in all phases of atherogenesis. Science (New York, N.Y.) 248, 1009–1012.

[15] Campbell, G. R., and Campbell, J. H. (1985) Smooth muscle phenotypic changes in arterial wall homeostasis: implications for the pathogenesis of atherosclerosis. Experimental and Molecular Pathology 42, 139–162.

[16] Doran, A. C., Meller, N., and McNamara, C. A. (2008) Role of smooth muscle cells in the initiation and early progression of atherosclerosis. Arteriosclerosis, Thrombosis, and Vascular Biology 28, 812–819.

[17] Rensen, S. S. M., Doevendans, P. a. F. M., and van Eys, G. J. J. M. (2007) Regulation and characteristics of vascular smooth muscle cell phenotypic diversity. Netherlands Heart Journal: Monthly Journal of the Netherlands Society of Cardiology and the Netherlands Heart Foundation 15, 100–108.

[18] Jaeger, E., Rust, S., Roessner, A., Kleinhans, G., Buchholz, B., et al. (1991) Joint occurrence of collagen mRNA containing cells and macrophages in human atherosclerotic vessels. Atherosclerosis 86, 55–68.

[19] O'Callaghan, C. J., and Williams, B. (2000) Mechanical strain-induced extracellular matrix production by human vascular smooth muscle cells: role of TGF-beta(1). Hypertension (Dallas, Tex.: 1979) 36, 319–324.

[20] Newby, A. C., and Zaltsman, A. B. (1999) Fibrous cap formation or destruction--the critical importance of vascular smooth muscle cell proliferation, migration and matrix formation. Cardiovascular Research 41, 345–360.

[21] Loree, H. M., Kamm, R. D., Stringfellow, R. G., and Lee, R. T. (1992) Effects of fibrous cap thickness on peak circumferential stress in model atherosclerotic vessels. Circulation Research 71, 850–858.

[22] Guyton, J. R., and Klemp, K. F. (1994) Development of the atherosclerotic core region. Chemical and ultrastructural analysis of microdissected atherosclerotic lesions from human aorta. Arteriosclerosis and Thrombosis: A Journal of Vascular Biology 14, 1305–1314.

[23] Bruschke, A. V., Kramer, J. R., Bal, E. T., Haque, I. U., Detrano, R. C., et al. (1989) The dynamics of progression of coronary atherosclerosis studied in 168 medically treated patients who underwent coronary arteriography three times. American Heart Journal 117, 296–305.

[24] Falk, E. (1983) Plaque rupture with severe pre-existing stenosis precipitating coronary thrombosis. Characteristics of coronary atherosclerotic plaques underlying fatal occlusive thrombi. British Heart Journal 50, 127–134.

[25] Davies, M. J. (1996) Stability and instability: two faces of coronary atherosclerosis. The Paul Dudley White Lecture 1995. Circulation 94, 2013–2020.

[26] Falk, E. (1992) Why do plaques rupture? Circulation 86, III30-42.

[27] Demer, L. L., Watson, K. E., and Boström, K. (1994) Mechanism of calcification in atherosclerosis. Trends in Cardiovascular Medicine 4, 45–49.

[28] Galis, Z. S., Sukhova, G. K., Lark, M. W., and Libby, P. (1994) Increased expression of matrix metalloproteinases and matrix degrading activity in vulnerable regions of human atherosclerotic plaques. The Journal of Clinical Investigation 94, 2493–2503.

[29] Burke, A. P., Kolodgie, F. D., Farb, A., Weber, D. K., Malcom, G. T., et al. (2001) Healed plaque ruptures and sudden coronary death: evidence that subclinical rupture has a role in plaque progression. Circulation 103, 934–940.

[30] Nemoto, T., Ueda, Y., Matsuo, K., Nishio, M., Hirata, A., et al. (2013) Regression of luminal stenosis at the site of silent plaque disruption in the era of optimal medical therapy. Low high-density lipoprotein cholesterol level isa potential risk of stenosis progression. Circulation Journal: Official Journal of the Japanese Circulation Society 77, 2573–2577.

[31] Zhao, Y., Vanhoutte, P. M., and Leung, S. W. S. (2015) Vascular nitric oxide: Beyond eNOS. Journal of Pharmacological Sciences 129, 83–94.

[32] Wilson, P. W., Castelli, W. P., and Kannel, W. B. (1987) Coronary risk prediction in adults (the Framingham Heart Study). The American Journal of Cardiology 59, 91G-94G.

[33] Mayer, B., Erdmann, J., and Schunkert, H. (2007) Genetics and heritability of coronary artery disease and myocardial infarction. Clinical Research in Cardiology: Official Journal of the German Cardiac Society 96, 1–7.

[34] Andresdottir, M. B., Sigurdsson, G., Sigvaldason, H., Gudnason, V., and Reykjavik Cohort Study (2002) Fifteen percent of myocardial infarctions and coronary revascularizations explained by family history unrelated to conventional risk factors. The Reykjavik Cohort Study. European Heart Journal 23, 1655–1663.

[35] Boer, J. M., Feskens, E. J., Verschuren, W. M., Seidell, J. C., and Kromhout, D. (1999) The joint impact of family history of myocardial infarction and other risk factors on 12-year coronary heart disease mortality. Epidemiology (Cambridge, Mass.) 10, 767–770.

[36] Marenberg, M. E., Risch, N., Berkman, L. F., Floderus, B., and de Faire, U. (1994) Genetic susceptibility to death from coronary heart disease in a study of twins. The New England Journal of Medicine 330, 1041–1046.

[37] Chakravarti, A. (1999) Population genetics--making sense out of sequence. Nature Genetics 21, 56–60.

[38] Björkegren, J. L. M., Kovacic, J. C., Dudley, J. T., and Schadt, E. E. (2015) Genome-wide significant loci: how important are they? Systems genetics to understand heritability of coronary artery disease and other common complex disorders. Journal of the American College of Cardiology 65, 830–845.

[39] Lieb, W., Jansen, H., Loley, C., Pencina, M. J., Nelson, C. P., et al. (2013) Genetic predisposition to higher blood pressure increases coronary artery disease risk. Hypertension (Dallas, Tex.: 1979) 61, 995–1001.

[40] Schadt, E. E., and Björkegren, J. L. M. (2012) NEW: network-enabled wisdom in biology, medicine, and health care. Science Translational Medicine 4, 115rv1.

[41] Collins, F. S., Brooks, L. D., and Chakravarti, A. (1998) A DNA polymorphism discovery resource for research on human genetic variation. Genome Research 8, 1229–1231.

[42] Reich, D. E., and Lander, E. S. (2001) On the allelic spectrum of human disease. Trends in genetics: TIG 17, 502–510.

[43] Altshuler, D., Daly, M. J., and Lander, E. S. (2008) Genetic mapping in human disease. Science (New York, N.Y.) 322, 881–888.

[44] Genome-wide association study of 14,000 cases of seven common diseases and 3,000 shared controls - PubMed.

[45] Samani, N. J., Erdmann, J., Hall, A. S., Hengstenberg, C., Mangino, M., et al. (2007) Genomewide association analysis of coronary artery disease. The New England Journal of Medicine 357, 443–453.

[46] Brookes, A. J. (1999) The essence of SNPs. Gene 234, 177–186.

[47] International HapMap Consortium (2005) A haplotype map of the human genome. Nature 437, 1299–1320.

[48] Sachidanandam, R., Weissman, D., Schmidt, S. C., Kakol, J. M., Stein, L. D., et al. (2001) A map of human genome sequence variation containing 1.42 million single nucleotide polymorphisms. Nature 409, 928–933.

[49] Barrett, J. C., and Cardon, L. R. (2006) Evaluating coverage of genome-wide association studies. Nature Genetics 38, 659–662.

[50] Collins, A. (2009) Allelic association: linkage disequilibrium structure and gene mapping. Molecular Biotechnology 41, 83–89.

[51] Broman, K. W., and Feingold, E. (2004) SNPs made routine. Nature Methods 1, 104–105.

[52] Ha, N.-T., Freytag, S., and Bickeboeller, H. (2014) Coverage and efficiency in current SNP chips. European journal of human genetics: EJHG 22, 1124–1130.

[53] Wang, D. G., Fan, J. B., Siao, C. J., Berno, A., Young, P., et al. (1998) Large-scale identification, mapping, and genotyping of single-nucleotide polymorphisms in the human genome. Science (New York, N.Y.) 280, 1077–1082.

[54] Hirschhorn, J. N., and Daly, M. J. (2005) Genome-wide association studies for common diseases and complex traits. Nature Reviews. Genetics 6, 95–108.

[55] Jannot, A.-S., Ehret, G., and Perneger, T. (2015) $P < 5 \times 10(-8)$ has emerged as a standard of statistical significance for genome-wide association studies. Journal of Clinical Epidemiology 68, 460–465.

[56] Risch, N., and Merikangas, K. (1996) The future of genetic studies of complex human diseases. Science (New York, N.Y.) 273, 1516–1517.

[57] Yang, X. (2012) Use of functional genomics to identify candidate genes underlying human genetic association studies of vascular diseases. Arteriosclerosis, Thrombosis, and Vascular Biology 32, 216–222.

[58] Helgadottir, A., Thorleifsson, G., Manolescu, A., Gretarsdottir, S., Blondal, T., et al. (2007) A common variant on chromosome 9p21 affects the risk of myocardial infarction. Science (New York, N.Y.) 316, 1491–1493.

[59] McPherson, R., Pertsemlidis, A., Kavaslar, N., Stewart, A., Roberts, R., et al. (2007) A common allele on chromosome 9 associated with coronary heart disease. Science (New York, N.Y.) 316, 1488–1491.

[60] CARDIoGRAMplusC4D Consortium, Deloukas, P., Kanoni, S., Willenborg, C., Farrall, M., et al. (2013) Large-scale association analysis identifies new risk loci for coronary artery disease. Nature Genetics 45, 25–33.

[61] Clarke, R., Peden, J. F., Hopewell, J. C., Kyriakou, T., Goel, A., et al. (2009) Genetic variants associated with Lp(a) lipoprotein level and coronary disease. The New England Journal of Medicine 361, 2518–2528.

[62] Erdmann, J., Grosshennig, A., Braund, P. S., König, I. R., Hengstenberg, C., et al. (2009) New susceptibility locus for coronary artery disease on chromosome 3q22.3. Nature Genetics 41, 280–282.

[63] Erdmann, J., Willenborg, C., Nahrstaedt, J., Preuss, M., König, I. R., et al. (2011) Genome-wide association study identifies a new locus for coronary artery disease on chromosome 10p11.23. European Heart Journal 32, 158–168.

[64] Lu, X., Wang, L., Chen, S., He, L., Yang, X., et al. (2012) Genome-wide association study in Han Chinese identifies four new susceptibility loci for coronary artery disease. Nature Genetics 44, 890–894.

[65] Myocardial Infarction Genetics Consortium, Kathiresan, S., Voight, B. F., Purcell, S., Musunuru, K., et al. (2009) Genome-wide association of early-onset myocardial infarction with single nucleotide polymorphisms and copy number variants. Nature Genetics 41, 334–341.

[66] Nikpay, M., Goel, A., Won, H.-H., Hall, L. M., Willenborg, C., et al. (2015) A comprehensive 1,000 Genomes-based genome-wide association meta-analysis of coronary artery disease. Nature Genetics 47, 1121–1130.

[67] Schunkert, H., König, I. R., Kathiresan, S., Reilly, M. P., Assimes, T. L., et al. (2011) Large-scale association analysis identifies 13 new susceptibility loci for coronary artery disease. Nature Genetics 43, 333–338.

[68] Aragam, K. G., Jiang, T., Goel, A., Kanoni, S., Wolford, B. N., et al. (2022) Discovery and systematic characterization of risk variants and genes for coronary artery disease in over a million participants. Nature Genetics 54, 1803–1815.

[69] Koyama, S., Ito, K., Terao, C., Akiyama, M., Horikoshi, M., et al. (2020) Population-specific and trans-ancestry genome-wide analyses identify distinct and shared genetic risk loci for coronary artery disease. Nature Genetics 52, 1169–1177.

[70] Tcheandjieu, C., Zhu, X., Hilliard, A. T., Clarke, S. L., Napolioni, V., et al. (2022) Large-scale genome-wide association study of coronary artery disease in genetically diverse populations. Nature Medicine 28, 1679–1692.

[71] van der Harst, P., and Verweij, N. (2018) Identification of 64 Novel Genetic Loci Provides an Expanded View on the Genetic Architecture of Coronary Artery Disease. Circulation Research 122, 433–443.

[72] Aherrahrou, R., Reinberger, T., Hashmi, S., and Erdmann, J. (2024) GWAS breakthroughs: mapping the journey from one locus to 393 significant CAD associations. Cardiovascular Research, cvae161.

[73] Civelek, M., and Lusis, A. J. (2014) Systems genetics approaches to understand complex traits. Nature Reviews. Genetics 15, 34–48.

[74] Brænne, I., Civelek, M., Vilne, B., Di Narzo, A., Johnson, A. D., et al. (2015) Prediction of Causal Candidate Genes in Coronary Artery Disease Loci. Arteriosclerosis, Thrombosis, and Vascular Biology 35, 2207–2217.

[75] Nurnberg, S. T., Zhang, H., Hand, N. J., Bauer, R. C., Saleheen, D., et al. (2016) From Loci to Biology: Functional Genomics of Genome-Wide Association for Coronary Disease. Circulation Research 118, 586–606.

[76] Allayee, H., Ghazalpour, A., and Lusis, A. J. (2003) Using mice to dissect genetic factors in atherosclerosis. Arteriosclerosis, Thrombosis, and Vascular Biology 23, 1501–1509.

[77] Daugherty, A. (2002) Mouse models of atherosclerosis. The American Journal of the Medical Sciences 323, 3–10.

[78] Fazio, S., and Linton, M. F. (2001) Mouse models of hyperlipidemia and atherosclerosis. Frontiers in Bioscience: A Journal and Virtual Library 6, D515-525.

[79] Maeda, N. (2011) Development of apolipoprotein E-deficient mice. Arteriosclerosis, Thrombosis, and Vascular Biology 31, 1957–1962.

[80] Shah, P. W., Reinberger, T., Hashmi, S., Aherrahrou, Z., and Erdmann, J. (2024) MRAS in coronary artery disease-Unchartered territory. IUBMB life 76, 300–312.

[81] Haas, U., Sczakiel, G., and Laufer, S. D. (2012) MicroRNA-mediated regulation of gene expression is affected by disease-associated SNPs within the 3'-UTR via altered RNA structure. RNA biology 9, 924–937.

[82] Ye, M., Shima, F., Muraoka, S., Liao, J., Okamoto, H., et al. (2005) Crystal structure of M-Ras reveals a GTP-bound "off" state conformation of Ras family small GTPases. The Journal of Biological Chemistry 280, 31267–31275.

[83] Young, L. C., and Rodriguez-Viciana, P. (2018) MRAS: A Close but Understudied Member of the RAS Family. Cold Spring Harbor Perspectives in Medicine 8, a033621.

[84] Kimmelman, A., Tolkacheva, T., Lorenzi, M. V., Osada, M., and Chan, A. M. (1997) Identification and characterization of R-ras3: a novel member of the RAS gene family with a non-ubiquitous pattern of tissue distribution. Oncogene 15, 2675–2685.

[85] Watanabe-Takano, H., Takano, K., Keduka, E., and Endo, T. (2010) M-Ras is activated by bone morphogenetic protein-2 and participates in osteoblastic determination, differentiation, and transdifferentiation. Experimental Cell Research 316, 477–490.

[86] Matsumoto, K., Asano, T., and Endo, T. (1997) Novel small GTPase M-Ras participates in reorganization of actin cytoskeleton. Oncogene 15, 2409–2417.

[87] Liu, L., You, L., Tan, L., Wang, D. W., and Cui, W. (2015) Genetic insight into the role of MRAS in coronary artery disease risk. Gene 564, 63–66.

[88] Endo, T. (2020) M-Ras is Muscle-Ras, Moderate-Ras, Mineral-Ras, Migration-Ras, and Many More-Ras. Experimental Cell Research 397, 112342.

[89] Kimmelman, A. C., Nuñez Rodriguez, N., and Chan, A. M.-L. (2002) R-Ras3/M-Ras induces neuronal differentiation of PC12 cells through cell-type-specific activation of the mitogen-activated protein kinase cascade. Molecular and Cellular Biology 22, 5946–5961.

[90] Fishilevich, S., Nudel, R., Rappaport, N., Hadar, R., Plaschkes, I., et al. (2017) GeneHancer: genome-wide integration of enhancers and target genes in GeneCards. Database: The Journal of Biological Databases and Curation 2017, bax028.

[91] Jiang, F., Dong, Y., Wu, C., Yang, X., Zhao, L., et al. (2011) Fine mapping of chromosome 3q22.3 identifies two haplotype blocks in ESYT3 associated with coronary artery disease in female Han Chinese. Atherosclerosis 218, 397–403.

[92] Alshahid, M., Wakil, S. M., Al-Najai, M., Muiya, N. P., Elhawari, S., et al. (2013) New susceptibility locus for obesity and dyslipidaemia on chromosome 3q22.3. Human Genomics 7, 15.

[93] Ellis, K. L., Frampton, C. M., Pilbrow, A. P., Troughton, R. W., Doughty, R. N., et al. (2011) Genomic Risk Variants at 1p13.3, 1q41, and 3q22.3 Are Associated With Subsequent Cardiovascular Outcomes in Healthy Controls and in Established Coronary Artery Disease. Circulation: Cardiovascular Genetics 4, 636–646.

[94] Song, Y., Ma, R., and Zhang, H. (2019) The influence of MRAS gene variants on ischemic stroke and serum lipid levels in Chinese Han population. Medicine 98, e18065.

[95] Edwards, S. L., Beesley, J., French, J. D., and Dunning, A. M. (2013) Beyond GWASs: Illuminating the Dark Road from Association to Function. American Journal of Human Genetics 93, 779–797.

[96] Wen, X., Pique-Regi, R., and Luca, F. (2017) Integrating molecular QTL data into genome-wide genetic association analysis: Probabilistic assessment of enrichment and colocalization. PLoS genetics 13, e1006646.

[97] Hormozdiari, F., Kostem, E., Kang, E. Y., Pasaniuc, B., and Eskin, E. (2014) Identifying causal variants at loci with multiple signals of association. Genetics 198, 497–508.

[98] Munz, M., Wohlers, I., Simon, E., Reinberger, T., Busch, H., et al. (2020) Qtlizer: comprehensive QTL annotation of GWAS results. Scientific Reports 10, 20417.

[99] World Health Organization. Regional Office for Europe (2011) Global atlas on cardiovascular disease prevention and control: published by the World Health Organization in collaboration with the World Heart Federation and the World Stroke Organization. World Health Organization. Regional Office for Europe, Copenhagen.

[100] Fan, J., and Watanabe, T. (2022) Atherosclerosis: Known and unknown. Pathology International 72, 151–160.

[101] Fruchart, J.-C., Nierman, M. C., Stroes, E. S. G., Kastelein, J. J. P., and Duriez, P. (2004) New risk factors for atherosclerosis and patient risk assessment. Circulation 109, III15-19.

[102] D'Agostino, R. B., Vasan, R. S., Pencina, M. J., Wolf, P. A., Cobain, M., et al. (2008) General cardiovascular risk profile for use in primary care: the Framingham Heart Study. Circulation 117, 743–753.

[103] Han, A. L. (2022) Association between lipid ratio and depression: a cross-sectional study. Scientific Reports 12, 6190.

[104] Wu, J., Yin, R.-X., Guo, T., Lin, Q.-Z., Shi, G.-Y., et al. (2015) Association between the MARS rs6782181 polymorphism and serum lipid levels. International Journal of Clinical and Experimental Pathology 8, 1855–1866.

[105] Muslin, A. J. (2008) MAPK signalling in cardiovascular health and disease: molecular mechanisms and therapeutic targets. Clinical Science (London, England: 1979) 115, 203–218.

[106] Turner, A. W., Hu, S. S., Mosquera, J. V., Ma, W. F., Hodonsky, C. J., et al. (2022) Single-nucleus chromatin accessibility profiling highlights regulatory mechanisms of coronary artery disease risk. Nature Genetics 54, 804–816.

[107] Higgins, E. M., Bos, J. M., Dotzler, S. M., John Kim, C. S., and Ackerman, M. J. (2019) MRAS Variants Cause Cardiomyocyte Hypertrophy in Patient-Specific Induced Pluripotent Stem Cell-Derived Cardiomyocytes: Additional Evidence for MRAS as a Definitive Noonan Syndrome-Susceptibility Gene. Circulation. Genomic and Precision Medicine 12, e002648.

[108] Tasaka, G., Negishi, M., and Oinuma, I. (2012) Semaphorin 4D/Plexin-B1-Mediated M-Ras GAP Activity Regulates Actin-Based Dendrite Remodeling through Lamellipodin. Journal of Neuroscience 32, 8293–8305.

[109] Yoshikawa, Y., Satoh, T., Tamura, T., Wei, P., Bilasy, S. E., et al. (2007) The M-Ras-RA-GEF-2-Rap1 pathway mediates tumor necrosis factor-alpha dependent regulation of integrin activation in splenocytes. Molecular Biology of the Cell 18, 2949–2959.

[110] Lavoie, H., and Therrien, M. (2015) Regulation of RAF protein kinases in ERK signalling. Nature Reviews Molecular Cell Biology 16, 281–298.

[111] Sun, P., Watanabe, H., Takano, K., Yokoyama, T., Fujisawa, J., et al. (2006) Sustained activation of M-Ras induced by nerve growth factor is essential for neuronal differentiation of PC12 cells. Genes to Cells: Devoted to Molecular & Cellular Mechanisms 11, 1097–1113.

[112] Young, L. C., Hartig, N., Muñoz-Alegre, M., Oses-Prieto, J. A., Durdu, S., et al. (2013) An MRAS, SHOC2, and SCRIB complex coordinates ERK pathway activation with polarity and tumorigenic growth. Molecular Cell 52, 679–692.

[113] Higgins, E. M., Bos, J. M., Mason-Suares, H., Tester, D. J., Ackerman, J. P., et al. (2017) Elucidation of MRAS-mediated Noonan syndrome with cardiac hypertrophy. JCI insight 2, e91225.

[114] Motta, M., Sagi-Dain, L., Krumbach, O. H. F., Hahn, A., Peleg, A., et al. (2020) Activating MRAS mutations cause Noonan syndrome associated with hypertrophic cardiomyopathy. Human Molecular Genetics 29, 1772–1783.

[115] Kimmelman, A. C., Osada, M., and Chan, A. M. (2000) R-Ras3, a brain-specific Ras-related protein, activates Akt and promotes cell survival in PC12 cells. Oncogene 19, 2014–2022.

[116] Dudek, H., Datta, S. R., Franke, T. F., Birnbaum, M. J., Yao, R., et al. (1997) Regulation of neuronal survival by the serine-threonine protein kinase Akt. Science (New York, N.Y.) 275, 661–665.

[117] Philpott, K. L., McCarthy, M. J., Klippel, A., and Rubin, L. L. (1997) Activated Phosphatidylinositol 3-Kinase and Akt Kinase Promote Survival of Superior Cervical Neurons. Journal of Cell Biology 139, 809–815.

[118] Poznyak, A. V., Sukhorukov, V. N., Zhuravlev, A., Orekhov, N. A., Kalmykov, V., et al. (2022) Modulating mTOR Signaling as a Promising Therapeutic Strategy for Atherosclerosis. International Journal of Molecular Sciences 23, 1153.

[119] Galkina, E., and Ley, K. (2007) Vascular adhesion molecules in atherosclerosis. Arteriosclerosis, Thrombosis, and Vascular Biology 27, 2292–2301.

[120] Ward, K. R., Zhang, K.-X., Somasiri, A. M., Roskelley, C. D., and Schrader, J. W. (2004) Expression of activated M-Ras in a murine mammary epithelial cell line induces epithelial-mesenchymal transition and tumorigenesis. Oncogene 23, 1187–1196.

[121] Fatkhullina, A. R., Peshkova, I. O., and Koltsova, E. K. (2016) The Role of Cytokines in the Development of Atherosclerosis. Biochemistry. Biokhimiia 81, 1358–1370.

[122] Ait-Oufella, H., Taleb, S., Mallat, Z., and Tedgui, A. (2011) Recent advances on the role of cytokines in atherosclerosis. Arteriosclerosis, Thrombosis, and Vascular Biology 31, 969–979.

[123] Szmitko, P. E., Wang, C.-H., Weisel, R. D., de Almeida, J. R., Anderson, T. J., et al. (2003) New markers of inflammation and endothelial cell activation: Part I. Circulation 108, 1917–1923.

[124] Hansson, G. K., Libby, P., and Tabas, I. (2015) Inflammation and plaque vulnerability. Journal of Internal Medicine 278, 483–493.

[125] Tabas, I., García-Cardeña, G., and Owens, G. K. (2015) Recent insights into the cellular biology of atherosclerosis. The Journal of Cell Biology 209, 13–22.

[126] Moss, J. W. E., and Ramji, D. P. (2017) Chapter 6 - Cytokines in Atherosclerosis. In *Cytokine Effector Functions in Tissues*, (Foti M, Locati M, eds.). . pp. 109–118, Academic Press.

[127] Gisterå, A., and Hansson, G. K. (2017) The immunology of atherosclerosis. Nature Reviews Nephrology 13, 368–380.

[128] Poznyak, A. V., Bharadwaj, D., Prasad, G., Grechko, A. V., Sazonova, M. A., et al. (2021) Anti-Inflammatory Therapy for Atherosclerosis: Focusing on Cytokines. International Journal of Molecular Sciences 22, 7061.

[129] Cao, G., Xuan, X., Hu, J., Zhang, R., Jin, H., et al. (2022) How vascular smooth muscle cell phenotype switching contributes to vascular disease. Cell Communication and Signaling 20, 1–22.

[130] Haybar, H., Bandar, B., Torfi, E., Mohebbi, A., and Saki, N. (2023) Cytokines and their role in cardiovascular diseases. Cytokine 169, 156261.

[131] Kalliolias, G. D., and Ivashkiv, L. B. (2016) TNF biology, pathogenic mechanisms and emerging therapeutic strategies. Nature Reviews. Rheumatology 12, 49–62.

[132] Canault, M., Peiretti, F., Poggi, M., Mueller, C., Kopp, F., et al. (2008) Progression of atherosclerosis in ApoE-deficient mice that express distinct molecular forms of TNF-alpha. The Journal of Pathology 214, 574–583.

[133] Ohta, H., Wada, H., Niwa, T., Kirii, H., Iwamoto, N., et al. (2005) Disruption of tumor necrosis factor-alpha gene diminishes the development of atherosclerosis in ApoE-deficient mice. Atherosclerosis 180, 11–17.

[134] Jacobsson, L. T. H., Turesson, C., Gülfe, A., Kapetanovic, M. C., Petersson, I. F., et al. (2005) Treatment with tumor necrosis factor blockers is associated with a lower incidence of first cardiovascular events in patients with rheumatoid arthritis. The Journal of Rheumatology 32, 1213–1218.

[135] Jones, L. L., and Vignali, D. A. A. (2011) Molecular interactions within the IL-6/IL-12 cytokine/receptor superfamily. Immunologic Research 51, 5–14.

[136] Akdis, M., Burgler, S., Crameri, R., Eiwegger, T., Fujita, H., et al. (2011) Interleukins, from 1 to 37, and interferon-γ: receptors, functions, and roles in diseases. The Journal of Allergy and Clinical Immunology 127, 701-721.e1–70.

[137] Chia, Y. C., Kieneker, L. M., van Hassel, G., Binnenmars, S. H., Nolte, I. M., et al. (2021) Interleukin 6 and Development of Heart Failure With Preserved Ejection Fraction in the General Population. Journal of the American Heart Association 10, e018549.

[138] Vasques-Nóvoa, F., Pedro Ferreira, J., Marques, P., Sergio Neves, J., Vale, C., et al. (2022) Interleukin-6, infection and cardiovascular outcomes in acute heart failure: Findings from the EDIFICA registry. Cytokine 160, 156053.

[139] Garbers, C., Hermanns, H. M., Schaper, F., Müller-Newen, G., Grötzinger, J., et al. (2012) Plasticity and cross-talk of interleukin 6-type cytokines. Cytokine & Growth Factor Reviews 23, 85–97.

[140] Xing, Z., Gauldie, J., Cox, G., Baumann, H., Jordana, M., et al. (1998) IL-6 is an antiinflammatory cytokine required for controlling local or systemic acute inflammatory responses. The Journal of Clinical Investigation 101, 311–320.

[141] Huber, S. A., Sakkinen, P., Conze, D., Hardin, N., and Tracy, R. (1999) Interleukin-6 exacerbates early atherosclerosis in mice. Arteriosclerosis, Thrombosis, and Vascular Biology 19, 2364–2367.

[142] Schieffer, B., Selle, T., Hilfiker, A., Hilfiker-Kleiner, D., Grote, K., et al. (2004) Impact of interleukin-6 on plaque development and morphology in experimental atherosclerosis. Circulation 110, 3493–3500.

[143] Rose-John, S. (2012) IL-6 trans-signaling via the soluble IL-6 receptor: importance for the pro-inflammatory activities of IL-6. International Journal of Biological Sciences 8, 1237–1247.

[144] Schuett, H., Oestreich, R., Waetzig, G. H., Annema, W., Luchtefeld, M., et al. (2012) Transsignaling of interleukin-6 crucially contributes to atherosclerosis in mice. Arteriosclerosis, Thrombosis, and Vascular Biology 32, 281–290.

[145] Dinarello, C. A. (2009) Immunological and inflammatory functions of the interleukin-1 family. Annual Review of Immunology 27, 519–550.

[146] Kirii, H., Niwa, T., Yamada, Y., Wada, H., Saito, K., et al. (2003) Lack of interleukin-1beta decreases the severity of atherosclerosis in ApoE-deficient mice. Arteriosclerosis, Thrombosis, and Vascular Biology 23, 656–660.

[147] Mills, K. H. G. (2008) Induction, function and regulation of IL-17-producing T cells. European Journal of Immunology 38, 2636–2649.

[148] Clarke, M. C. H., Talib, S., Figg, N. L., and Bennett, M. R. (2010) Vascular smooth muscle cell apoptosis induces interleukin-1-directed inflammation: effects of hyperlipidemia-mediated inhibition of phagocytosis. Circulation Research 106, 363–372.

[149] Pascual-Figal, D. A., Bayes-Genis, A., Asensio-Lopez, M. C., Hernández-Vicente, A., Garrido-Bravo, I., et al. (2019) The Interleukin-1 Axis and Risk of Death in Patients With

Acutely Decompensated Heart Failure. Journal of the American College of Cardiology 73, 1016–1025.

[150] Silvain, J., Kerneis, M., Zeitouni, M., Lattuca, B., Galier, S., et al. (2020) Interleukin-1β and Risk of Premature Death in Patients With Myocardial Infarction. Journal of the American College of Cardiology 76, 1763–1773.

[151] Everett, B. M., MacFadyen, J. G., Thuren, T., Libby, P., Glynn, R. J., et al. (2020) Inhibition of Interleukin-1β and Reduction in Atherothrombotic Cardiovascular Events in the CANTOS Trial. Journal of the American College of Cardiology 76, 1660–1670.

[152] Isoda, K., Sawada, S., Ishigami, N., Matsuki, T., Miyazaki, K., et al. (2004) Lack of interleukin-1 receptor antagonist modulates plaque composition in apolipoprotein E-deficient mice. Arteriosclerosis, Thrombosis, and Vascular Biology 24, 1068–1073.

[153] Sheedy, F. J., Grebe, A., Rayner, K. J., Kalantari, P., Ramkhelawon, B., et al. (2013) CD36 coordinates NLRP3 inflammasome activation by facilitating intracellular nucleation of soluble ligands into particulate ligands in sterile inflammation. Nature Immunology 14, 812–820.

[154] Freigang, S., Ampenberger, F., Weiss, A., Kanneganti, T.-D., Iwakura, Y., et al. (2013) Fatty acid-induced mitochondrial uncoupling elicits inflammasome-independent IL-1α and sterile vascular inflammation in atherosclerosis. Nature Immunology 14, 1045–1053.

[155] Kamari, Y., Shaish, A., Shemesh, S., Vax, E., Grosskopf, I., et al. (2011) Reduced atherosclerosis and inflammatory cytokines in apolipoprotein-E-deficient mice lacking bone marrow-derived interleukin-1α. Biochemical and Biophysical Research Communications 405, 197–203.

[156] Merhi-Soussi, F., Kwak, B. R., Magne, D., Chadjichristos, C., Berti, M., et al. (2005) Interleukin-1 plays a major role in vascular inflammation and atherosclerosis in male apolipoprotein E-knockout mice. Cardiovascular Research 66, 583–593.

[157] Devlin, C. M., Kuriakose, G., Hirsch, E., and Tabas, I. (2002) Genetic alterations of IL-1 receptor antagonist in mice affect plasma cholesterol level and foam cell lesion size. Proceedings of the National Academy of Sciences of the United States of America 99, 6280–6285.

[158] Bartoschek, M., and Pietras, K. (2018) PDGF family function and prognostic value in tumor biology. Biochemical and Biophysical Research Communications 503, 984–990.

[159] Lu, Q.-B., Wan, M.-Y., Wang, P.-Y., Zhang, C.-X., Xu, D.-Y., et al. (2018) Chicoric acid prevents PDGF-BB-induced VSMC dedifferentiation, proliferation and migration by suppressing ROS/NFκB/mTOR/P70S6K signaling cascade. Redox Biology 14, 656–668.

[160] Chen, S., Liu, B., Kong, D., Li, S., Li, C., et al. (2015) Atorvastatin calcium inhibits phenotypic modulation of PDGF-BB-induced VSMCs via down-regulation the Akt signaling pathway. PloS One 10, e0122577.

[161] Zhou, J., Shao, L., Yu, J., Huang, J., and Feng, Q. (2021) PDGF-BB promotes vascular smooth muscle cell migration by enhancing Pim-1 expression via inhibiting miR-214. Annals of Translational Medicine 9, 1728.

[162] Smyth, L. C. D., Highet, B., Jansson, D., Wu, J., Rustenhoven, J., et al. (2022) Characterisation of PDGF-BB:PDGFRβ signalling pathways in human brain pericytes: evidence of disruption in Alzheimer's disease. Communications Biology 5, 235.

[163] Dash, B. C., Jiang, Z., Suh, C., and Qyang, Y. (2015) Induced pluripotent stem cell-derived vascular smooth muscle cells: methods and application. The Biochemical Journal 465, 185–194.

[164] Drab, M., Haller, H., Bychkov, R., Erdmann, B., Lindschau, C., et al. (1997) From totipotent embryonic stem cells to spontaneously contracting smooth muscle cells: a retinoic acid and db-cAMP *in vitro* differentiation model. FASEB journal: official publication of the Federation of American Societies for Experimental Biology 11, 905–915.

[165] Sinha, S., Iyer, D., and Granata, A. (2014) Embryonic origins of human vascular smooth muscle cells: implications for *in vitro* modeling and clinical application. Cellular and molecular life sciences: CMLS 71, 2271–2288.

[166] Alexander, M. R., and Owens, G. K. (2012) Epigenetic control of smooth muscle cell differentiation and phenotypic switching in vascular development and disease. Annual Review of Physiology 74, 13–40.

[167] Beamish, J. A., He, P., Kottke-Marchant, K., and Marchant, R. E. (2010) Molecular regulation of contractile smooth muscle cell phenotype: implications for vascular tissue engineering. Tissue Engineering. Part B, Reviews 16, 467–491.

[168] Adam, P. J., Regan, C. P., Hautmann, M. B., and Owens, G. K. (2000) Positive- and negative-acting Kruppel-like transcription factors bind a transforming growth factor beta control element required for expression of the smooth muscle cell differentiation marker SM22alpha *in vivo*. The Journal of Biological Chemistry 275, 37798–37806.

[169] Bennett, M. R., Sinha, S., and Owens, G. K. (2016) Vascular Smooth Muscle Cells in Atherosclerosis. Circulation Research 118, 692–702.

[170] Hayashi, K., Shibata, K., Morita, T., Iwasaki, K., Watanabe, M., et al. (2004) Insulin receptor substrate-1/SHP-2 interaction, a phenotype-dependent switching machinery of insulin-like growth factor-I signaling in vascular smooth muscle cells. The Journal of Biological Chemistry 279, 40807–40818.

[171] Understanding PCR von Sarah Maddocks | ISBN 978-0-12-802683-0 | Fachbuch online kaufen - Lehmanns.de.

[172] Love, M. I., Huber, W., and Anders, S. (2014) Moderated estimation of fold change and dispersion for RNA-seq data with DESeq2. Genome Biology 15, 550.

[173] Elizarraras, J. M., Liao, Y., Shi, Z., Zhu, Q., Pico, A. R., et al. (2024) WebGestalt 2024: faster gene set analysis and new support for metabolomics and multi-omics. Nucleic Acids Research 52, W415–W421.

[174] Watkins, H., and Farrall, M. (2006) Genetic susceptibility to coronary artery disease: from promise to progress. Nature Reviews. Genetics 7, 163–173.

[175] Ferrières, J., Lambert, J., Lussier-Cacan, S., and Davignon, J. (1995) Coronary artery disease in heterozygous familial hypercholesterolemia patients with the same LDL receptor gene mutation. Circulation 92, 290–295.

[176] Kessler, T., Vilne, B., and Schunkert, H. (2016) The impact of genome-wide association studies on the pathophysiology and therapy of cardiovascular disease. EMBO molecular medicine 8, 688–701.

[177] Mathieu, M.-E., Faucheux, C., Saucourt, C., Soulet, F., Gauthereau, X., et al. (2013) MRAS GTPase is a novel stemness marker that impacts mouse embryonic stem cell plasticity and Xenopus embryonic cell fate. Development (Cambridge, England) 140, 3311–3322.

[178] Monk, B. A., and George, S. J. (2015) The Effect of Ageing on Vascular Smooth Muscle Cell Behaviour--A Mini-Review. Gerontology 61, 416–426.

[179] Seawright, J. W., Sreenivasappa, H., Gibbs, H. C., Padgham, S., Shin, S. Y., et al. (2018) Vascular Smooth Muscle Contractile Function Declines With Age in Skeletal Muscle Feed Arteries. Frontiers in Physiology 9, 856.

[180] Lacolley, P., Regnault, V., and Avolio, A. P. (2018) Smooth muscle cell and arterial aging: basic and clinical aspects. Cardiovascular Research 114, 513–528.

[181] Davis, R., Pillai, S., Lawrence, N., Sebti, S., and Chellappan, S. P. (2012) TNFα-mediated proliferation of vascular smooth muscle cells involves Raf-1-mediated inactivation of Rb and transcription of E2F1-regulated genes. Cell Cycle 11, 109–118.

[182] Gomez, D., and Owens, G. K. (2012) Smooth muscle cell phenotypic switching in atherosclerosis. Cardiovascular Research 95, 156–164.

[183] Bochaton-Piallat, M.-L., and Gabbiani, G. (2005) Modulation of Smooth Muscle Cell Proliferation and Migration: Role of Smooth Muscle Cell Heterogeneity. In *Atherosclerosis: Diet and Drugs*, (von Eckardstein A, ed.). . pp. 645–663, Springer, Berlin, Heidelberg.

[184] Salabei, J. K., Cummins, T. D., Singh, M., Jones, S. P., Bhatnagar, A., et al. (2013) PDGF-mediated autophagy regulates vascular smooth muscle cell phenotype and resistance to oxidative stress. The Biochemical journal 451, 375–388.

[185] Libby, P., Ridker, P. M., and Hansson, G. K. (2011) Progress and challenges in translating the biology of atherosclerosis. Nature 473, 317–325.

[186] Virmani, R., Kolodgie, F. D., Burke, A. P., Farb, A., and Schwartz, S. M. (2000) Lessons from sudden coronary death: a comprehensive morphological classification scheme for atherosclerotic lesions. Arteriosclerosis, Thrombosis, and Vascular Biology 20, 1262–1275.

[187] Lutgens, E., de Muinck, E. D., Kitslaar, P. J., Tordoir, J. H., Wellens, H. J., et al. (1999) Biphasic pattern of cell turnover characterizes the progression from fatty streaks to ruptured human atherosclerotic plaques. Cardiovascular Research 41, 473–479.

[188] Hariri, R. J., Hajjar, D. P., Coletti, D., Alonso, D. R., Weksler, M. E., et al. (1988) Aging and arteriosclerosis. Cell cycle kinetics of young and old arterial smooth muscle cells. The American Journal of Pathology 131, 132–136.

[189] Moon, S.-K., Cha, B.-Y., and Kim, C.-H. (2003) *In vitro* cellular aging is associated with enhanced proliferative capacity, G1 cell cycle modulation, and matrix metalloproteinase-9 regulation in mouse aortic smooth muscle cells. Archives of Biochemistry and Biophysics 418, 39–48.

[190] Stemerman, M. B., Weinstein, R., Rowe, J. W., Maciag, T., Fuhro, R., et al. (1982) Vascular smooth muscle cell growth kinetics *in vivo* in aged rats. Proceedings of the National Academy of Sciences of the United States of America 79, 3863–3866.

[191] Bennett, M. R., Evan, G. I., and Schwartz, S. M. (1995) Apoptosis of human vascular smooth muscle cells derived from normal vessels and coronary atherosclerotic plaques. The Journal of Clinical Investigation 95, 2266–2274.

[192] O'Brien, E. R., Alpers, C. E., Stewart, D. K., Ferguson, M., Tran, N., et al. (1993) Proliferation in primary and restenotic coronary atherectomy tissue. Implications for antiproliferative therapy. Circulation Research 73, 223–231.

[193] Patel, V. A., Zhang, Q. J., Siddle, K., Soos, M. A., Goddard, M., et al. (2001) Defect in insulin-like growth factor-1 survival mechanism in atherosclerotic plaque-derived vascular smooth muscle cells is mediated by reduced surface binding and signaling. Circulation Research 88, 895–902.

[194] Matthews, C., Gorenne, I., Scott, S., Figg, N., Kirkpatrick, P., et al. (2006) Vascular smooth muscle cells undergo telomere-based senescence in human atherosclerosis: effects of telomerase and oxidative stress. Circulation Research 99, 156–164.

[195] O'Sullivan, M., Scott, S. D., McCarthy, N., Figg, N., Shapiro, L. M., et al. (2003) Differential cyclin E expression in human in-stent stenosis smooth muscle cells identifies targets for selective anti-restenosis therapy. Cardiovascular Research 60, 673–683.

[196] Feil, S., Fehrenbacher, B., Lukowski, R., Essmann, F., Schulze-Osthoff, K., et al. (2014) Transdifferentiation of Vascular Smooth Muscle Cells to Macrophage-Like Cells During Atherogenesis. Circulation Research 115, 662–667.

[197] Boyle, J. J., Weissberg, P. L., and Bennett, M. R. (2002) Human macrophage-induced vascular smooth muscle cell apoptosis requires NO enhancement of Fas/Fas-L interactions. Arteriosclerosis, Thrombosis, and Vascular Biology 22, 1624–1630.

[198] Bauriedel, G., Hutter, R., Welsch, U., Bach, R., Sievert, H., et al. (1999) Role of smooth muscle cell death in advanced coronary primary lesions: implications for plaque instability. Cardiovascular Research 41, 480–488.

[199] Ihling, C., Szombathy, T., Nampoothiri, K., Haendeler, J., Beyersdorf, F., et al. (1999) Cystic medial degeneration of the aorta is associated with p53 accumulation, Bax upregulation, apoptotic cell death, and cell proliferation. Heart (British Cardiac Society) 82, 286–293.

[200] Sawabe, M. (2010) Vascular aging: from molecular mechanism to clinical significance. Geriatrics & Gerontology International 10 Suppl 1, S213-220.

[201] Bennett, M. R., Gibson, D. F., Schwartz, S. M., and Tait, J. F. (1995) Binding and phagocytosis of apoptotic vascular smooth muscle cells is mediated in part by exposure of phosphatidylserine. Circulation Research 77, 1136–1142.

[202] Cabrera, J. T. O., and Makino, A. (2022) Efferocytosis of vascular cells in cardiovascular disease. Pharmacology & therapeutics 229, 107919.

[203] Kojima, Y., Downing, K., Kundu, R., Miller, C., Dewey, F., et al. (2014) Cyclin-dependent kinase inhibitor 2B regulates efferocytosis and atherosclerosis. The Journal of Clinical Investigation 124, 1083–1097.

[204] Zernecke, A., Schober, A., Bot, I., von Hundelshausen, P., Liehn, E. A., et al. (2005) SDF-1alpha/CXCR4 axis is instrumental in neointimal hyperplasia and recruitment of smooth muscle progenitor cells. Circulation Research 96, 784–791.

[205] Yu, H., Stoneman, V., Clarke, M., Figg, N., Xin, H.-B., et al. (2011) Bone marrow-derived smooth muscle-like cells are infrequent in advanced primary atherosclerotic plaques but promote atherosclerosis. Arteriosclerosis, Thrombosis, and Vascular Biology 31, 1291–1299.

[206] Worssam, M. D., and Jørgensen, H. F. (2021) Mechanisms of vascular smooth muscle cell investment and phenotypic diversification in vascular diseases. Biochemical Society Transactions 49, 2101–2111.

[207] Grootaert, M. O. J., and Bennett, M. R. (2021) Vascular smooth muscle cells in atherosclerosis: time for a re-assessment. Cardiovascular Research 117, 2326–2339.

[208] Wu, Y.-T., Chen, L., Tan, Z.-B., Fan, H.-J., Xie, L.-P., et al. (2018) Luteolin Inhibits Vascular Smooth Muscle Cell Proliferation and Migration by Inhibiting TGFBR1 Signaling. Frontiers in Pharmacology 9.

[209] Girona, J., Rosales, R., Plana, N., Saavedra, P., Masana, L., et al. (2013) FABP4 Induces Vascular Smooth Muscle Cell Proliferation and Migration through a MAPK-Dependent Pathway. PLOS ONE 8, e81914.

[210] Bennett, M. R. (1999) Apoptosis of vascular smooth muscle cells in vascular remodelling and atherosclerotic plaque rupture. Cardiovascular Research 41, 361–368.

[211] McVey, D. G., Andreadi, C., Gong, P., Stanczyk, P. J., Solomon, C. U., et al. (2024) Genetic influence on vascular smooth muscle cell apoptosis. Cell Death & Disease 15, 1–12.

[212] Tsai, E. J., and Kass, D. A. (2009) Cyclic GMP signaling in cardiovascular pathophysiology and therapeutics. Pharmacology & Therapeutics 122, 216–238.

[213] Rybalkin, S. D., Hinds, T. R., and Beavo, J. A. (2013) Enzyme assays for cGMP hydrolysing Phosphodiesterases. Methods in molecular biology (Clifton, N.J.) 1020, 51–62.

[214] Delhaye, S., and Bardoni, B. (2021) Role of phosphodiesterases in the pathophysiology of neurodevelopmental disorders. Molecular Psychiatry 26, 4570–4582.

[215] Omori, K., and Kotera, J. (2007) Overview of PDEs and Their Regulation. Circulation Research 100, 309–327.

[216] C, B., and C, G. (2015) Cardiac cAMP: production, hydrolysis, modulation and detection. Frontiers in pharmacology 6.

[217] Fukumoto, S., Koyama, H., Hosoi, M., Yamakawa, K., Tanaka, S., et al. (1999) Distinct Role of cAMP and cGMP in the Cell Cycle Control of Vascular Smooth Muscle Cells. Circulation Research 85, 985–991.

[218] Hildebrand, S., Ibrahim, M., Schlitzer, A., Maegdefessel, L., Röll, W., et al. (2022) PDGF regulates guanylate cyclase expression and cGMP signaling in vascular smooth muscle. Communications Biology 5, 197.

[219] Lorigo, M., Oliveira, N., and Cairrao, E. (2021) PDE-Mediated Cyclic Nucleotide Compartmentation in Vascular Smooth Muscle Cells: From Basic to a Clinical Perspective. Journal of Cardiovascular Development and Disease 9, 4.

[220] Azevedo, M. F., Faucz, F. R., Bimpaki, E., Horvath, A., Levy, I., et al. (2014) Clinical and Molecular Genetics of the Phosphodiesterases (PDEs). Endocrine Reviews 35, 195–233.

[221] Ma, J., Li, Y., Yang, X., Liu, K., Zhang, X., et al. (2023) Signaling pathways in vascular function and hypertension: molecular mechanisms and therapeutic interventions. Signal Transduction and Targeted Therapy 8, 1–30.

[222] Orr, A. W., Hastings, N. E., Blackman, B. R., and Wamhoff, B. R. (2010) Complex Regulation and Function of the Inflammatory Smooth Muscle Cell Phenotype in Atherosclerosis. Journal of Vascular Research 47, 168–180.

[223] Lehners, M., Dobrowinski, H., Feil, S., and Feil, R. (2018) cGMP Signaling and Vascular Smooth Muscle Cell Plasticity. Journal of Cardiovascular Development and Disease 5, 20.

[224] Melichar, V. O., Behr-Roussel, D., Zabel, U., Uttenthal, L. O., Rodrigo, J., et al. (2004) Reduced cGMP signaling associated with neointimal proliferation and vascular dysfunction in late-stage atherosclerosis. Proceedings of the National Academy of Sciences of the United States of America 101, 16671–16676.

[225] Robichaux, W. G., Mei, F. C., Yang, W., Wang, H., Sun, H., et al. (2020) Epac1 (Exchange Protein Directly Activated by cAMP 1) Upregulates LOX-1 (Oxidized Low-Density Lipoprotein Receptor 1) to Promote Foam Cell Formation and Atherosclerosis Development. Arteriosclerosis, Thrombosis, and Vascular Biology 40, e322–e335.

[226] Robichaux, W. G., Mei, F. C., Yang, W., Wang, H., Sun, H., et al. (2020) Epac1 upregulates LOX-1 to promote foam cell formation and atherosclerosis development. Arteriosclerosis, thrombosis, and vascular biology 40, e322–e335.

[227] Nakashima, Y., Wight, T. N., and Sueishi, K. (2008) Early atherosclerosis in humans: role of diffuse intimal thickening and extracellular matrix proteoglycans. Cardiovascular Research 79, 14–23.

[228] Zhao, A., Li, D., Mao, X., Yang, M., Deng, W., et al. (2022) GNG2 acts as a tumor suppressor in breast cancer through stimulating MRAS signaling. Cell Death & Disease 13, 260.

[229] Young, L. C., Hartig, N., Boned Del Río, I., Sari, S., Ringham-Terry, B., et al. (2018) SHOC2-MRAS-PP1 complex positively regulates RAF activity and contributes to Noonan syndrome pathogenesis. Proceedings of the National Academy of Sciences of the United States of America 115, E10576–E10585.

[230] Rodriguez-Viciana, P., Oses-Prieto, J., Burlingame, A., Fried, M., and McCormick, F. (2006) A phosphatase holoenzyme comprised of Shoc2/Sur8 and the catalytic subunit of PP1 functions as an M-Ras effector to modulate Raf activity. Molecular Cell 22, 217–230.

[231] Khalid, K., Padda, J., Ismail, D., Abdullah, M., Gupta, D., et al. (2021) Correlation of Coronary Artery Disease and Left Ventricular Hypertrophy. Cureus 13, e17550.

[232] Cinti, S., Mitchell, G., Barbatelli, G., Murano, I., Ceresi, E., et al. (2005) Adipocyte death defines macrophage localization and function in adipose tissue of obese mice and humans. Journal of Lipid Research 46, 2347–2355.

[233] Young, H. E., Mancini, M. L., Wright, R. P., Smith, J. C., Black, A. C., et al. (1995) Mesenchymal stem cells reside within the connective tissues of many organs. Developmental Dynamics: An Official Publication of the American Association of Anatomists 202, 137–144.

[234] Van Gaal, L. F., Mertens, I. L., and De Block, C. E. (2006) Mechanisms linking obesity with cardiovascular disease. Nature 444, 875–880.

[235] Apovian, C. M., Bigornia, S., Mott, M., Meyers, M. R., Ulloor, J., et al. (2008) Adipose macrophage infiltration is associated with insulin resistance and vascular endothelial dysfunction in obese subjects. Arteriosclerosis, Thrombosis, and Vascular Biology 28, 1654–1659.

[236] Gesta, S., Tseng, Y.-H., and Kahn, C. R. (2007) Developmental origin of fat: tracking obesity to its source. Cell 131, 242–256.

[237] Owens, G. K. (1989) Control of hypertrophic versus hyperplastic growth of vascular smooth muscle cells. The American Journal of Physiology 257, H1755-1765.

9. Appendix

9.1 List of PDEs downregulated in *Mras* KO SMCs

A table of phosphodiesterases (PDEs) downregulated and upregulated in the *Mras* KO SMCs is depicted below.

Table 26 – HSMC Phosphodiesterases *Mras KO* SMCs vs *B6.ApoE*$^{-/-}$ SMCs

Gene_id	baseMean	log_2Fold change	pvalue	padj	Gene Name
ENSMUSG00000021684	81.67933473	-4.975434265	4.64585E-17	2.05242E-16	**Pde8b**
ENSMUSG00000041741	461.3436416	-2.273930074	6.1245E-104	1.984E-102	**Pde3a**
ENSMUSG00000053965	439.6002116	-2.081898271	1.91442E-93	5.39878E-92	**Pde5a**
ENSMUSG00000023868	90.5483805	-1.752188451	0.000226624	0.000461511	**Pde10a**
ENSMUSG00000030671	313.9870917	-1.333859482	4.53852E-41	4.56946E-40	**Pde3b**
ENSMUSG00000019990	165.0630801	-1.29904774	5.99067E-12	2.05401E-11	**Pde7b**
ENSMUSG00000059173	196.2844382	-1.170179058	6.90065E-18	3.15241E-17	**Pde1a**
ENSMUSG00000041119	72.21914173	1.452571104	0.00797869	0.013644648	**Pde9a**

The blue colour is for downregulation; the orange colour is for upregulation in *Mras* KO SMCs.

9.2 Abbreviations

Acronym	Extended name
Acta 2	Actin alpha 2
AKT	Ak strain transforming/ Protein kinase B
ANG=II	Angiotensin II
ApoE	Apolipoprotein E
Aqua dest.	Aqua destillata (distilled water)
bFGF	Basic fibroblast growth factor
Ca & Mg	Calcium and Magnesium
CAD	Coronary Artery Disease
CALD1	Caldesmon 1
cAMP	Cyclic adenosine monophosphate
CD36	Cluster of differentiation 36
cDNA	Complementary DNA
cGMP	Cyclic guanosine monophosphate
CSFs	Colony- stimulating factors
Cts	Threshold cycles

Cts	Threshold cycles
CVD	Cardiovascular disease
DAPI	4',6- diamidino-2-phenylindole
DAPI	4’, 6- diamidino-2-phenylindole
DEGs	Differentially expressed genes
DEVD-p-NA	N-Acetyl-Asp-Glu-Val-Asp p-nitroanilide
dKO	Double knockout
DMEM	Dulbecco’s modified eagle medium
DNA	Deoxyribonucleic acid
dNTPs	Deoxyribose nucleoside triphosphates
DTT	Dithiothreitol
ECM	Extracellular matrix
ECs	Endothelial cells
EDTA	Ethylenediamine tetra acetic acid
EGF	Epidermal growth factor
EMT	Epithelial-to-mesenchymal transition
Epac1	Exchange protein activated by cAMP1
eQTL	expression quantitative trait locus
ER	Endoplasmic reticulum
ERK	Extracellular signal- regulated kinase
FBS	Fetal bovine serum
GAPDH	Glyceraldehyde-3-phosphate dehydrogenase
GEFs	Guanine nucleotide exchange factors
GIMP	GNU Image Manipulation program
GNG2	G protein subunit gamma 2
GOTM	General ocean turbulence model
gp130	Glycoprotein 130
GSEA	Gene set enrichment analysis
GWAS	Genome-wide association Studies
HRP	Horseradish peroxidase
HSMCs	Human smooth muscle cells
ICAM-1	Intercellular adhesion molecule 1
IDT	Integrated DNA technologies
IFNs	Interferons
IFN-γ	Interferon-gamma

IGF1	Insulin-like growth factor 1
IGFs	Insulin-like growth factors
IL-1RA	Interleukin 1 receptor antagonist
IL-1ß	Interleukin 1 beta
IL-6	Interleukin 6
ILs	Interleukins
JNK	c-Jun N-terminal kinase
KO	knockout
LB	Lysogeny broth
LDL-C	Low density lipoprotein- cholesterol
Lox1	Lectin-like Oxidized Low density lipoprotein receptor 1
LVH	Left ventricular hypertrophy
MAPK	Mitogen-activated protein kinase
MCP-1	Monocyte chemotactic protein 1
MEF-2	Myocyte enhancer factor 2
MI	Myocardial Infarction
MoMa	Monocytes and macrophages
MRAS	Muscle RAS oncogene
MSMCs	Murine smooth muscle cells
mTOR	Mammalian target of rapamycin
MYH10	Myosin heavy chain 10
MYH11	Myosin heavy chain 11
NCBI	National Centre for Biotechnology Information
NLRP3	Nacht, LRR and PYD domains-containing protein 3
ORF	Open reading frame
ORO	Oil red O
oxLDLs	Oxidized low density lipoproteins
PBS	Phosphate buffered saline
PCA	Principal component analysis
PCs	Pericytes
PDE	Phosphodiesterase
PDGF	Platelet- derived growth factor
PenStrep (P/S)	Penicillin/ streptomycin
PI3K	Phosphatidylinositol-3 kinase
PMSF	Phenylmethylsulphonyl fluoride

PP1	Protein phosphatase 1
PVDF	Polyvinylidene fluoride
qPCR	Quantitative polymerase chain reaction
RAF	Rapidly accelerated fibrosarcoma
RAP1	Ras-related protein 1
RAPGEF6	Rap guanine nucleotide exchange factor 6
RAS	Rat sarcoma virus
RBP1	Retinol binding protein 1
RNA	Ribonucleic acid
RNAi	RNA interference
RNA-seq	RNA sequencing
RUV	Remove unwanted variation
SCRIB	Scribble planar cell polarity protein
SDS	Sodium dodecyl sulphate
SHOC2	Soc-2 suppressor of clear homolog leucine rich repeat scaffold protein
siRNA	Small interfering RNA
SM22α	Smooth muscle protein 22 alpha
SMCs	Smooth muscle cells
SMDS	Smooth muscle cell differentiation supplement
SMGS	Smooth muscle cell growth supplement
SMTN	Smoothelin
SMαA	Smooth muscle alpha actin
SNVs	Single nucleotide variants
SVA	Surrogate variable analysis
Tagln	Transgelin
TBS	Tris buffered saline
TBS-T	Tris buffered saline with tween 20
TGF	Transforming growth factor
TGF-ß1	Transforming growth factor- beta 1
TLR4	Toll-like receptor 4
TLR6	Toll-like receptor 6
TNF	Tumour necrosis factor
TPM4	Tropomyosin 4
VCAM-1	Vascular cell adhesion protein 1
VIM	Vimentin

VSMCs	Vascular smooth muscle cells
WT	Wild-type
Xa	Coagulation Factor Xa

9.3 Amino acids

Amino Acid	Three-letter code	Symbol
Arginine	Arg	R
Aspartic acid	Asp	D
Glutamic acid	Glu	E
Glutamine	Gln	Q
Glycine	Gly	G
Isoleucine	Ile	I
Threonine	Thr	T
Valine	Val	V

9.4 Units

Symbol	Unit
°C	Degrees centigrade
µ	Micro
µg	Microgram
µl	Microliter
h	Hour
min	Minute
ml	Millilitre
mM	Milli molar mass
pmol/ µl	Pico mol per microliter
Rpm	Revolutions per minute
s	Second
U/µl	Unit per microliter
v	Volume
w/v	Weight per volume

9.10 Own Publications

1. ***Shah PW***, Reinberger T, et al. (2024). MRAS in coronary artery disease- Unchartered territory. IUBMB Life. PMID: 38251784; (IF: 4.7)
2. **Shah PW**, Hashmi S, Reinberger T, et al. (2023). In memoriam: Prof. Dr. rer. nat. Jeanette Erdmann. IUBMB Life. PMID: 38095343; (IF: 4.7)
3. **Hashmi S, Shah PW, et al.** (2023). Beyond the Basics: Unravelling the complexity of Coronary Artery Calcification. Cells. PMID: 3813214; (IF: 5.1)
4. **Abdullah, Shah PW, et al.** (2020). A homozygous nonsense variant in DYM underlies Dyggve-Melchior-Clausen syndrome associated with ectodermal features. Mol Biol Rep. PMID: 32886330; (IF: 2.6)
5. **Ullah A, Ali RH, Majeed AI, Liaqat K, Shah PW, et al.**, (2019). A novel insertion and deletion mutation in the BHLHA9 underlies camptosynpolydactyly and mesoaxial synostotic syndactyly with phalangeal reduction. Eur J Med Genet. PMID: 30107244; (IF: 2.7)

9.12 Acknowledgements

All glories to the Almighty ALLAH, The most Gracious and the most Merciful who bestowed me with everything I wished for. Praise to the Holy Prophet (PBUH) who became our ultimate source of knowledge and taught us to probe into the secrets of nature.

First, and foremost, I extend my deepest gratitude to my beloved supervisor ***Prof. Dr. rer. nat. Jeanette Erdmann,*** former Director Institute for Cardiogenetics, University of Lübeck, who provided me with this fascinating project. Her scholastic guidance, immense patience and valuable suggestions made my way throughout the first three years of my PhD. Unfortunately, she passed away in July, 2023 and left a deep void in my heart and life.

I am very grateful to ***Prof. Dr. med. Malte Spielmann,*** Director of Institute of Human Genetics, University of Lübeck, for accepting me as his student in the hardest times of my PhD. His kind supervision, unwavering support, and encouragement has been very instrumental in fostering an environment where my intellectual and academic pursuits could flourish. I am truly thankful to him for his dedication to not only nurturing the progress of my doctoral research and thesis but also my overall professional growth.

I owe my deep respect to ***Dr. Zouhair Aherrahrou,*** Deputy head, Institute for Cardiogenetics, who provided me an opportunity to work in a constructive research environment.

This project was funded by **DAAD (Deutscher Akademischer Austauschdienst)**, and I am deeply thankful for their financial assistance and trust in my research work.

No words in any dictionary of the whole world can express my feelings of love, practical support and sacrifices of my parents, my keys to success, my beloved father ***Prof. Dr Sayed Wiqar Ali Shah***, Professor of History and my loving mother ***Mrs. Nazia Wiqar Shah.*** I have been blessed with the best of the best, my beautiful siblings ***Zalanda Wiqar Shah, Zalan Wiqar Shah*** & ***Roshaana Wiqar Shah*** and my cute little nephew ***Sayed Bahlol Shah Bacha***, who not only supported me during my research work and studies but in all phases of life. My family has always remained by my side in thick and thin and given me generous support, continuous motivation, and inspiring guidance throughout the course of my life.

I wish to express sincere thanks to ***Dr. Tobias Reinberger***, whose expert guidance, valuable suggestions and moral support made this project possible. From the very first day of my PhD, Tobias has been by my side through every phase, and we have faced the challenges of this project together.

I would like to extend my sincere gratitude to my esteemed lab colleagues, ***Dr. Redouane Aherrahrou, Dr. Naseeb Kakar, Haider, Franzi, Marlon, Nadine, Luis,*** and ***Daria*** for their cooperation, insightful suggestions and camaraderie that made my time in the lab both productive and enjoyable. I am thankful from the core of my heart to ***Sandra, Maren, Annett, Petra*** and ***Maria*** for their unwavering assistance and generous cooperation, which played a vital role in the successful completion of this research project at this prestigious lab.

I would also thank my dear friends ***Imad Ali, Laila, Abdullah, Hammal,*** and ***Neelam***, for their remarkable support, love and prayers. Despite the physical distance, our connection transcends borders, bringing me a sense of home no matter where I am. Your friendship has been a constant source of comfort, laughter and understanding, making the challenges of distance feel lighter. Our bond is a cherished treasure, and I know it will last a lifetime.

Throughout my PhD journey, I was fortunate to have wonderful friends who brought joy and happiness into my life. I am particularly thankful to ***Aida, Shela, Cholpon, PJ, Litizia,*** and ***Yuliia*** for their amazing company – not just during lunch breaks, but for their encouragement and motivation throughout these four years. Thank you for inspiring me to pursue my goals and ambitions. I love you all.

Finally, I want to specially thank my husband, ***Hamza Wahab*** for his boundless love, steadfast support, and invaluable life advice. This work would not be possible without your patience, understanding and constant motivation during all the hard times. Thank you for being my pillar of support and sharing in both the triumphs and trails of this journey.

Lastly, I offer my regards and blessings to everyone who has supported me in anyway throughout the completion of this project.

Pashmina Wiqar Shah